ELECTROCHEMICAL HYDROGENATION OF AROMATIC COMPOUNDS CHEMISORBED AT POLYCRYSTALLINE AND SINGLE-CRYSTAL Pd SURFACES

A Dissertation

by

JEAN SANABRIA-CHINCHILLA

Submitted to the Office of Graduate Studies of
Texas A&M University
in partial fulfillment of the requirements for the degree of

DOCTOR OF PHILOSOPHY

August 2006

Major Subject: Chemistry

ELECTROCHEMICAL HYDROGENATION OF AROMATIC COMPOUNDS CHEMISORBED AT POLYCRYSTALLINE AND SINGLE-CRYSTAL Pd SURFACES

A Dissertation

by

JEAN SANABRIA-CHINCHILLA

Submitted to the Office of Graduate Studies of
Texas A&M University
in partial fulfillment of the requirements for the degree of

DOCTOR OF PHILOSOPHY

Approved by:

Chair of Committee, Manuel P. Soriaga
Committee Members, Paul S. Cremer
Edward Fry
Gyula Vigh
Head of Department, Emile A. Schweikert

August 2006

Major Subject: Chemistry

ABSTRACT

Electrochemical Hydrogenation of Aromatic Compounds Chemisorbed at
Polycrystalline and Single-Crystal Pd Surfaces. (August 2006)
Jean Sanabria-Chinchilla, B.S., Universidad de Costa Rica
Chair of Advisory Committee: Dr. Manuel P. Soriaga

The chemisorption and electrochemical hydrogenation of hydroquinone (H_2Q) at polycrystalline (pc) Pd, well-ordered Pd(100), and Pd-modified Au(*hkl*) electrodes were studied using a combination of ultra-high vacuum (UHV) surface spectroscopy, electrochemistry (EC), and electrochemical mass spectrometry (EC-MS). H_2Q was found to form a slightly tilted flat-oriented quinone (Q) adlayer, when adsorbed from low concentrations; when chemisorbed from high concentrations, an edgewise-oriented H_2Q adlayer was indicated.

The hydrogenation of the chemisorbed layer is initiated at potentials before the onset of the hydrogen evolution region. As expected, the kinetics increases as the applied potential is increased, but the hydrogenation pathway appears to be independent of the potential. Hydrogenation in the absence of absorbed hydrogen (sub-surface) was studied at ultra-thin Pd films on Au single-crystal substrates. Hydrogenation and/or potential induced desorption were established, although non-volatile and/or hydrophobic products were detected. In comparison, negative excursions with benzene-coated electrodes resulted in nothing more than potential-induced desorption of the starting material. Negative-potential electro-desorption was more facile at terraces than at steps. Vibrational spectroscopic measurements suggested that hydrogenation occurs one molecule at a time to the fullest extent that resulted in desorption of product; that is, partially hydrogenated species do not exist on the surface.

DEDICATION

To my loving wife, Silvia, for always being there, in the sunny and rainy days of my life; for her patience and unconditional love; and for her unflinching support during the last conquest of this crusade.

ACKNOWLEDGMENTS

All conceivable strength, mental and spiritual, needed to accomplish this project duly belongs to God who has made everything possible.

I would like to thank my advisor, Dr. M. P. Soriaga, for his invaluable help in the development of this project. His unending support during my stay at Texas A&M University is gratefully acknowledged. By patiently sharing his vast knowledge, he has taught me what a model scientist is truly made of. I would also like to thank my committee members, Dr. Gy. Vigh, Dr. P. Cremer, and Dr. E. Fry, for their advice on my research project.

I would like to express my special gratitude to Dr. Helmut Baltruschat (Bonn University, Germany) for inviting me to his laboratory and allowing me to use the facilities therein.

Thank you to the present and former members of Dr. Soriaga's research group: Dr. Y.-G. Kim, Dr. X. Chen, Dr. Y.-S. Park, Juan, Ding, Akhtar, Raj, and Kyle. Special thanks go to Dr. X. Chen for serving as my mentor. To my friend, Jack, with whom I spent countless hours in the lab, thanks for sharing your priceless opinions at different stages of this project. Thanks to all my colleagues for making the laboratory an enjoyable place to work in.

I would like to thank Silvia, my wife, for all the unconditional spiritual support, help and comprehension she offered me during these tumultuous years. Without her, accomplishing this work would have been twice as difficult.

A mis padres José F. Sanabria González y Gladys Chinchilla Barboza por darme la vida y por el amor y soporte espiritual durante todo este tiempo desde la distancia. Gracias por educarme y hacer de mi una persona de bien.

This project was financially supported by the National Science Foundation and the Robert A. Welch Foundation.

TABLE OF CONTENTS

Page

LIST OF FIGURES

Page

Page

Page

INTRODUCTION

The catalytic properties of palladium metal are well known [1], although it is not as widely used or as extensively studied as platinum. This, however, does not mean that further investigations on the interfacial properties of Pd are not warranted. In fact, the unique behavior of the metal, in addition to absorbing unusually large amounts of hydrogen, may result from the anomalously weak intermetallic Pd-Pd bond. For example, the cohesive energy (enthalpy of atomization) and the dissociation enthalpy of Pd are much smaller than that for nickel. Such an anomaly has been shown to enhance adsorbed-induced surface mobilities and facilitate the disruption of substrate-substrate bonds and/or the formation of substrate-adsorbate bonds [2].

As a catalyst, Pd has demonstrated its ability to catalyze both homogeneous [3] and heterogeneous [1,3,4] reactions. As a homogeneous catalyst, Pd-based compounds, complexes, and ligands have been extensively used in organic synthesis. Pd offers many possibilities of carbon-carbon bond formation, which are not available with other catalysts. Another important feature is its tolerance towards several functional groups such as carbonyl and hydroxy groups. Reactions can be carried out without protection of these functional groups [3].

In heterogeneous catalysis, Pd is the catalyst of choice in important reactions related with the manufacture of fine chemicals such as pharmaceuticals, pesticides, and flavors and fragrances. For example, Pd is the most successful industrial alkyne hydrogenation catalyst because it offers the best combination of activity and selectivity at a reasonable price. Palladium has been used in the selective hydrogenation of α,β-unsaturated aldehydes; allylic acetoxilation, amination and oxidation; glucose and glycerol oxidation; and Heck coupling [4]. In electrocatalysis, the successful use of Pd has been documented [5-10].

Hydrogenation of organic compounds is a very important reaction from the synthetic point of view. Several functional groups are efficiently hydrogenated, often

---

This dissertation follows the style of the Journal of Electroanalytical Chemistry.

with chemo-, regio-, and stereoselectivity. In the liquid phase, three fundamental hydrogenation methods are employed: gas-phase catalytic hydrogenation (CH), direct electroreduction and protonation (EP), and electrocatalytic hydrogenation (ECH) [6].

Electrocatalytic hydrogenation bears some advantages over the other two methods. Specifically, it provides gentle reaction conditions (ambient pressure and room temperature) and enhanced selectivity by careful electrode potential control. The method employs electrochemical sources of hydrogen (*in situ* generation of hydrogen) and avoids the hazards of high pressures of $H_{2(g)}$. Most of the electrocatalytic hydrogenation reactions follow the Langmuir-Hinshelwood mechanism, which leads to lower energy consumption since hydrogen gas formation occurs at more negative potentials [4,6,11-15].

In the Langmuir-Hinshelwood mechanism, chemisorbed hydrogen is formed by either the reduction of water or hydronium ions at the electrode surface (M) following the Volmer reaction:

$$H_2O(H_3O)^+ + e^- + M \rightleftharpoons M\text{-}H + OH^-(H_2O) \quad (1)$$

The chemisorbed hydrogen reacts with unsaturated organic molecules and hydrogenation takes place through Eqs. 2 to 5:

$$M + (C{=}C) \rightleftharpoons M(C{=}C) \quad (2)$$

$$M(C{=}C) + M\text{-}H \rightleftharpoons M(C\text{-}CH) \quad (3)$$

$$M(C\text{-}CH) + M\text{-}H \rightleftharpoons M(CH\text{-}CH) \quad (4)$$

$$M(CH\text{-}CH) \rightleftharpoons M + (CH\text{-}CH) \quad (5)$$

$$M(CH\text{-}CH) + 2MH \longrightarrow 2\,CH_2 + 3M \quad (6)$$

A sufficiently weak C-C bond leads to hydrogenolysis via Eq. 6.

The electrocatalytic hydrogenation of aromatic compounds is valued for its potential commercial and fundamental role in providing new, attractive synthesis routes

of totally or partially hydrogenated derivatives [14]. The choice of electrocatalytic methods is based in the following advantages: (i) the control of potential provides comparatively mild reaction conditions and may lead to better catalytic selectivity; (ii) there are experimental parameters unique only to the electrode-electrolyte interface which may be manipulated to dictate a certain reaction pathway; (iii) the presence of solvent and/or supporting electrolyte may protect the electrode surface such that extensive decomposition of the starting material, typical of pure/supported metal surfaces at elevated temperatures, would be minimized; (iv) catalyst poisons due to reagent decomposition tend to form less readily under electrochemical conditions at ambient temperatures; (v) the chemical behavior of surface intermediates formed in aqueous solutions can be closely modeled after analogous well-characterized homogeneous compounds; (vi) for hydrogenation reactions, the aqueous solvent functions as a convenient *in situ* source of hydrogen; and vii) because electrocatalysis employs two electrodes, application of the concept of "paired electrosynthesis" becomes possible [15].

Background

Studies on the orientation of chemisorbed molecules and its influence in electrochemical oxidation or reduction reactions were first attempted by indirect measurements using thin-layer electrochemistry (TLE) by Hubbard and coworkers [16,17]. Central to the molecular orientation studies was the measurement of the surface coverage or packing density (Γ, mol/cm^2) of the intact chemisorbed molecules [18,19]. Dihydroxy substituted benzene compounds were popular subject molecules because of their well-established electrochemical reactions [20-29].

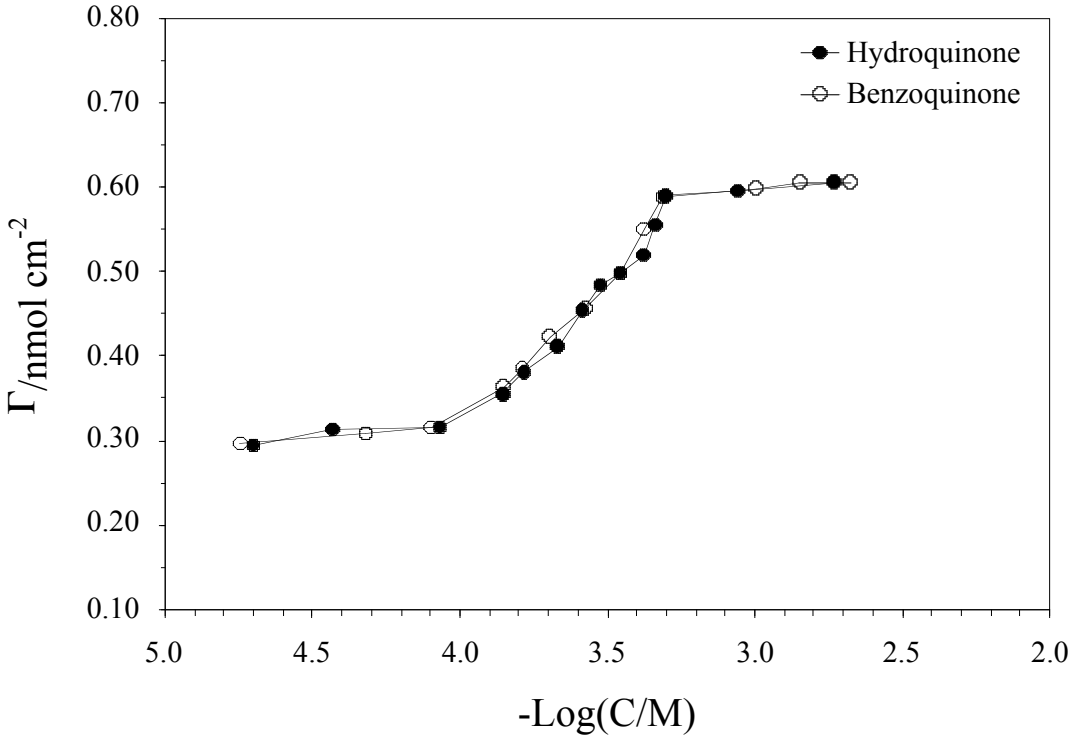

Fig. 1. Chemisorption isotherms, Γ vs. –log(C/*M*) plots, from H_2Q and BQ solutions at smooth polycrystalline Pt electrodes [21].

The chemisorption of several organic molecules on Pt electrodes has been demonstrated to be a nonrandom, irreversible process. Fig. 1 shows the chemisorption isotherm of hydroquinone and benzoquinone on polycrystalline Pt electrodes. The plateaus represented specific molecular adsorption modes of H_2Q on the electrode surface. The correlation of these plateaus to the adsorbed-molecular orientations depends upon comparison of the measured (using covalent and van der Waals radii [30]) and calculated molecular cross-sections ($\sigma, Å^2$/molecule). Fig. 2 illustrates the method to calculate the molecular cross-sections for flat and edge orientations of chemisorbed H_2Q. The measured molecular cross-sections were obtained from the packing density values using Eq. 7,

$$\sigma = 10^{16}/(N_A\Gamma) \tag{7}$$

where N_A represents Avogadro's constant and Γ is obtained from Fig. 1. The lower plateau (σ_{exp} = 52.7 $Å^2$) was assigned to a flat-oriented (η^6) adsorbate (σ_{calc} = 53.8 $Å^2$); whereas, the higher plateau (σ_{exp} = 27.9 $Å^2$) was assigned to an edwise-oriented (η^2) adsorbate (σ_{calc} = 28.6 $Å^2$). These orientational assignments have been verified using independent techniques such as infrared reflection-adsorption spectroscopy (IRAS) [31] and radiochemistry [32].

The effects of the adsorbed-molecule orientation on the electrochemical oxidation and reduction of aromatic compounds were first studied on Pt electrodes [15,33-36]. The initial work involved a direct measurement of the number of electrons transferred during the oxidation (n_{ox}, Eq. 8) or reduction (n_H, Eq. 9).

$$\text{Organics}_{(ads)} \longrightarrow \text{Oxidation products} + n_{ox}H^+ + n_{ox}e^- \tag{8}$$

$$\text{Organics}_{(ads)} + n_HH^+ + n_He^- \longrightarrow \text{Hydrogenation products} \tag{9}$$

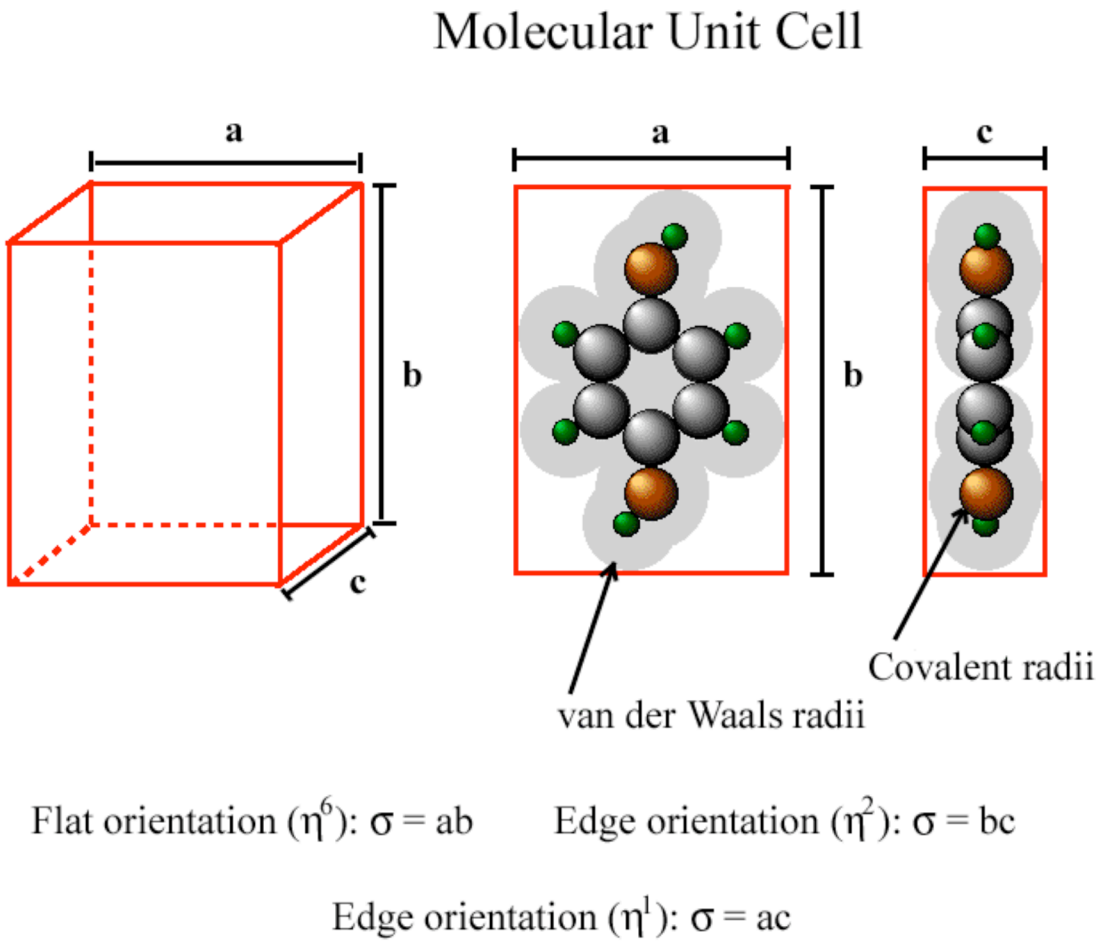

Fig. 2. Molecular unit cells employed in the calculations of the adsorbate molecule cross-sections [16]. Grey balls represent carbon atoms, orange balls represent oxygen atoms, and green balls represent hydrogen atoms.

The extraction of n_{ox} and n_H values from the Γ and faradaic charge is described in the experimental section.

Figs. 3 and 4 summarize the chemisorption and oxidation/reduction products of H_2Q intermediates on polycrystalline Pt electrodes. Most of the proposed products were inferred from the n_{ox} and n_H values. The use of gas chromatography (GC) with derivatization by silylation was employed to confirm oxidation products such as maleic acid [37]. Long optical path length thin-layer spectroelectrochemistry was employed to identify 1,4-cyclohexandiol as the product of the electrocatalytic reduction of H_2Q [38]. The use of the long optical path length and the large ratio of electrode area-to-solution volume were meaningful aspects in the detection of these species since organic monolayers account for just fractions of nmol/cm^2.

Orientational studies have also been performed also on well-defined single crystals. Hubbard *et al.* studied the adsorbate orientation of several organic molecules on Pt(111) using a combination of electrochemistry (EC), Auger electron spectroscopy (AES), low energy electron diffraction (LEED), and electron energy loss spectroscopy (EELS) [18,39-44]. Chemisorption isotherms were affected profoundly by electrode cycling and by the crystallinity of the electrode surface. It has been claimed that only flat-oriented H_2Q species are observed on Pt(111) surfaces.

Itaya and coworkers has also studied H_2Q chemisorption from dilute solutions (HF supporting electrolyte) and from vacuum [45]. By using scanning tunneling microscopy (STM) in solution, they reported that H_2Q formed an ordered structure on Pt(111) with a strong attractive interaction between two adjacent hydroxyl groups in the neighboring HQ molecules. After the sample was transfer into vacuum, LEED measurements were performed, which showed that the (2.56×2.56)R16° incommensurate structure of the H_2Q adlayer was formed in solution. The H_2Q adlayer on Pt(111) was also formed by vapor deposition and the identical (2.56×2.56)R16° adlayer structure was found by LEED and STM in vacuum. Identical results were obtained with Rh(111) [46].

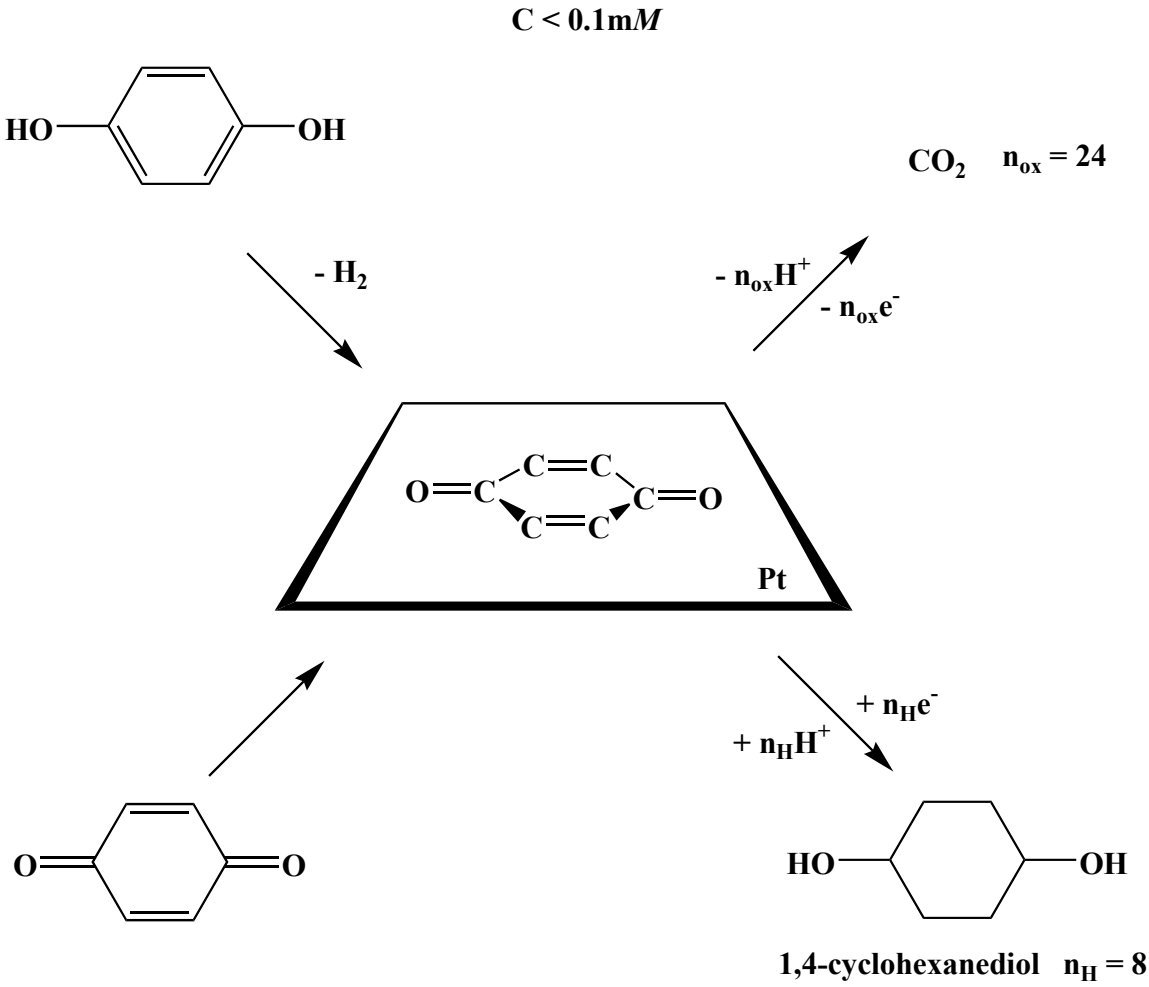

Fig. 3. Schematics of the electroreactivity of H_2Q and Q chemisorbed from low concentration solutions on Pt(pc) electrodes.

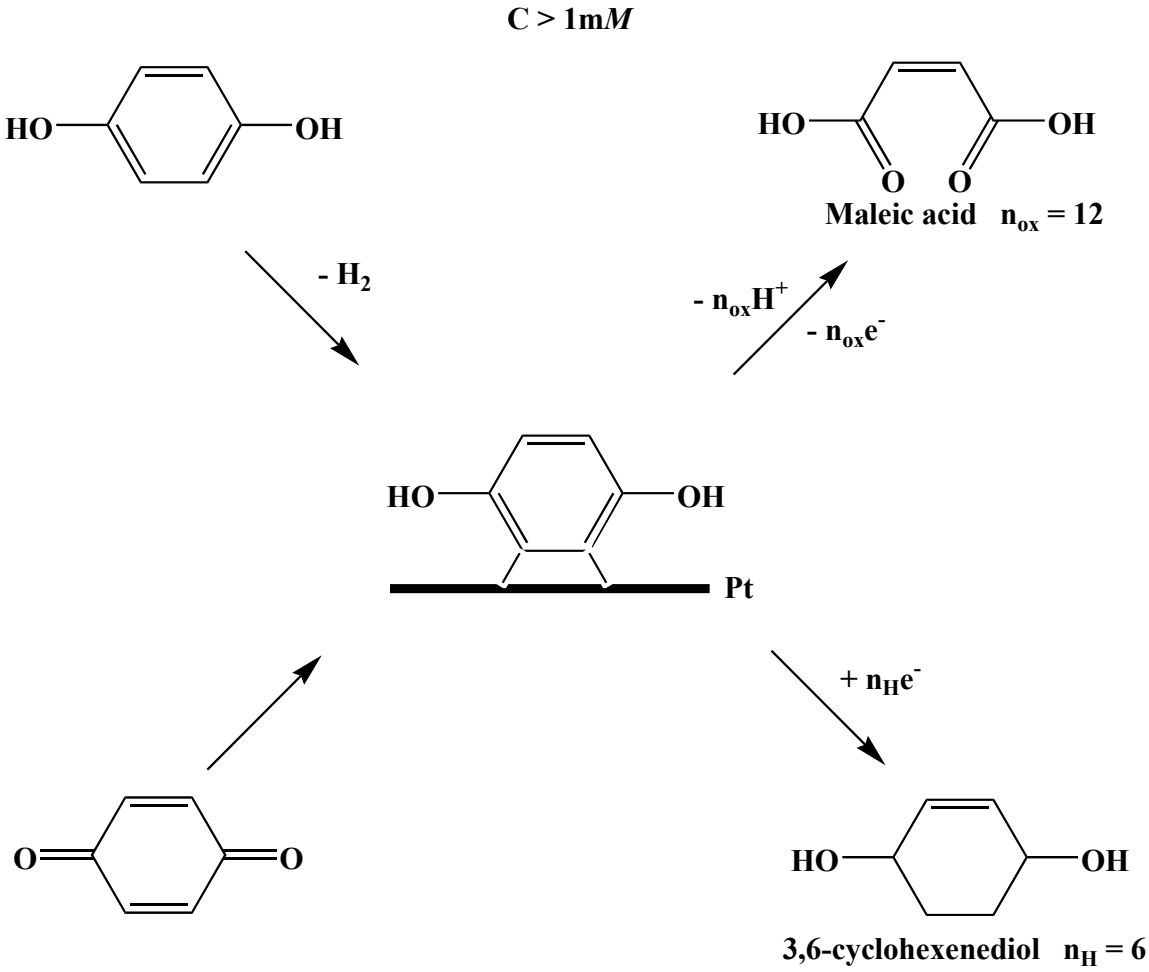

Fig. 4. Schematics of the electroreactivity of H_2Q and Q chemisorbed from high concentration solutions on Pt(pc) electrodes.

The chemisorption and electrochemical activity of several aromatic compounds on polycrystalline and single crystal Pd electrodes have been studied [2,47-51]. Chemisorption isotherms for H_2Q and Q on Pd(pc) surfaces have been recently reported [52]; behavior very similar to that on Pt(pc) was observed. For example, two plateaus were observed, although the lower plateau was not as well-defined and the lower-to-upper transition was not as sharp as in the Pt case. The higher plateau (σ_{exp} = 27.5 $Å^2$) can be assigned to an edge-wise oriented adsorbate (σ_{calc} = 28.6 $Å^2$); whereas, the higher molecular cross-section value associated with the lower plateau (σ_{exp} = 46.5 $Å^2$) was taken to indicate that the adsorbate is a predominant flat species on the Pd surface. HREELS indicated that quinonoid rather than diphenolic species were adsorbed on Pd(111) substrates because no OH vibrational modes were observed in the 3600 cm^{-1} region. The presence of a weak in-plane vibrational stretch suggested that slightly tilted parallel oriented species were present [49]. The tilt was also indicated by STM images in which one oxygen was higher (brighter) that the other one [53].

Objectives

While most of the studies are related with Pd on technical applications, fundamental studies such as surface-reaction mechanisms are scarce. This project aims to the study of the chemisorption and electrochemical hydrogenation of model aromatic compounds, benzene and p-dihydroxybenzene, at polycrystalline and well-defined single crystal surfaces of Pd by a combination of surface-sensitive and electrochemical techniques.

EXPERIMENTAL

Thin-layer electrochemistry (TLE)

In thin-layer electrochemistry, the processes are confined to an analyte solution of thickness 2-25 μm, which is smaller than the Nernst diffusion layer. In this configuration, TLE provides advantages over conventional electrochemical methods: (i) at moderate scan rates the electrochemical reactions do not suffer diffusional mass transport from the bulk solution; (ii) minimal surface contamination from solution impurities due to the exceeding small volumes (*c.a.* few μL); and (iii) enhanced sensitivity to surface processes due to the high surface area-to-volume ratio. This last feature makes TLE an important tool in the study of chemisorbed organic monolayers since the amount of species at the adlayer is usually in the order of a fraction of nmol/cm^2 [16,54,55]. TLE was employed in this research to obtain information on the Γ, molecular orientation, and surface reactivity of the subject compounds on Pd(pc) surfaces. Selected results from TLE experiments were investigated in greater detail using a combination of electrochemistry ultra-high vacuum and mass spectrometry (EC-UHV-MS).

Fig. 5 shows the TLE cell used in the present work. A cylindrical Pd(pc) electrode is located inside of a precision bore glass capillary whose dimensions are just slightly larger that those of the metal. A thin layer of electrolytic solution fills the cell via two pin holes at the bottom of the glass container. Spent solution is removed from the cell when pressurized high purity N_2 gas (BOTCO, Bryan, TX) is blown through it. When gas flow is arrested, the TLE cell is replenished with a fresh aliquot of solution.

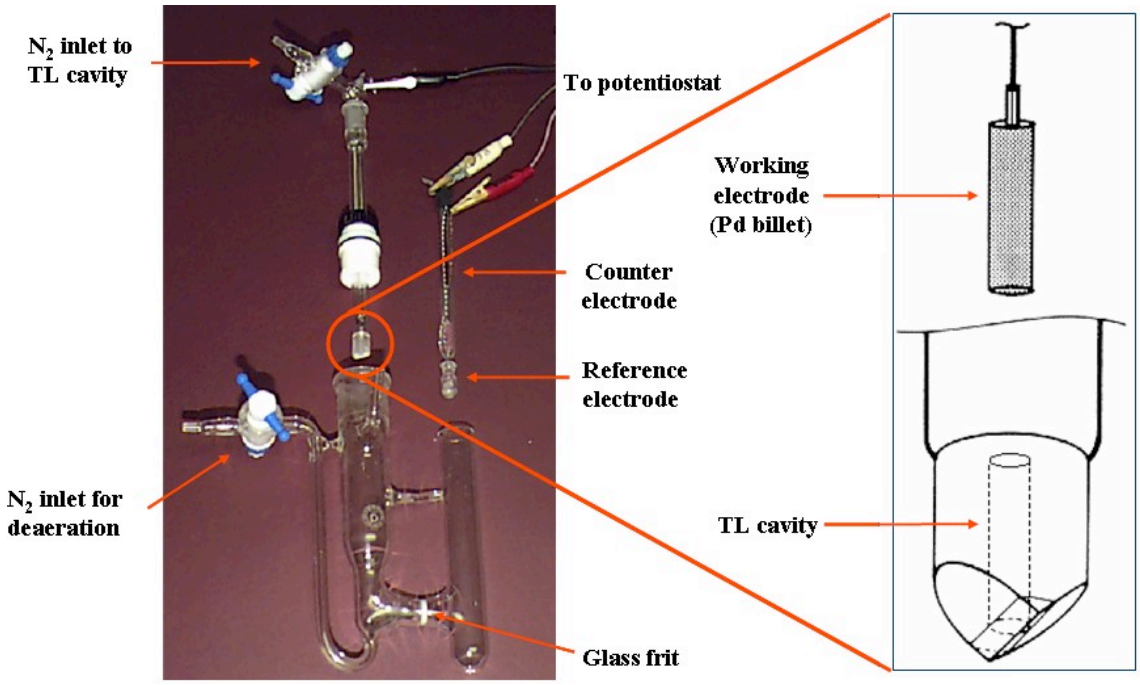

a b

Fig. 5. (a) Thin-layer electrode and H-cell set-up. (b) Magnified thin-layer cavity and Pd billet.

The Pd(pc) TLE electrode was fabricated from a Pd rod (99.99 % purity, Wilkinson Co., Westlake Village, CA). The surface was first metallographically polished by successive finer grades of diamond paste compounds (Beuhler Ltd., Evanston, IL) to a mirror finish. The electrode was then thermally annealed to redness in a hydrogen-oxygen flame and quenched in N_2-saturated Milli-Q® Plus water (Houston TX). Electrodes prepared by this procedure have less than 5 % surface roughness [56]; hence, the surface area (1.272 cm^2) of the working electrode was determined from the geometrical area adding an area roughness factor of 1.05. The volume of the thin-layer cavity [(3.68 ± 0.01) μL] was measured coulometrically from Faraday's law by using the Fe^{3+}/Fe^{2+} redox couple. The working solution consisted of 10.0 m*M* Fe^{2+} in 1 *M* H_2SO_4 [55].

TLE experiments were limited to linear sweep voltammetry (LSV) and potential-step coulometry (PSC) to characterize the organic adlayer. These methods are well known and are not going to be elaborated here [57].

Surface coverage measurements

If the clean thin-layer electrode is filled only once, a single aliquot of electrolyte containing a precise molar amount of solute enters the thin-layer cavity. When this solute is surface active and its initial concentration is moderately low ($C° \leq 10^{-4}$ *M*), a major portion of the solute is adsorbed, producing a significant change in solute concentration, C° [16]

$$VC = VC^{o} - A\Gamma \tag{10}$$

where V is the volume of the confined solution in the thin-layer cavity, and A represents the electrode surface area.

The electrolytic charge, Q, required for electrolysis of unadsorbed solute in the thin-layer cavity, is related to the interfacial concentration of adsorbed solute, Γ, by the Faraday's law, Eq. 11:

$$(Q_l - Q_b) = nFVC = nFVC^o - nFA\Gamma \quad (11)$$

where Q_l denotes the electrolytic charge observed for a single filling of the thin-layer cavity, Q_b is the background electrolytic charge consumed in an otherwise identical experiment in which the dissolved reactant has been rinsed from the cell, and n is the number of faradays of charge F consumed per mole.

On the other hand, if the thin-layer cavity is rinsed with an excess of the reactant solution, then the reactant concentration equals that in the bulk solution, C°, so that the electrolytic charge, Q, is given by Eq. 12. Combining Eqs. 11 and 12 yields

$$Q - Q_b = nFVC^o \quad (12)$$

an expression for interfacial concentration, Γ, in terms of measured charges:

$$Q - Q_l = nFA\Gamma \quad (13)$$

Measurement of n_{ox} and n_H

Eqs. 8 and 9 show general reactions for the electrochemical oxidation and hydrogenation of organic adlayers. n_{ox} (n_H) represents the number of electrons transferred during the oxidation (hydrogenation) per chemisorbed species. The greater the value, the more oxidized (reduced) the species are.

Determination of n_{ox} (n_H) is based upon precise measurements of Γ and Q_{ox} (Q_H), the electrolytic charge needed to oxidize (reduce) and desorbs this material [34]. Q_{ox} (Q_H) is determined as follows: (i) the clean thin-layer electrode was exposed for 180 s to a surfactant solution for which Γ had been measured; (ii) excess dissolved material was then removed by rinsing with a pure supporting electrolyte; and (iii) the electrolytic charge Q'_{ox} (Q'_H), for oxidation (hydrogenation) was determined at a potential just below that for oxygen (hydrogen) evolution. The background charge $Q_{ox,b}$ ($Q_{H,b}$) was determined by an identical procedure except for omission of the adsorbed material; Q_{ox}

(Q_H) and $Q_{ox,b}$ ($Q_{H,b}$) were evaluated where the charge-time curves became parallel, indicating complete oxidation (hydrogenation) of the organic material. Values of n_{ox} (n_H), were extracted from the data by using Faraday's law in the form of Eqs. 14 and 15 respectively:

$$Q_{ox} = (Q'_{ox} - Q'_{ox,b}) = n_{ox}FA\Gamma \quad (14)$$

$$Q_H = (Q'_H - Q'_{H,b}) = n_H FA\Gamma \quad (15)$$

where F is Faraday's constant and A the electrode surface area.

Ultra-high vacuum electrochemistry (UHV-EC)

Since the TLE work employs polycrystalline electrodes, the information obtained represents the ensemble behavior of various crystallographic faces. More detailed investigations were conduced using surface-sensitive analytical methods at well-defined single crystal electrodes. A combination of Auger electron spectroscopy (AES), low-energy electron diffraction (LEED), and high-resolution electron energy loss spectroscopy (HREELS) were employed in this research. The bases of these techniques will be described below [58].

The main difficulty in the surface characterization of single-crystal surfaces lies in the exceedingly low population of surface atoms (10^{15} atoms cm^{-2}) relative to that of bulk species (10^{23} atoms cm^{-3}). Experiments intended to examine the physical and chemical properties of surfaces must employ methods that interact only with the inter-facial layers. Therefore, standard structural tools such as X-ray diffraction would thus not be readily applicable to single-crystal surfaces since X-rays penetrate into the bulk and extract information characteristic of the bulk rather than the surface.

The majority of inter-facial characterization techniques take advantage of the unique surface sensitivity of low-energy electrons. This surface influence arises because the mean free path of an electron through a solid is dependent upon its kinetic energy. As shown in the so-called "universal curve" reproduced in Fig. 6, the electron mean free

path falls to a minimum (4 to 20 Å) when the kinetic energy is between 10 and 500 eV. This signifies that all experimental techniques based upon the low-energy electron incidence onto and/or emergence from surfaces will bear information diagnostic of the topmost surface layers.

A solid surface subjected to a beam of electrons of incident or primary energy E_p gives rise to the appearance of backscattered (primary) and emitted (secondary) electrons; the energy distribution, a plot of the number of electrons N(E) as a function of energy E, of these electrons is shown in Fig. 7. This spectrum can be divided into four regions according to the origin of the scattered electrons: (i) true *secondary* electrons, created as a result of multiple inelastic interactions between the incident and bound electrons; these electrons give rise to the prominent broad band at the lower end of the spectrum. (ii) Auger electrons emitted and primary electrons inelastically scattered due to interactions with electronic states in the solid; the small peaks in the medium-energy range of the spectrum are attributed to these electrons. (iii) Primary electrons inelastically scattered upon interactions with the vibrational states of the surface; peaks resulting from these electrons reside close to the inelastic peak since their energy losses are comparatively minute. (iv) Primary electrons scattered elastically; these electrons, which comprise only a few percent of the total incident electrons, give rise to the elastic peak at E_p. Regions (ii) to (iv) of the energy distribution spectrum have been exploited in modern surface analysis. The elastic peak, for example, is used in diffraction experiments; the other peaks provide information on electronic and vibrational structures.

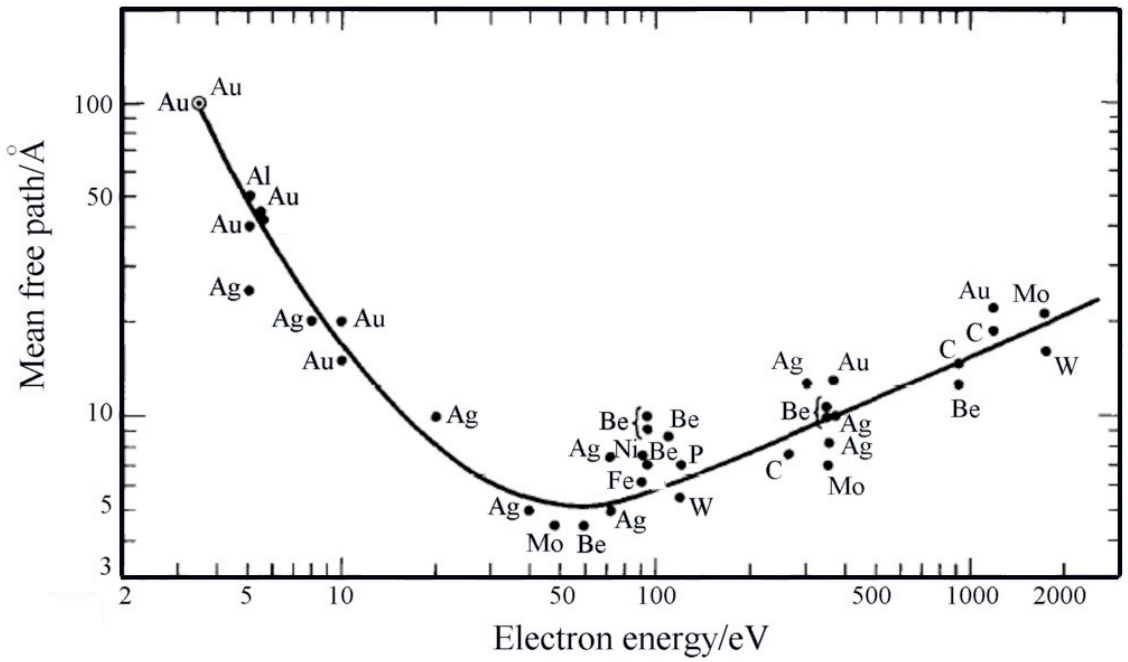

Fig. 6. Electron mean free path as a function of electron kinetic energy.

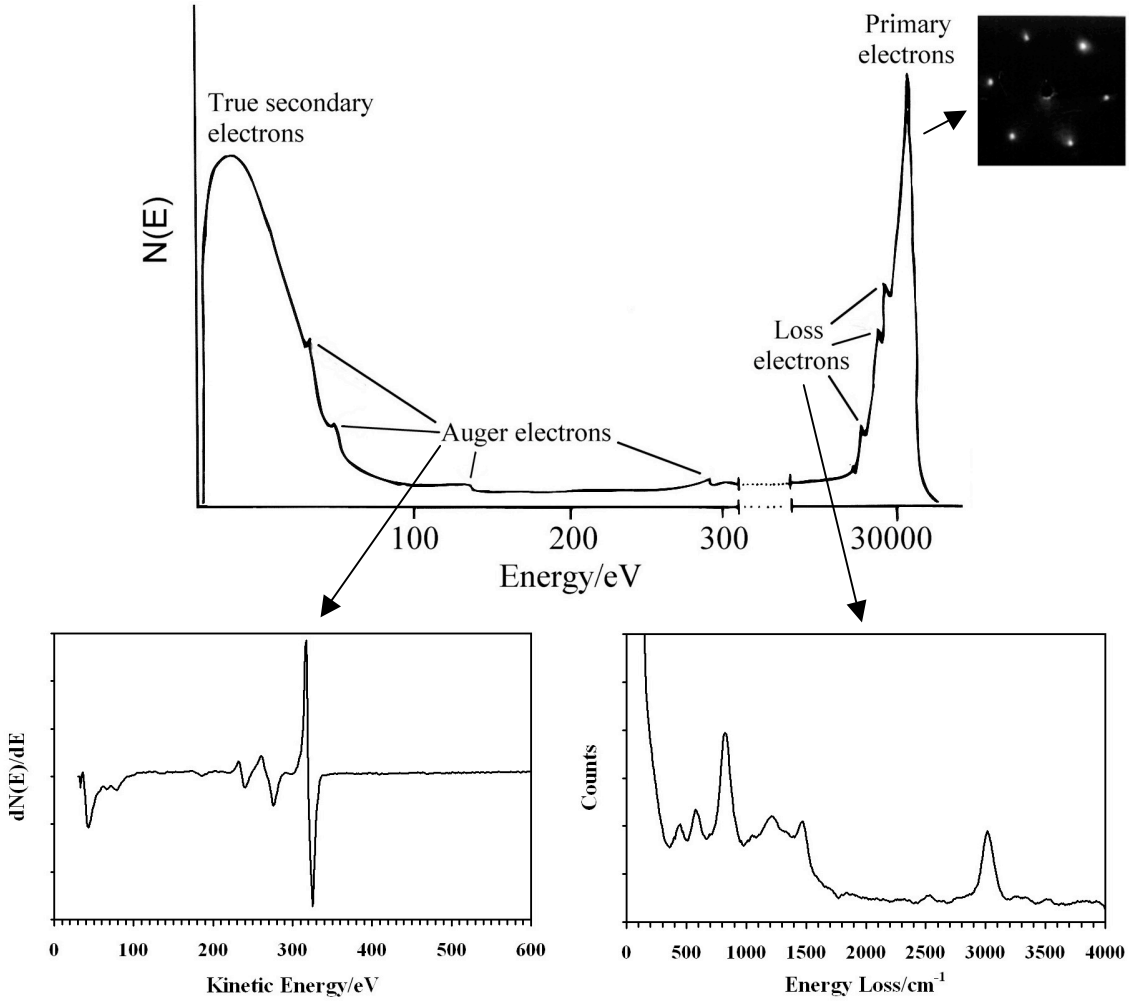

Fig. 7. Energy distribution of backscattered electrons.

Low-energy electron diffraction (LEED)

In this method, the surface is irradiated with a monoenergetic beam of electrons and the elastically backscattered electrons are collected onto a phosphor screen. The virtue of LEED as a surface structural technique is a result of the low kinetic energies used (50 to 500 eV) since (i) the electron mean free path is at a minimum, which affords LEED its surface sensitivity; (ii) the de Broglie wavelengths, $\lambda_e \approx (150/E_e)^{-}$ (where E_e is in eV and λ_e is in Å) correspond to crystal lattice dimensions which render the low-energy electrons suitable for diffraction studies; and (iii) electron backscattering is strong which minimizes incident electron fluxes at, and subsequent scattering from, non-surface layers. In LEED, therefore, the presence (or absence) of diffraction patterns on the fluorescent screen is a consequence of the order (or disorder) of the atomic arrangements near the surface.

The locations of the diffracted beams define the reciprocal lattice of the real surface. The real-space surface structure itself can be reconstructed from the real-space unit cell vectors generated from the reciprocal lattice vectors according to the following relationships:

$$\vec{a}^{*} = \frac{\vec{b} \times \vec{z}}{\vec{a} \cdot \vec{b} \times \vec{z}} \tag{16}$$

$$\vec{b}^{*} = \frac{\vec{z} \times \vec{a}}{\vec{a} \cdot \vec{b} \times \vec{z}} \tag{17}$$

where $\vec{a}$ and $\vec{b}$ are the real-space lattice vectors, $\vec{a}^{*}$ and $\vec{b}^{*}$ are the reciprocal unit mesh vectors, and $\vec{z}$ is the surface normal. The coherence width of electron beam sources in LEED is typically 100 Å. That is, sharp diffraction features appear only if well-ordered domains are at least $(100\ \text{Å})^2$ in size; diffraction from smaller domains leads to beam broadening.

The analysis of LEED data based solely upon the geometry of the diffraction spots provides information on the periodicity of the electron scatterers on the surface. In

some favorable instances, other information such as adsorbate coverages or point group symmetries can also be inferred. However, the actual location of the atoms within the surface lattice cannot be determined without an analysis of the intensities of the diffracted beams.

There are two schemes for the notation of interfacial adlattice structures. The matrix notation, which is applicable to any system, is based upon the relationship between the real-space lattice vectors of the *adsorbate* mesh and the *substrate* (clean-surface) mesh. For example, if the adsorbate unit cell vectors $\vec{a}'$ and $\vec{b}'$ are related to those of the substrate mesh according to

$$\vec{a}' = m_{11}\vec{a} + m_{12}\vec{b} \tag{18}$$

$$\vec{b}' = m_{21}\vec{a} + m_{22}\vec{b} \tag{19}$$

Then the matrix M defined by the coefficients $m_{ij,}$

$$M = \begin{pmatrix} m_{11} & m_{12} \\ m_{21} & m_{22} \end{pmatrix} \tag{20}$$

denotes the real-space surface structure. The other method, known as the Wood notation, is more widely used, but is applicable only if the angle between $\vec{a}'$ and $\vec{b}'$ is the same as that between $\vec{a}$ and $\vec{b}$. The surface structure is labeled using the general form (nxm)Rϕ°

or c(nxm)Rϕ°, where c designates a centered unit cell, Rϕ° the angle of rotation of the adsorbate unit cell relative to the substrate unit mesh, and n and m are scale factors relating the adsorbate and substrate unit cell vectors:

$$\left|\vec{a}'\right| = n\left|\vec{a}\right| \tag{21}$$

$$\left|\vec{b}'\right| = m\left|\vec{b}\right| \tag{22}$$

A schematic diagram of a "rear view" type LEED optics similar to that used in the present work (PE 15-120, Perkin-Elmer, Eden Praire, MN) is shown in Fig. 8. It consists of a phosphor-coated hemispherical screen, at the center of which is a normal-incidence, electrostatically focused electron gun. In front are four concentric grids; the first and fourth grids are held at ground potential, while the inner two are maintained at a voltage just below that of the electron gun, in order to reject *inelastically* backscattered electrons. The elastically diffracted electrons which pass through the suppressor grids are accelerated onto the fluorescent screen by a 5 kV potential applied to the screen.

The electrode-surface unit mesh was initially established by visual inspection of the diffraction spots through the view port. The patterns were compared with those calculated for model structures [59]. A photograph of the LEED pattern for the Pd(100) electrode surface used in the present work is shown in Fig. 8b. The sharp and distinct (1x1) pattern of square symmetry is characteristic of a clean and well-ordered face center cubic crystal with a (100) low index plane.

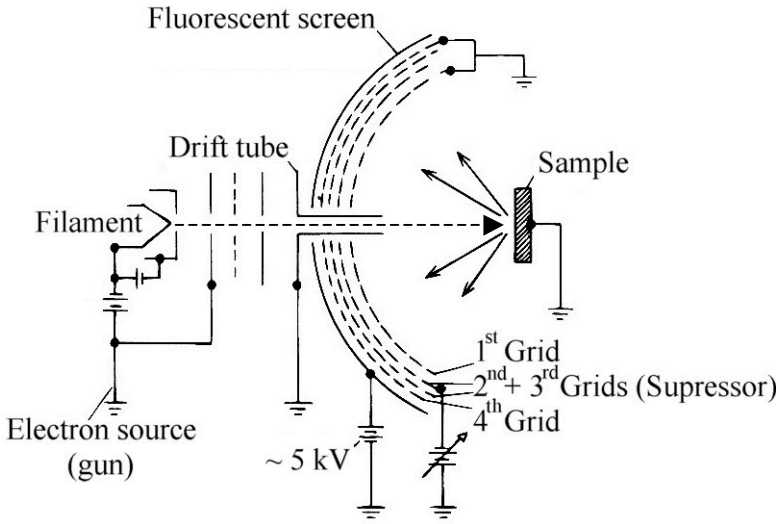

a

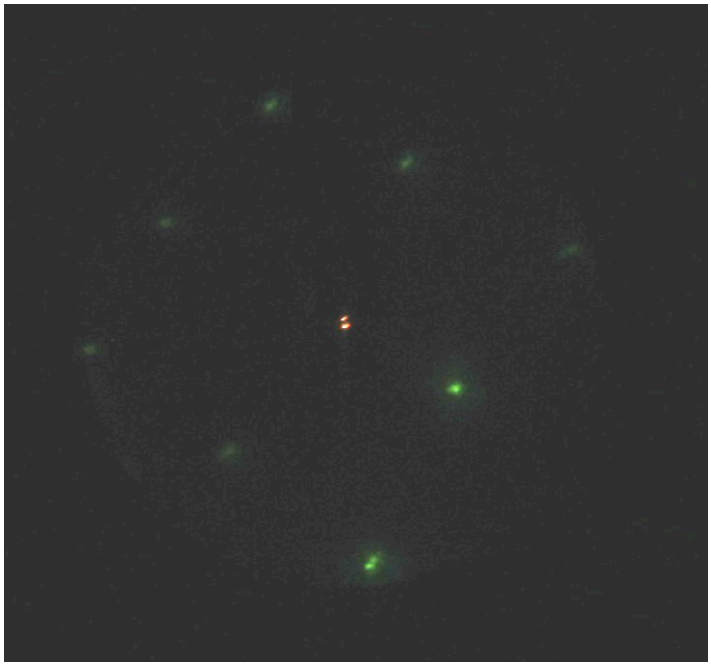

b

Fig. 8. (a) Schematic diagram of LEED optics. (b) Picture of a LEED pattern for a freshly-prepared, well-ordered Pd(100) surface. Experimental conditions: Beam energy, 59.7 eV; screen voltage, 3 kV.

High-resolution electron energy loss spectroscopy (HREELS)

Almost all of the incident electrons impinged at a solid surface undergo inelastic events which cause them to be backscattered at energies lower than the primary energy E_p. If E_l is the energy lost to the surface, peaks would appear in the energy distribution spectrum (Fig. 7) at energies $\Delta E = E_p - E_l$. Such peaks, commonly referred to as electron energy loss peaks, are of several types according to the origin of the energy loss. These types include core-level ionization, valence-level excitations, plasmon losses, and vibrational excitations. For the latter, the energy losses are small since $E_{vib} < 4000$ cm^{-1} < 0.5 eV. Hence, the loss peaks due to vibrational interactions at $\Delta E = E_{vib}$, lie close to the elastic peak and can be observed only if electron energy loss measurements are done at high resolution.

At solid surfaces, there are two mechanisms that give rise to vibrational HREELS spectra: dipole scattering and impact scattering. In dipole scattering, the incident electron interacts with the oscillating electric dipole moment induced by the vibration of species at the surface. Such interactions occur at long range and can be described either classically or quantum mechanically. Two important selection rules apply for surface dipole scattering: (i) only vibrations whose dynamic dipole moments perpendicular to the surface are non-zero contribute to HREELS spectra. (ii) The intensity distribution with respect to scattering angle is sharply peaked in the specular direction; that is, loss peaks due to dipole scattering disappear when the backscattered electrons are collected at an angle different from that of the specularly reflected beam. The first selection rule is the same as that for surface infrared reflection-absorption spectroscopy (IRAS).

The mechanism for impact scattering at solids, which can only be treated quantum mechanically, involves exceedingly short-range interactions between the incident electron and the oscillator at the surface. The surface dipole selection rules do not apply to impact scattering. Theoretical considerations have predicted and experimental studies have confirmed the following properties of this type of scattering mechanism: (i) Impact scattering vanishes in the specular direction; that is, loss peaks due to impact scattering can be observed only if the scattered electrons are detected at

angles removed from the specular direction. (ii) Impact scattering is more likely to prevail at higher energies. (iii) Strong dipole scatters are weak impact scatterers; conversely, weak dipole scatterers are strong impact scatterers.

It is clear that the combination of specular and off-specular HREELS could provide a means for the complete identification of the normal modes of an adsorbed molecular species; point and space group theoretical considerations would, of course, be required. HREELS is an extremely sensitive technique. The limit of detection for strong dipole scatterers such as CO can be as low as 0.0001 monolayer; for weak scatterers such as hydrogen, the limit is 0.01 monolayer. In comparison, IRAS for chemisorbed CO, a strong infrared absorber, is restricted to coverages above 0.1 monolayer.

Fig. 9 shows a schematic diagram of the HREELS spectrometer used in this research (LK 2000 HREELS spectrometer, L.K. Technologies Inc., Bloomington, IN). The energy of incident electrons can be varied from 1 to 10 eV. To afford high resolution, energy monochromation and analysis are done with a 127° cylindrical deflection analyzers (CDA) in combination with retarding field optics. Due to extremely low signals (10^{10} Å), continuous dynode electron multiplier detectors have been recommended. The analyzer in this LK 2000 system cannot be rotated; therefore, all HREELS spectra are recorded at specular direction (62° with respect to the surface normal).

Assignments of HREELS loss peaks were performed by comparing the vibrational bands in HREELS spectra with characteristics IR group frequencies of molecules in the liquid, solid, and gaseous states [60]. Since the vibrational modes of a molecule shifts after chemisorption due to its chemical bonding to the surface and lateral interactions from neighboring molecules, it is important to consider the interaction of the molecules with metal surfaces as in organometallic complexes [61].

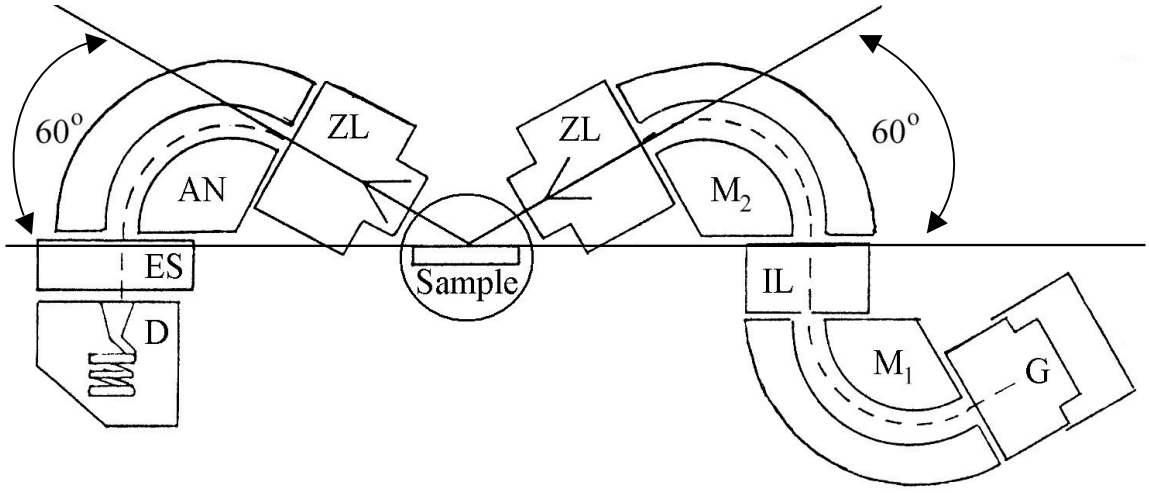

Fig. 9. Schematic diagram of a HREEL instrument.

Normalization of the HREEL spectra was performed by matching the spectral background (featureless) region before and after chemisorption of the aromatics on the metal surface [62]. The chemisorbed adlayer usually introduces a certain degree of roughness to the surface; thus, more electrons are inelastically scattered. This causes the elastic peak intensity to decrease dramatically. For the normalization procedure, a clean Pd spectrum is obtained and its elastic peak count rate is set to 2.5×10^5 cps, the maximum counts obtained on a clean spectrum. Each spectrum for adsorbed organic species is then multiplied by a factor to normalize the background of a spectrum (2100~2700 cm^{-1}) to that of the clean Pd spectrum. This method assumes that the background region of a spectrum is mainly due to impact scattering. In other words, the intensity of the background spectrum has a direct relationship with the incident electron beam energy. This normalization method works well with the chemisorption of H_2Q on Pd surfaces.

Fig. 10 shows the HREEL spectra of a freshly cleaned, well-ordered Pd(100) single crystal. Two vibrational bands are observed at 354 cm^{-1} and 1923 cm^{-1}; they have been identified as the ν(Pd-C) and ν(CO) stretching modes, respectively, emanating from background CO chemisorbed at the Pd surface. Even though the cleanliness of the substrate has been checked by AES, the detection of CO with HREELS proves that this technique is more sensitive especially with strong dipole scatters such as CO. It will be of interest to note that when the UHV-prepared Pd surface is immersed in supporting electrolyte, such as the ones used in this work, the CO peaks are not observed in a subsequent HREELS measurements.

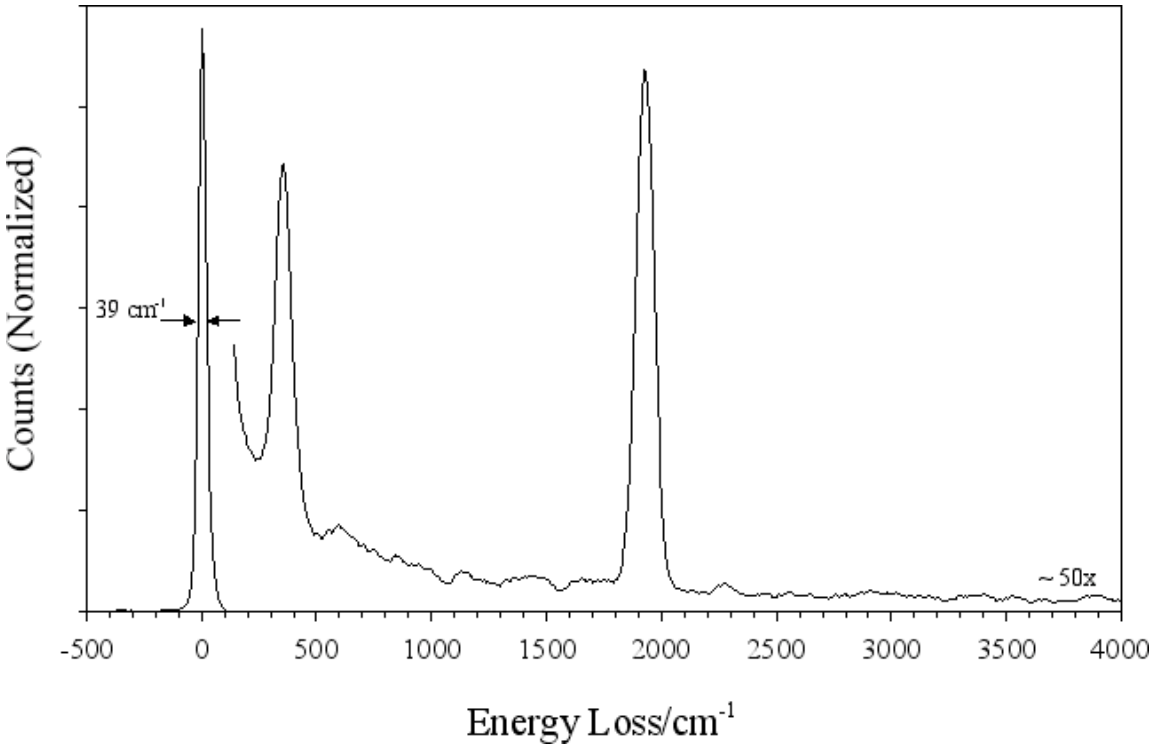

Fig. 10. HREEL spectra of a freshly-prepared, well-ordered Pd(100) surface. Experimental conditions: Incidence and detection angles = 62° from surface normal.

Auger electron spectroscopy (AES)

AES is one of the more widely used techniques for surface elemental analysis. In the Auger process, illustrated schematically in Fig. 11a, a core (K) level electron is emitted when a beam of electrons, typically with energies between 2 to 10 keV, is impinged onto the sample surface. In the decay process, an electron in an upper (L_1) level falls into the vacant core level and another electron in a different upper ($L_{2,3}$) level is ejected; the second, emitted, electron is the Auger electron and this particular process is labeled as a $KL_1L_{2,3}$ in order to specify which energy levels are involved. The kinetic energy of the Auger electron is dependent upon the binding energies of the K, L_1, and $L_{2,3}$ electrons but not upon the energy of the incident or primary electrons. The appropriate relationship is given by

$$E_{KL_1L_{2,3}} = E_K - E_{L_1} - E_{L_{2,3}} - e\varphi_{sp} \tag{23}$$

where *e* is the electronic charge and φ_{sp} the spectrometer work function. The exact application of Eq. (23) must realize that the energy difference is actually between singly ionized (one-hole) and doubly ionized (two-hole) binding energy states. Nevertheless, $E_{KL_1L_{2,3}}$, as obtained from empirical spectra, is characteristic of a given atom which affords AES its element-specificity. Since the overall Auger process involves three electrons, AES is clearly not applicable for the analysis of H and He. It should also be noted that, although the incident electrons are of high energies, AES is still a surface sensitive method because the emitted Auger electrons are generally of much lower energies and correspond to the minimum in the universal curve (Fig. 6).

An inherent difficulty in AES arises from the fact that the Auger emission peaks are actually of very low intensities superimposed on a large secondary emission background (Fig. 7). The usual approach to circumvent this problem combines electron-energy analysis with suitable modulation techniques; in this manner, spectra exclusive of the original background can be obtained.

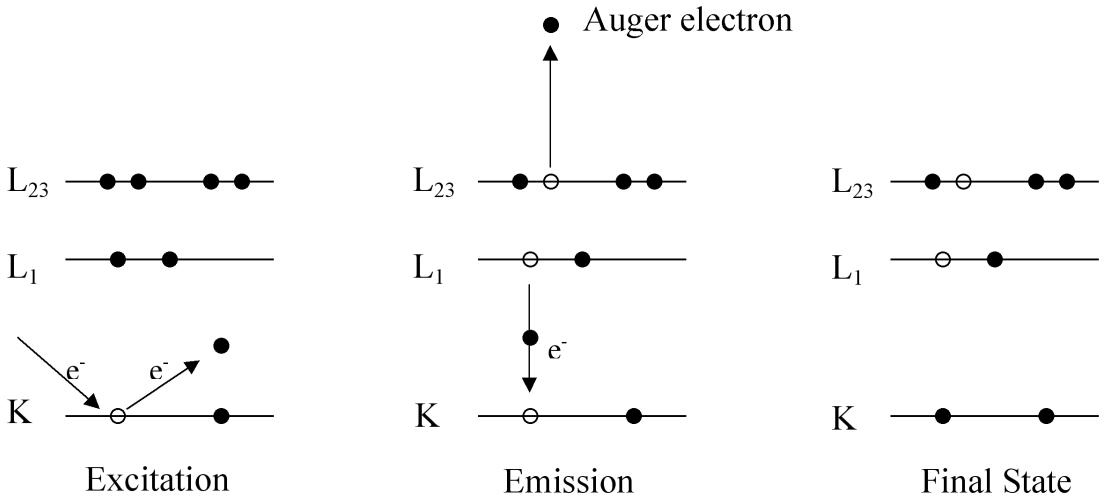

a

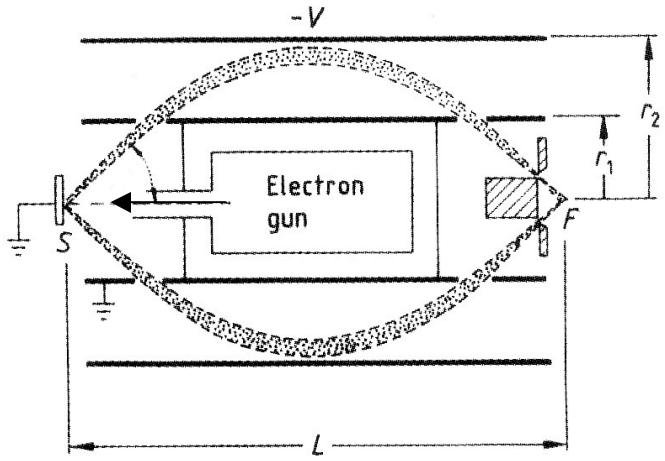

b

Fig. 11. (a) Auger emission process. (b) Schematic diagram of a cylindrical mirror analyzer (CMA).

A schematic diagram of the 10-155 cylindrical mirror analyzer (CMA, Perkin Elmer, Eden Praire, MN) (CMA) used in the present work is given in Fig. 11b. Energy analysis with a CMA is achieved by a negative ramp voltage (V) applied to the outer cylinder while the inner cylinder is held at ground. Only electrons of the appropriate energy can pass unhindered through the CMA and into the detector, which is usually a channel electron multiplier. The pass energy of the CMA is modulated and then synchronously demodulated with a lock-in amplifier. The resultant spectrum is a derivative spectrum. The resolution of a CMA is dependent upon its entrance and exit slits; improved resolution can be achieved by a double-pass CMA.

Conventionally, Auger spectra are plotted as the differentiated energy distribution dN(E)/dE in order to enhance the small Auger features observed in the undifferentiated form, depicted in Fig. 7. The peak assignment for the Auger peaks in the dN(E)/dE form is conventionally performed by using the negative minimum. Auger spectra of all elements have been documented for routine identification purposes [63]. A surface of a given composition possesses a signature Auger dN(E)/dE spectrum; this renders AES a powerful technique for qualitative surface elemental analysis.

Quantification of Auger signals was performed by obtaining the Auger current I_x through double integration of the adsorbate Auger derivative signal A corrected for the clean surface A_c

$$I_x = \frac{4}{k^2} \int_0^{E_p} \int_0^{E} (A - \phi_b A_c) dE' dE \tag{24}$$

where ϕ_b compensates for any observed adsorbate-induced attenuation of the substrate signal, and k is the modulation amplitude [64].

In quantifying the amount of each element at the adlayer, the Auger current (I_x) for the element x is calculated by integrating the energy distribution peak N(E) or by double-integrating the differentiated energy distribution feature dN(E)/dE. The Auger current is then normalized by the Auger current of the Pd substrate (I_{Pd}) obtained from

the same spectrum. The I_x/I_{Pd} ratio is independent of any changes in beam current and sample positioning from different runs.

Fig. 12 shows the Auger spectrum of a freshly clean, well-ordered Pd(100) surface. Surface cleanliness is verified by the appearance of only Pd Auger features in the spectrum.

Ultra-high vacuum electrochemical apparatus (UHV-EC)

The photograph of the all-stainless-steel UHV system employed in this research is shown in Fig. 13. The UHV system was built upon a TNB-X series 500 vacuum pump (Perkin Elmer, Eden Prairie, MN) and utilizes a three-stage pumping system to keep the base pressure at UHV levels. Two liquid-nitrogen chilled pumps reduce the pressure from atmospheric pressure to about 5×10^{-4} torr; a 56-L/s turbomolecular pump (Balzer, NH) lower the pressure further to 1×10^{-7} torr. Finally, a 300-L/s triode ionization pump and a liquid-nitrogen cooled titanium pump keep the base pressure *c.a.* 10^{-9} torr. The UHV system consists of two compartments: the electrochemistry (EC) and surface analysis (SA) chambers. An X-Y-Z-R manipulator (Huntington Laboratories, Mountain View, CA), installed on a twin-rail positioning table, allows the transfer of the crystal from the SA chamber to the EC chamber. A gate-valve (MDC Vacuum Products, Hayward, CA) allows the isolation of the surface analysis chamber when EC experiments are being performed at atmospheric pressure. The various surface analysis optics are shown in Fig. 12. To ensure the cleanliness of the system, the entire assembly was heated (back-out) to 470 K for at least two days until a base pressure of 10^{-10} torr was reached.

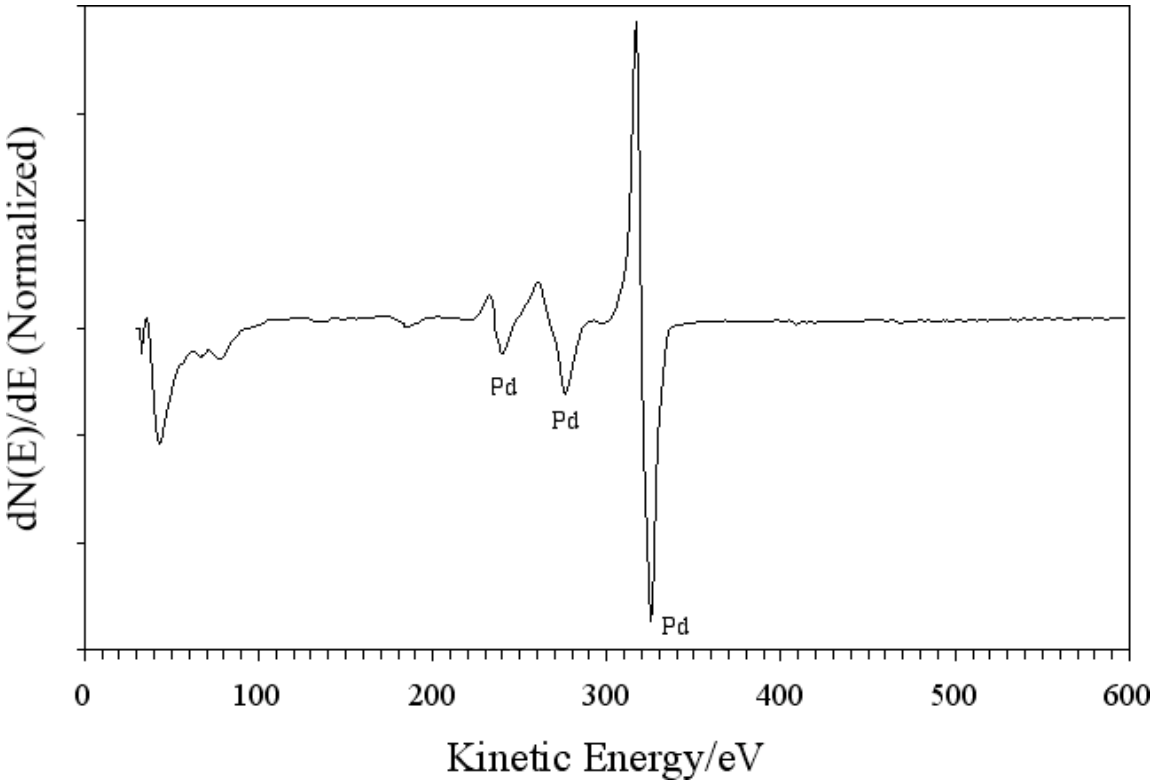

Fig. 12. Auger spectrum of a freshly cleaned, well-ordered Pd(100) surface. Experimental conditions: beam energy 2 keV; beam current, 1.6 μA.

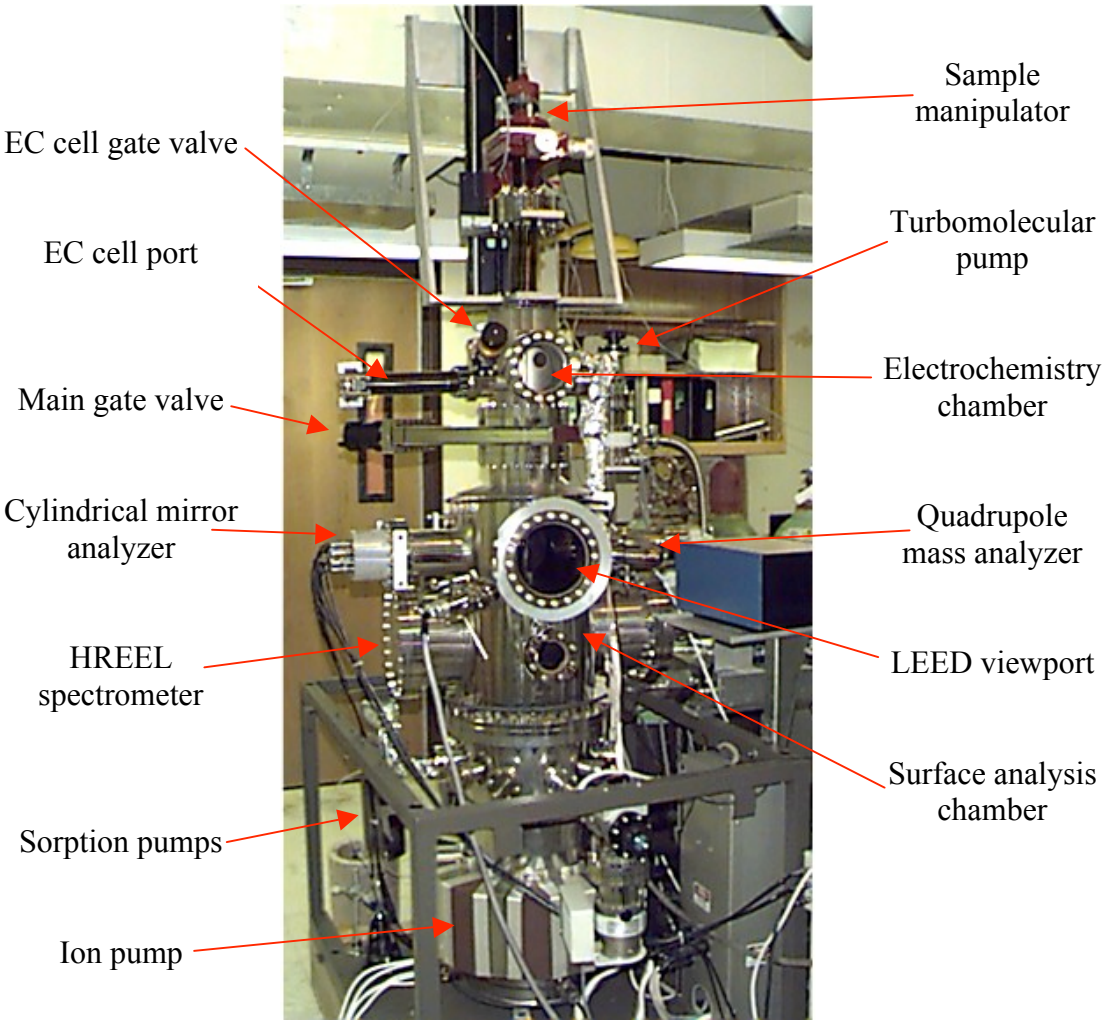

Fig. 13. Picture of the UHV chamber used for the UHV-EC studies.

The crystallographic-oriented Pd(100) single-crystal electrode (99.999 % purity) was purchased from Materials Research Center, Cornell University, Ithaca, NY. It was a circular disk with a diameter of 0.9 cm and a thickness of 0.3 cm. Both faces of the disc were aligned to within 0.5º of the (100) crystallographic plane and were metalographically polished to mirror finish. Although the edges were not oriented, they were metalographically polished. The crystal was attached to the crystal holder via two 0.5 mm Pd wires (99.99%, Aldrich, Milwaukee, WI); the wires also allow for electrical contact with the sample for potential control and resistive sample-heating. The sample temperature was controlled via a Pt-10 % Rh/Pt thermocouple wire (Omega Engineering, Stanford, CT) spot-welded to the top-edge of the sample for temperature measurements and feedback-control for the crystal temperature controller (Omega Engineering).

Cleaning of the Pd(100) single crystal was performed by multiple cycles of (i) thermal annealing at 1020 K in 5.0×10^{-5} torr of O_2 (99.8 % purity, BOTCO, Bryan, TX) and (ii) Ar^+-ion sputtering (2.5 mA) at 5.5×10^{-5} torr of Ar (99.9999 % purity, BOTCO, Bryan, TX). A final thermal annealing at 1020 K was performed to reestablish the atomic smoothness of the Pd surface. Surface cleanliness and ordering were then confirmed by AES and LEED, respectively.

A typical UHV-EC experiment follows these steps: (1) The Pd(100) substrate is cleaned and characterized. (2) The crystal is transferred to the EC chamber and the gate valve between the two chambers is closed so that the EC chamber is isolated from vacuum. (3) Ultra-high-purity Argon (99.9999%, BOTCO, Bryan, TX) is introduced into the EC chamber, and, once the pressure inside reaches 1 psig, the EC-cell gate valve is opened to insert the electrochemical cell into the EC chamber. (4) The EC cell is filled with solution and the crystal introduced. (5) After the EC experiment is conducted, the crystal is emmersed, the cell is drained, and retracted from the EC chamber. (6) The gate valve is closed, and the EC chamber is evacuated by the three-stage pumping system. (7) The main gate is opened and the crystal is then transferred back to the SA chamber for further characterization.

Electrochemical mass spectrometry (EC-MS)

In 1984, Dr. J. Heitbaum first showed that if a differentially pumped mass spectrometer (MS) is separated from an EC cell by a hydrophobic porous membrane, volatile species could be extracted from the aqueous phase and analyzed in the MS [65-68]. This method is more commonly referred to as differential electrochemical mass spectrometry (DEMS); although in this dissertation, the term DEMS will be interchangeably used with EC-MS.

EC-MS is an innovative and versatile technique that has provided a major boost in the research area of electrochemical surface science. It has been used in the detection of adsorbed molecules and intermediates in electrocatalytic reactions at metallic surfaces during the past 15 years. It has been successfully applied in the study of electrocatalytic hydrogenation of aromatic molecules. Examples of this are benzene on polycrystalline Pt [69], Pt(111) [70], Pt(110) and Pt(100) [71], and Pt(332) [72]; aniline and pyridine on polycrystalline and single-crystal Pt, Ru and Pd electrodes [73]; biphenyl, naphthalene and t-butylbenzene on Pt surfaces [74,75]; benzyl alcohol [76] and benzoic acid [77,78] on Pd and Pt electrodes; benzene on Pd-modified Au substrates [79] and hydroquinone on polycrystalline Pt and Pt(111) electrodes [80].

A schematic diagram of the EC-MS system used in this work is shown in Fig. 14. The electrochemical cell assembly consists of a circular block of passivated titanium (a) that rest above a stainless-steel support (l) that connects to the mass spectrometer. The space between the cell body and the support is a Teflon membrane (j) (75 μm thick, pore width 0.02 μm, porosity 50 %) mechanically supported by a steel frit (k); the volatile species is transferred from the solution to the gas phase through this membrane. A single-crystal disk (h) functions as the working electrode. The face of the crystal is in contact with the electrolyte solution and separated from the cell body by a Teflon membrane (i) (ID, 6 mm, OD, 12mm), which works as a spacer forming a 50-to-100-μm thick electrolyte layer (j). Stop or continuous flow electrolysis can be performed with this arrangement. For continuous flow, flow rates should be as low as 1 μL/s to allow enough time (< 2 s) for the electrogenerated products to reach the Teflon membrane.

Two capillaries positioned at opposite sides of the cell body (b, e) serve as electrolyte inlet and outlet and as connection to the reference [standard hydrogen electrode (SHE)] (f) and two auxiliary (Pt wire) (d, f) electrodes.

The vacuum system requires two turbomolecular pumps. A 200-L/s pump is located in the ionization chamber to keep the pressure around 10^{-4} torr; a 50-L/s pump is placed in the analyzer section to achieve a pressure below 10^{-5} torr. The EC cell is connected to the ionization chamber through a valve. A second valve is positioned in the same chamber for calibration experiments that introduces known volumes of gas.

When the species pass the Teflon membrane and enter the vacuum system, they are ionized by electron impact. A quadropole mass analyzer (QMS) separates the fragments by their m/z ratio and then they are detected in the secondary electron multiplier. The amplified signal (mass intensity) is displaced either as current transients, in which the ion mass current (i_I) is plotted as a function of time, and/or as mass spectrometrical cyclic voltammograms (MSCV), in which i_I is plotted as a function of applied potential.

Despite the hydrophobicity of the Teflon membrane, an appreciable amount of electrolyte evaporates. For a membrane porosity of 0.5 and a vapor pressure for water of 23 mbar at 20°C (0.25 mL of H_2O / hour), J' = 0.09 mbar L s^{-1} cm^{-2}.

Under stationary conditions, this amount has to be pumped by the pumping system:

$$J' = pS \tag{25}$$

with an upper limit of 10^{-3} mbar in the ion source and a pumping speed S of 200 L s^{-1}, a flow of 0.2 mbar L S is allowed and, therefore, an electrode area of 0.5 cm^2 is acceptable.

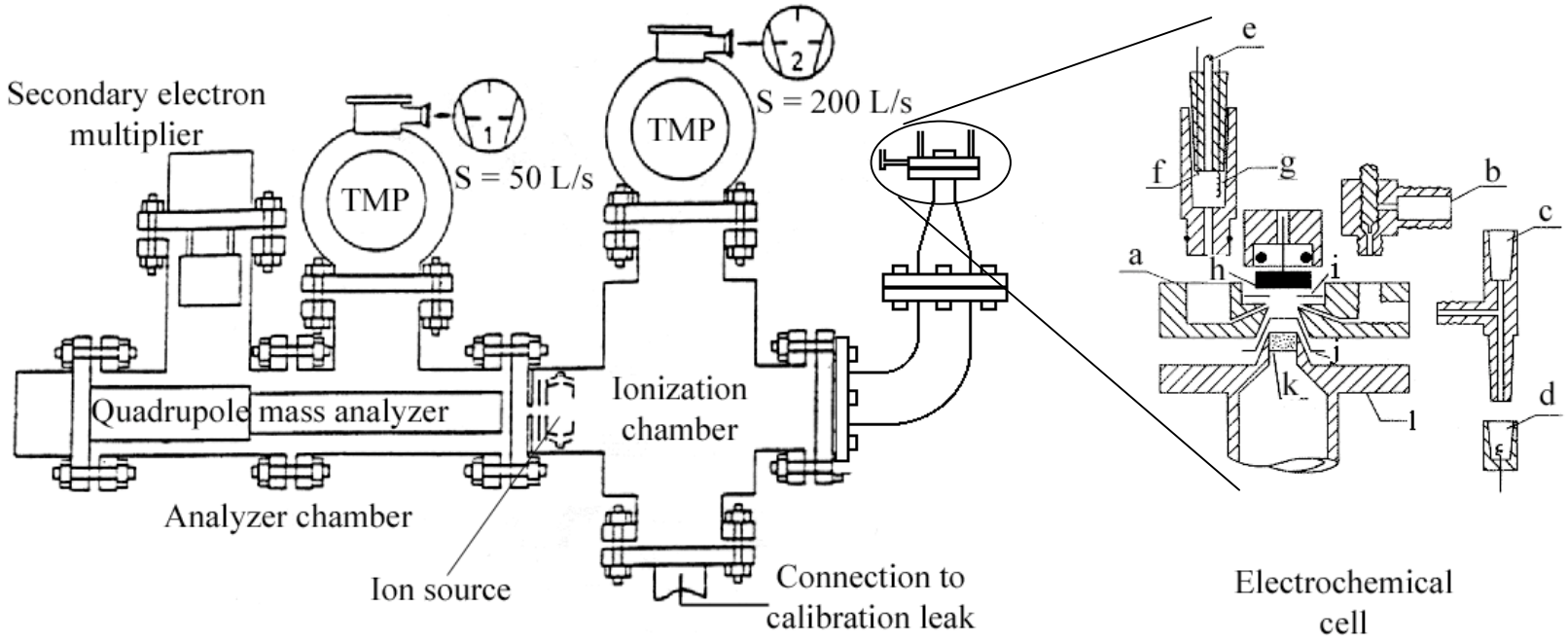

Fig. 14. Schematic diagram of a EC-MS system. This instrument is located in the laboratory of Dr. H. Baltruscht at the Institute for Physical and Theoretical Chemistry, University of Bonn, Germany

The time constant τ for the detection of a species is directly given by the ratio of the ionization chamber volume V_o (total volume of the chamber in which the ion source is situated; first pumping stage) to the pumping speed. Under nonstationary conditions, the change of pressure (e.g., after a sudden change of J') is given by

$$V_o\left(\frac{dp}{dt}\right) = J' - pS \tag{26}$$

with the solution

$$p = \left(\frac{J'}{S}\right)\left(1 - e^{\frac{-t}{\tau}}\right) \tag{27}$$

where $\tau = V_o / S$. With a pumping speed of 200 L/s and a volume V_o of 1 L, a time constant of 5 ms is obtained, which is much less than the time constant attainable with the electrochemical cells (see below).

The analyzer section, of course, has to be pumped separately to achieve a pressure below 10^{-5} mbar. A 50-L/s turbomolecular pump is sufficient. The electrochemical cell is connected to the first vacuum chamber via a valve (see Fig. 14). Another valve leads to the calibration volume. A shutter between the ionization chamber and the analyzer section allows the difference in pressure. The secondary electron multiplier is oriented 90° off axis, which has the advantage that light from the filament does not reach the multiplier. Higher stabilities are obtained using gas-tight ion sources because the filament operates at a lower pressure than that existing in the ionization chamber.

The effort of pumping can be largely reduced by allowing a much higher pressure in the chamber of the first pumping stage (e.g., 10^{-2} mbar) and by simply pumping with a rotational pump at an accordingly lower pumping speed. A sufficiently low time constant can easily be achieved by reducing its volume. In this case, the ion source has to be placed in a separate chamber that is pumped together with the analyzer

of the mass spectrometer by a simple turbo molecular pump of 50 L/s. A commercial gas inlet system can be used. The disadvantage of such a system is that condensation or multilayer adsorption of the species might occur in that pressure range; heating of the gas inlet system may be necessary.

Product formation rates can be easily monitored by recording the corresponding ion current. The mass spectrometrically determined ion intensity I_i is directly proportional to the partial pressure p_i of that species i and, therefore,

$$I_i = ap_i = \frac{aJ_i^{'}}{S} = \frac{RTJ_i a}{S} - K_o J_i \tag{28}$$

where a is a proportionality constant, $J_i = dn/dt = J_i^{'}/RT$ is the incoming flow in mol s^{-1}. K_o thus contains all settings of the mass spectrometer and the ionization probability of the corresponding species.

When the species is produced electrochemically, J_i is given by the faradaic current I_F corresponding to that process:

$$J_i = \frac{NI_F}{zF} \tag{29}$$

where z is the number of electrons, F is the Faraday constant, and N is the transfer efficiency, i.e., the ratio of the amount of the mass spectrometrically detected species to the total amount of species produced electrochemically. N may be less than 1 because a part of the produced species diffuses away from the electrode into the electrolyte. When the current efficiency is not equal to 100 %, I_F has to be replaced by its product with the current efficiency. Therefore,

$$I_i = \left(\frac{K_*}{z}\right) I_F \tag{30}$$

with $K_* = K_o N/F$. Experimentally, both the low time constant of the vacuum setup of several ms and the proportionality of I_i with the faradaic current were verified.

Calibration of the mass spectrometer is achieved by connecting a separate calibration volume, V_c, to the first vacuum chamber via a calibration leak (e.g., a leak valve). The inflow rate, J'_i, is then given by the pressure decrease in the calibration volume dp_c/dt:

$$J_i' = \frac{V_c dp_c}{dt} \tag{31}$$

$$I_i = K_o J_i = \frac{K_o J_i'}{RT} = \left(\frac{K_o}{RT}\right)\left(\frac{V_c dp_c}{dt}\right) \tag{32}$$

K_o can be calculated from the pressure decrease in the calibration volume, *i.e.*, from a plot of the ion current I_i vs. the differentiated pressure p_c.

This calibration procedure cannot only be used for gases (most commonly CO_2) but also for volatile liquids. Special care, however, has to be taken so that no gas adsorption or absorption occurs in any section of the calibration setup. Because of the limited linear range and a possible interference of the partial pressure of H_2O on the sensitivity, the same conditions that occurred during the measurement should exist during calibration of the instrument. In particular, this means that during calibration, the electrochemical cell is connected to the vacuum system.

In some cases calibration is possible by using a known electrochemical reaction, such as hydrogen evolution. From Eq. 30, K_* and NK_o are obtained straight away. Often the oxidation of adsorbed CO on Pt electrode is used to calibrate the mass spectrometer from CO_2. The integrated faradaic oxidation current and the integrated ion current for CO_2 have to be used. In this case, however, double-layer charging effects, which amount to 20% of the oxidation charge even after background subtraction, have to be taken into account. The reason of this is the different double-layer charge at a given potential in the

double-layer region with and without adsorbed CO and additionally the shift of the point of zero charge due to the adsorption of CO.

Disc-shaped gold single crystals (Metal Crystals and Oxides Ltd.), were employed in EC-MS. Prior to the insertion in the EC-MS system, the electrodes were flame-annealed for 4 minutes and cooled under a steady stream of ultrapure argon (Air Products) in the case of Au(111). A 2:1 volume mixture of argon and hydrogen was utilized in the case of Au(332), since the use of Ar results in disorder of the surface. The electrode was then transferred to an Ar-saturated 0.1 *M* H_2SO_4 (Merck) solution where crystallographic integrity of the single-crystal surface was verified by cyclic voltammetry [83,84]; voltammetric experiments were performed based on a "hanging meniscus" configuration [85].

Ultrathin films of palladium were potentiodynamically deposited at a slow scan rate (1 mV/s). The electroplating solutions consisted of 0.1 m*M* $PdCl_2$ (Merck), 0.6 m*M* HCl (Fluka) and 0.1 *M* H_2SO_4. The Pd surface coverage was estimated from the electrolytic charge accumulated during the deposition process; 1 monolayer (ML) was indicated by a charge of 492 $\mu C/cm^2$ [86]. The quality of the Pd-coated electrodes was assessed by cyclic voltammetry in chloride-free 0.1 *M* H_2SO_4 [87]. Removal of Pd to regenerate pure Au surfaces was performed with multiple potential cycles in a solution 0.6 m*M* HCl / 0.1 *M* H_2SO_4. Surface coverages (Γ, mol/cm^2) were calculated using the geometrical area of the Au(111) and Au(332) electrodes.

In a typical EC-MS experiment: the electrode, after deposition of the Pd adlayer and characterization by cyclic voltammetry, was emersed from 0.1 *M* H_2SO_4 at potentials within the double-layer region and immediately transferred to a one-compartment EC-MS thin-layer cell. The latter was rinsed with 1 mL of the adsorbate solution for 1 minute followed by a 3-minute equilibration at the double-layer region. The EC cell was then thoroughly rinsed with pure supporting electrolyte to ensure that *unadsorbed* material was no longer present. Current-potential scans were subsequently performed in organic-free 0.1 *M* H_2SO_4. Multiple cycles were run until no more changes were noted in both the current-potential curves and the mass spectrum.

EC-MS experiments were performed in the laboratory of Prof. Helmut Baltruschat at the Institute for Physical and Theoretical Chemistry, University of Bonn, Germany.

Reagents

The supporting electrolyte solutions used in the TLE (1.0 *M* H_2SO_4) and UHV-EC (10 m*M* H_2SO_4) experiments were prepared from fuming sulfuric acid (Aldrich Chemicals, Milwaukee, WI). The 0.1 *M* H_2SO_4 used for EC-MS studies was made from concentrated H_2SO_4 (Merck). p-dihydroxybenzene (hydroquinone, H_2Q), benzoquinone (Q), and 2,4-dihydroxybenzenesulfonate (hydroquinone sulfonate, H_2QS^-) were purchased from Aldrich; 2,5-dihydroxythiophenol (HQS) was synthesized following known procedures [88]. Milli-Q® Plus water was used to prepare all the aqueous solutions.

In the TLE cell arrangement (Fig. 6), a conventional H-cell was used. One compartment contained the thin layer cell, whereas the other one contained the auxiliary electrode (Pt wire) and the reference electrode (Ag/AgCl, 1 *M* NaCl). Potentials were controlled using a conventional potentiostat (CV-27, Bioanalytical Systems Inc., West Lafayette, IN) and the output was plotted on an X-Y recorder (Soltec VP-6414S, Sun Valley).

For the EC-UHV studies, a conventional cell was used. The cell consisted of two 5-mL compartments; one holds the Pd(100) crystal (working electrode) and one holds a Pt wire (auxiliary electrode) and a Ag/AgCl (1 m*M* Cl^-) reference electrode. The two compartments were separated by a fine glass frit to allow electrical contact without cross-contamination from the reference to the working electrode compartment. A long tube, connected to the working electrode compartment, served as the port where different solutions could be introduced in and out from that compartment. The resistance of this cell was calculated to be 1.5 kΩ as determined from the peak potential shift of the redox pair H_2Q/Q as a function of the applied scan rate. Electrochemical experiments performed in the UHV-EC system were carried out using the same kind of potentiostat

and X-Y recorder used in the TLE experiments. All potentials in this work are referenced to a Ag/AgCl (1 m*M* Cl^-) electrode.

RESULTS AND DISCUSSION

Polycrystalline palladium electrode

Studies on the chemisorption and electrochemical hydrogenation of aromatic molecules (H_2Q and Q) on Pd(pc) substrates were based upon thin-layer electrochemistry.

Coverage measurements and orientational assignments

The measurement of the packing densities (surface coverages) of H_2Q and Q along with the assignment of the mode of chemisorption (molecular orientation) from the interfacial concentrations have been described in a recent publication [52]. This article, which also discusses the anodic oxidation of the chemisorbed material, is reproduced in Appendix A. The latter should be perused at this point.

Electrochemical hydrogenation

Fig. 15 shows the cathodic portion of the current-potential curve of a clean and η^6-Q-coated Pd(pc) electrode in the hydrogen evolution region. The cathodic peak is featureless regardless of the presence or absence of chemisorbed organic, but the magnitude of the reductive current is larger for the organic-coated electrode. The featureless cathodic peak is in contrast to what is observed at platinum electrodes [15] because of the absence of site-specific hydrogen chemisorption peaks. The increase in cathodic current is most certainly due to hydrogenation of chemisorbed organic because hydrogen evolution and absorption are actually blocked by passivating adlayers like zerovalent sulfur [89]. It is clear, however, that the hydrogen reaction occurs over a wide range of potential because no distinctive peaks are observed.

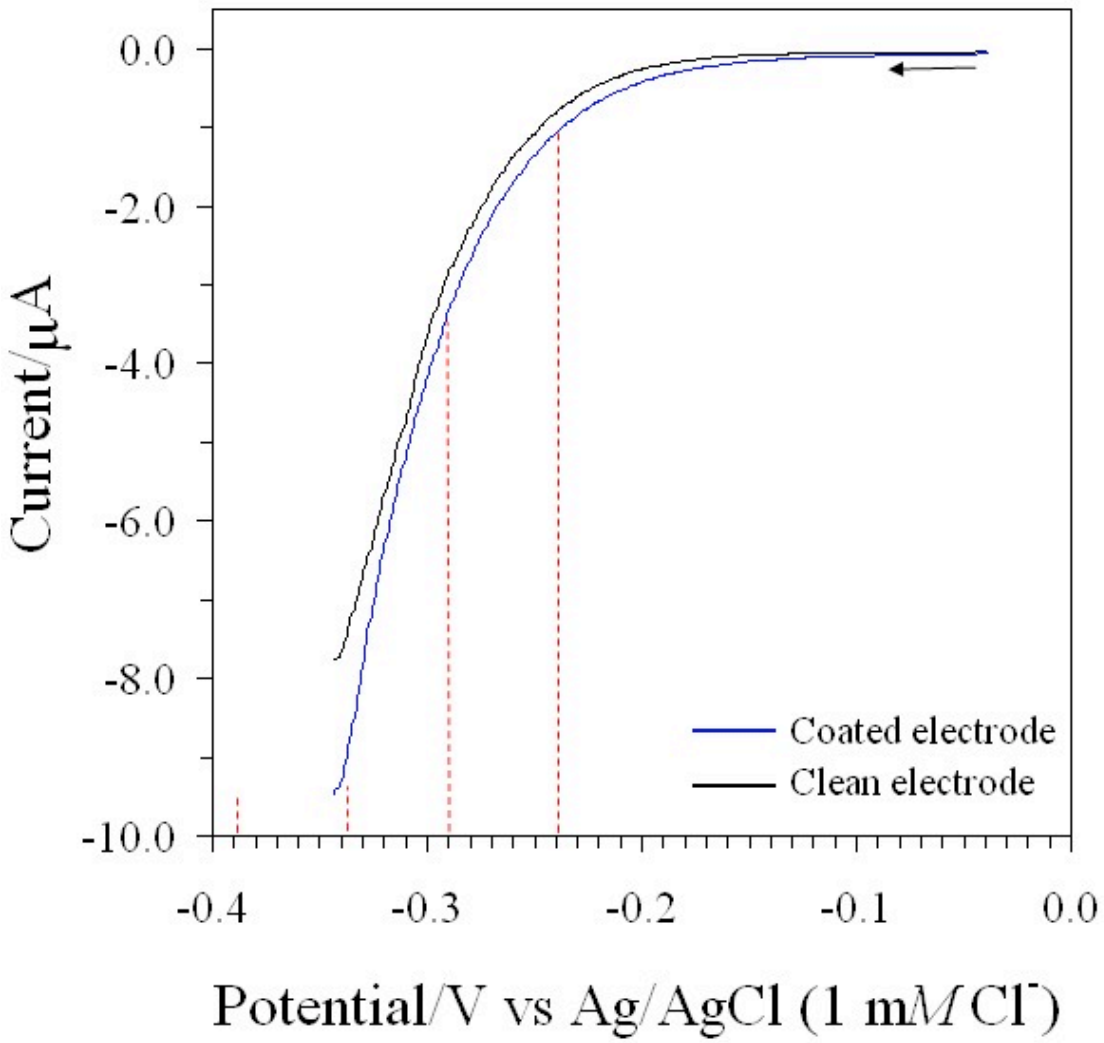

Fig. 15. Thin-layer cyclic current-potential curves of a Pd(pc) electrode before and after exposing the surface to a 0.10 m*M* H_2Q solution. The red broken lines mark the chosen potentials for the potential step experiments. Scan rate, 2 mV/s. Electrode area, 1.26 cm^2.

The extent of hydrogenation was monitored in terms of the n_H parameter (number of electrons transferred), as described in the experimental section. It is anticipated that n_H is strongly dependant upon the applied potential; this expectation is borne out by the n_H-vs-E plot shown in Fig. 16. Measurements at potentials much less than -0.35 V were not deemed meaningful because of intractable hydrogen evolution and bulk-absorption processess.

Unlike what was observed on Pt(pc) [15], the n_H-vs-E plot in Fig. 16 does not show a constant n_H at $E < -0.2$ V. This is unfortunate since the presence of a plateau would have indicated the limit of the extent of hydrogenative desorption of the adsorbed organic. It is evident that severely limited information on chemisorbed-organic hydrogenation can be extracted from the TLE measurements. Consequently, no additional TLE work was carried out; further investigations were undertaken with non-traditional approaches such as UHV-EC and EC-MS.

Ultra-high vacuum electrochemistry (UHV-EC)

As an extension of the TLE studies highlighted in the previous section, similar interfacial experiments were performed on a well-defined Pd(100) single-crystal electrode. The later was used because it is more reactive than the Pd(111) surface.

Experimental measurements were based upon LEED, AES, HREELS, and conventional EC. Experiments were not carried out unless clearly defined LEED patterns such as the one in Fig. 8b were observed. Likewise, the cleanliness of the electrode had to be confirmed by AES as in Fig. 12. The HREELS data was obtained before and after the electrode was dipped in supporting electrolyte. As mentioned in the experimental section, the HREEL spectrum of a freshly prepared Pd(100) surface indicates the presence of CO on the substrate surface (Fig. 10). The ubiquitous CO peaks are largely diminished after the electrode is emersed from a supporting electrolyte solution (Fig. 17). Assignment of the signals observed in Fig. 17 has been already established [90].

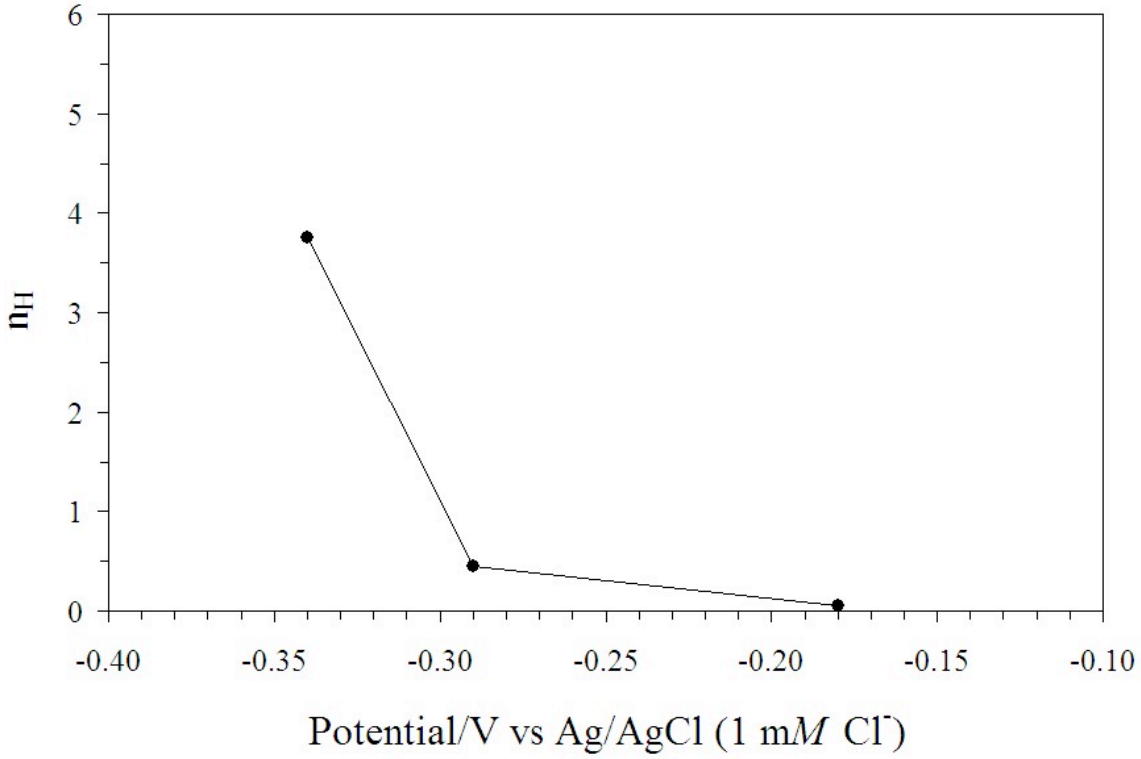

Fig. 16. Number of electrons (n_H) as a function of applied potential involved in the hydrogenation of chemisorbed species at Pd(pc) electrodes. Reaction time was 4 minutes.

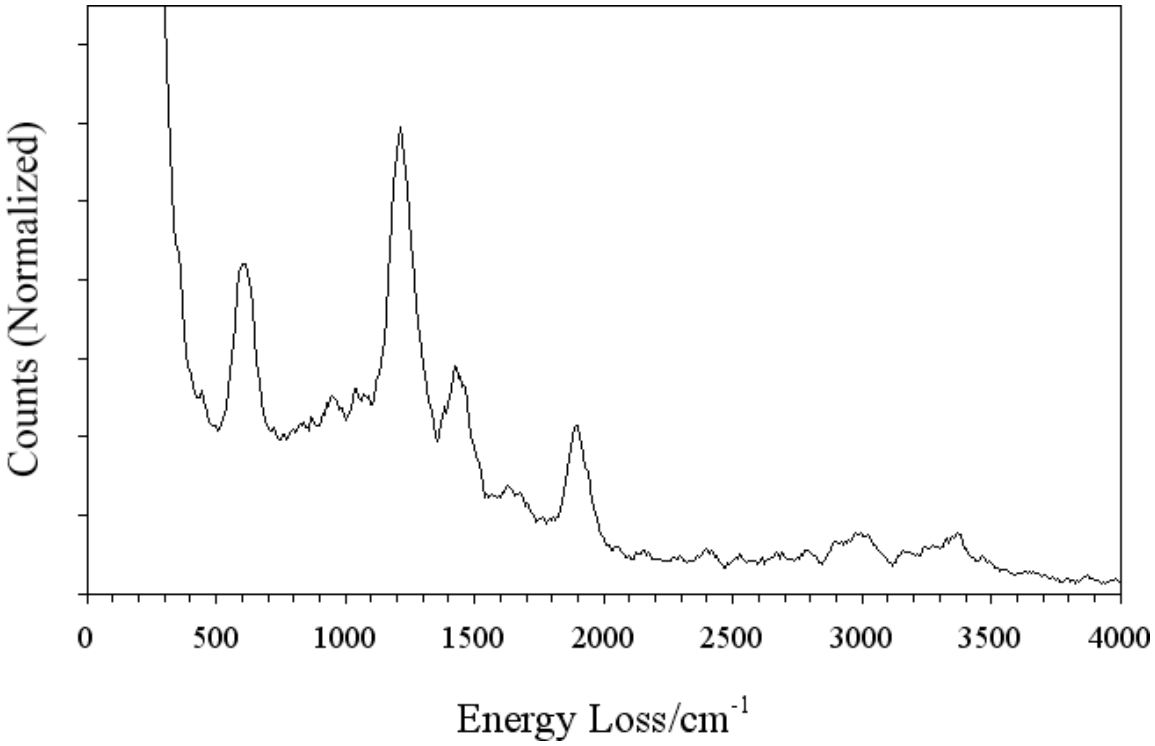

Fig. 17. HREELS spectrum of a well-ordered Pd(100) surface after emersion from a 10 m*M* H_2SO_4 solution.

HREELS-based chemisorption isotherms

It is first important to recall the results from previous measurements that compared HREEL spectra for species chemisorbed from H_2Q and from Q [53]. The relevant spectra are shown in Fig. 18. Three features in the H_2Q spectrum warrant extra attention: (i) the absence of a peak at 3600 cm^{-1} which, by comparison with the gas-phase H_2Q spectrum, would have indicated an in-plane ν(OH) stretch; (ii) the presence of peaks 2, 3 and 4 which, if the adsorbed molecule retained its aromatic functionality, would correspond to in-plane bending [δ(CH)] and stretch [ν(CC) and ν(CH)] modes, respectively; and (iii) the appearance of peak 1 that could be attributed to an out-of-plane bending mode, γ(CH), the intensity of which is the highest of all observed peaks.

The absence of a ν(OH) peak indicates either the absence of a phenolic O-H functionality group and/or the imposition of a rigid flat (η^6) adsorbed-aromatic orientation. In the later configuration, the metal-surface dipole selection rule would render the O-H stretch HREELS-inactive. However, if the dipole selection rule were strictly observed, peaks 2, 3 and 4 (if those were actually in-plane aromatic-ring modes) would likewise have been HREELS-inactive. Hence, the appearance of peaks 2 to 4 could be taken as an indication that the adsorbed molecule is not completely oriented parallel to the surface but is tilted, albeit only slightly. The minimal off-parallel tilt is evidenced by the out-of-plane peak being more intense than the in-plane modes. In the infrared spectrum of unbound H_2Q, the reverse is true: the in-planes modes are actually more intense than the out-of-plane vibration. It should also be noted that, for gas phase H_2Q, the O-H peak is considerably more intense than the C-H stretch; yet the HREEL spectrum of chemisorbed H_2Q shows only the C-H, without the O-H, peak. It may be postulated that H_2Q is oxidatively chemisorbed on Pd as Q in a slightly tilted η^6 orientation. It is clear that the HREEL spectrum of chemisorbed Q is essentially identical to that for H_2Q. The close similarity between the two spectra indicates that the adsorbed species derived from aqueous H_2Q is the same as that generated from aqueous Q.

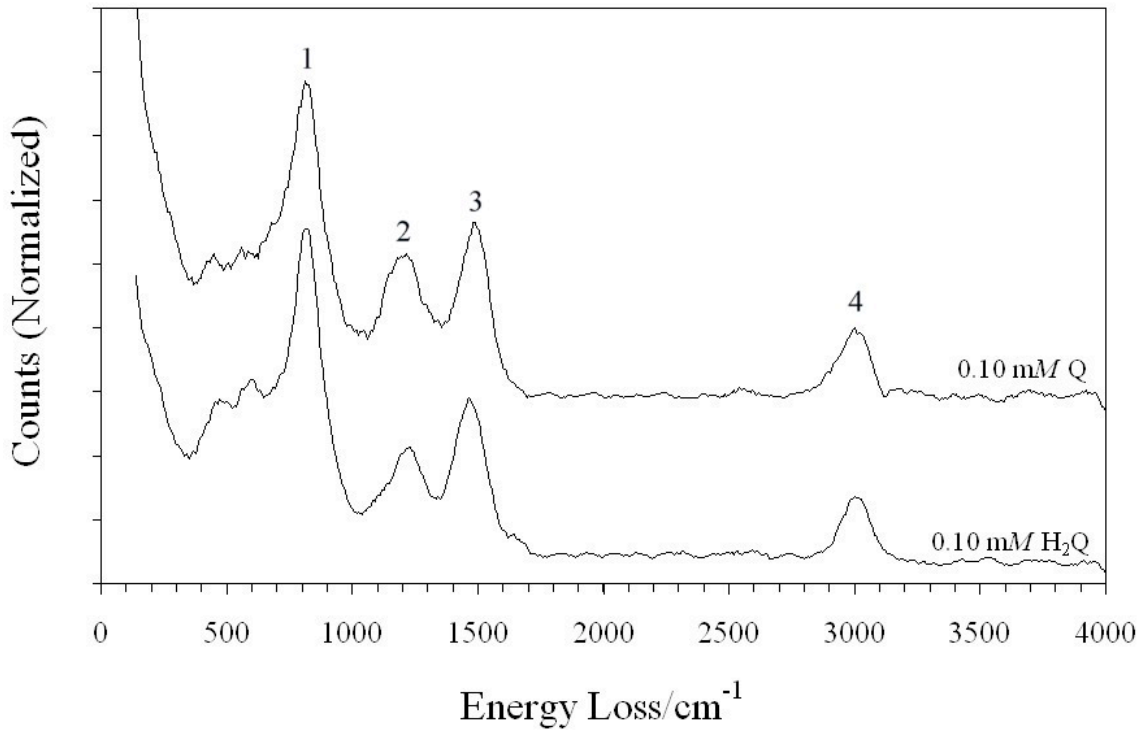

Fig. 18. HREEL spectra after emersion from 0.1 m*M* H_2Q and 0.1 m*M* Q solutions in 1 m*M* CF_3COOH.

An attempt was made to generate a chemisorption isotherm for H_2Q by exposure of the well-ordered Pd(100) electrode to various H_2Q solutions and subsequent surface analysis of the emersed crystal by HREELS The electrode was rinsed in pure water to remove unadsorbed material.

The results are displayed in Fig. 19. The main spectral features in Fig. 19 are identical to those in Fig. 2 in reference [53]; the apparently weaker and broader peaks in the region 300-600 cm^{-1} includes two δ(CC) bending modes; whereas, the region 1000-1400 cm^{-1} includes one ν(CC) and/or one δ(CH) mode. A cursory inspection of the data in Fig. 19 suggests little, if any, changes in the peak intensities as a function of the concentration at which chemisorption was carried out. The (erroneous) conclusion could be reached that the coverage and, hence the adsorbed-molecule orientation, is concentration-independent. Such a conclusion was the case for HREELS-based measurements at Pt(111) surfaces [44]. Quantitative AES measurements were used to buttress the assertion. However, AES employs much higher beam-electron energies than HREELS; hence, in the study of organic monolayers the use of AES may be questionable and it could easily lead to electron-stimulated decomposition of the organic species [44].

As previously described above in the experimental section, the proper use of HREEL spectra for quantitative surface coverage measurements must take into consideration three critical mandates: (i) integrated peak intensities (A), not peak heights, should be employed; (ii) the integrated peak intensities must be normalized; and (iii) the normalization must involve the integrated background intensity in the (featureless) 2100-2700 cm^{-1} region [62]. Neither integrated intensities nor background-based normalization were employed in the above cited work on Pt(111) electrodes [39,40,42]. In this study, the intensity of the γ(CH) and ν(CH) HREELS peaks were integrated and normalized and employed to generate the chemisorption isotherm shown in Fig. 20.

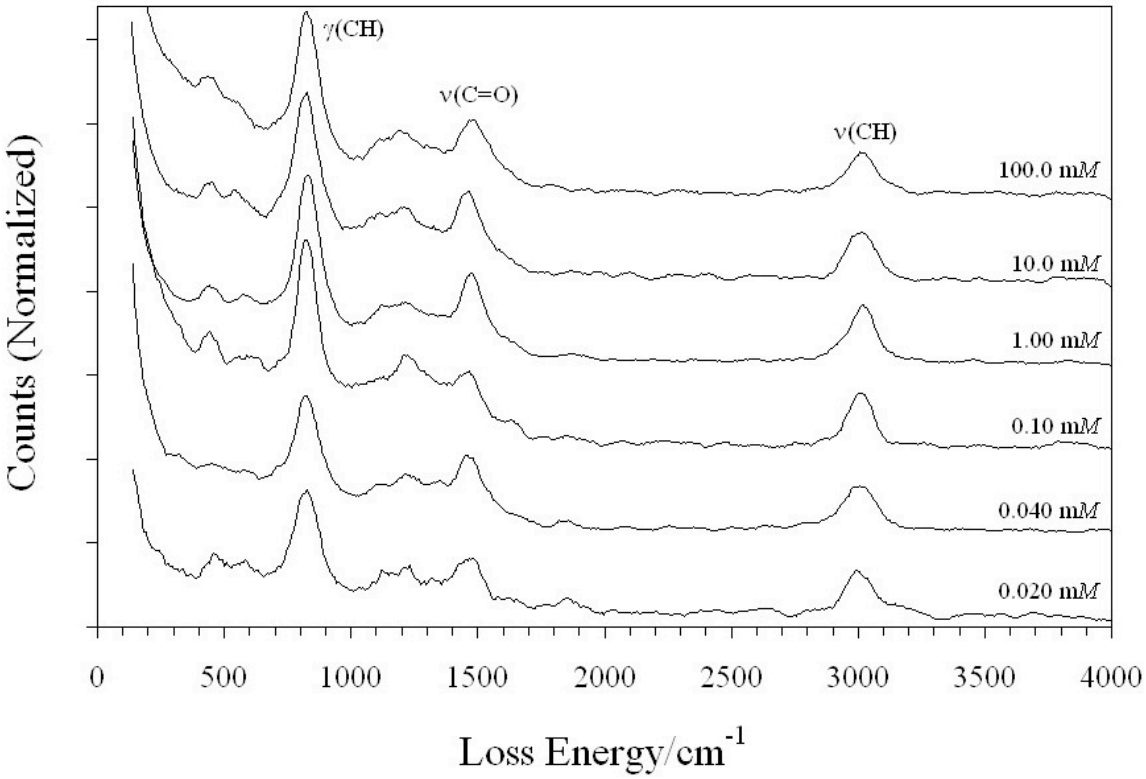

Fig. 19. HREEL spectra of Pd(100) surfaces after emersion from different H_2Q solutions in the millimolar concentration regime.

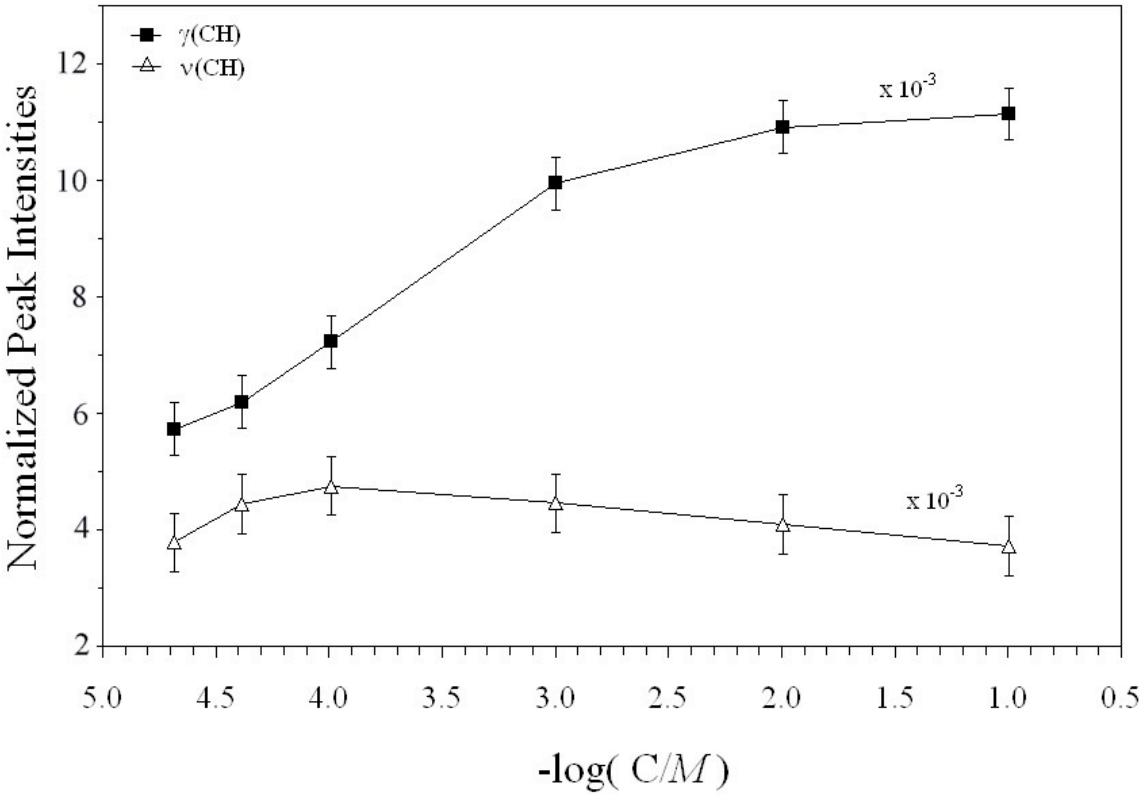

Fig. 20. Chemisorption isotherm: normalized γ(CH) and ν(CH) HREELS peak intensities as a function of solution H_2Q concentration. The solid lines simply interconnect the data points and do not represent any theoretical fit.

It is most interesting to note the two types of isotherms. The one generated from the out-of-plane bending (wagging) mode [γ(CH)] indicates a packing density transition from a lower plateau to an upper plateau with the upper-to-lower plateau ratio equal to 1.9; this is reminiscent of the chemisorption isotherm obtained from TLE measurements (cf. Fig. A-2 in Appendix A). It is quite striking to note that when the upper-to-lower plateau ratios of the surface coverage (Γ) and the integrated intensities (A) are superimposed on a simple plot, Fig. 21, the two sets of data follow the identical trend.

The γ(CH)-generated isotherm strongly suggests an orientational transition from a flat orientation at low concentrations to a vertical orientation at higher concentrations. On the other hand, no lower-to-upper plateau orientational transition is indicated in the chemisorption isotherm generated from the ν(CH) peak. Although there is an increase in the integrated peak intensity below 10^{-4} *M*, there is actually a slight decrease in the peak areas at higher concentrations. It may be of interest that the point at which a decrease in the plot for the ν(CH) isotherm coincides with the increase in the plot for the γ(CH) isotherm. If this point is actually the onset of a flat-to-vertical orientational transition, the unexpected decrease in the ν(CH) isotherm may be due to a complication afforded by the appreciable impact scattering mechanism of the mode in the flat oriented adlayer [90]; no impact scattering was noted for the γ(CH) mode in the flat orientation. The γ(CH) generated chemisorption isotherms (Figs. 20 and 21) has been used in this work to establish flat-to-vertical orientational transitions.

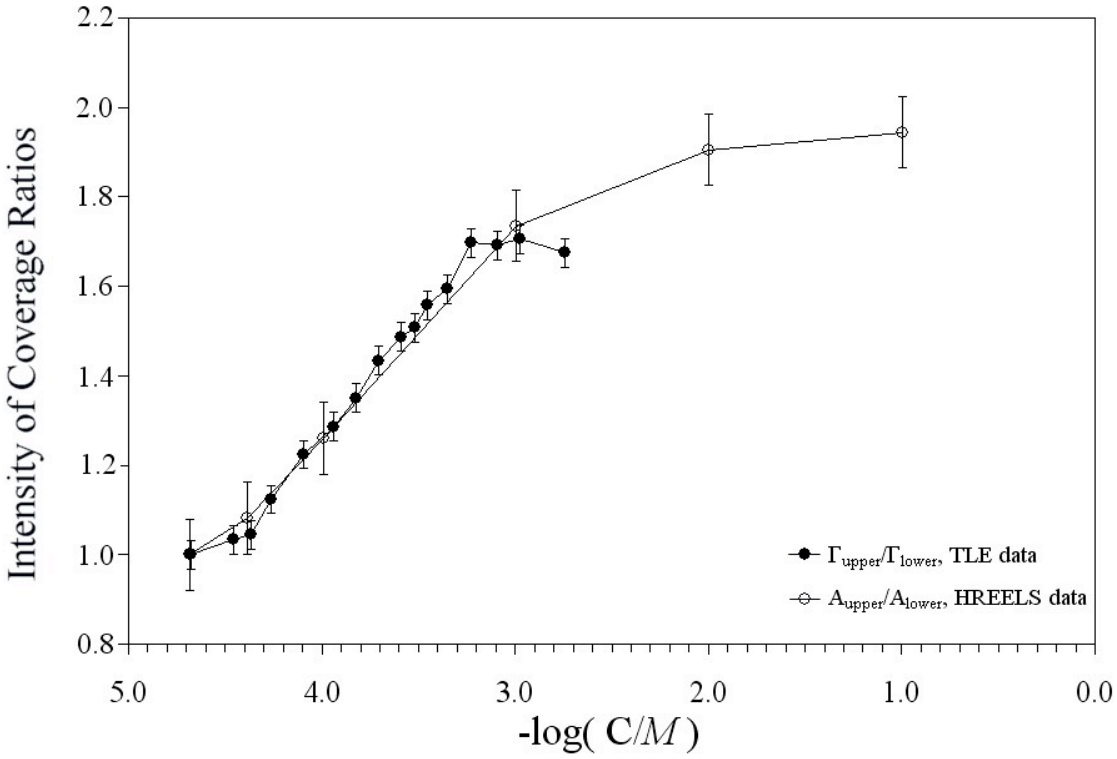

Fig. 21. Comparison of chemisorption isotherms obtained by thin-layer electrochemistry (TLE) [52] and the HREELS data from Fig. 20. Normalization procedure as explained in the text.

The missing O–H stretch

As can be seen in Fig. 20, the integrated band intensity-vs-concentration plot clearly shows an increase in surface coverage easily explainable in terms of the formation of vertically oriented (2,3-η^2-attached) organic–adsorbed species. It had been surmised, and later verified by surface infrared reflection-absorption spectroscopy [31], that in the η^2 configuration, two adjacent C-H bonds are broken and an ortho-di-σ-bonded diphenolic species is formed (species **I** in Fig. 22). However, the HREEL spectrum (Fig. 19) for the 2,3-η^2-attached species does not show an O-H stretch in the region near 3500 cm^{-1}. The possibility may exist that a quinone species such as species **II** in Fig. 22 may be formed on Pd, although from organometallic chemical considerations, the diphenolic species (**I**) would be more highly favored than the quinonoid species (**II**).

To provide a reference for the O-H stretch mode of unadsorbed diphenolic species, HREELS experiments were carried out with 5.0 m*M* and 100.0 m*M* of the potassium salt of hydroquinone sulfonate (H_2QS^-) in which the electrode was not rinsed with pure supporting electrolyte prior to the HREELS measurements; in this manner, a multilayer film of *unadsorbed* potassium hydroquinone sulfonate would be retained on the surface but the unadsorbed salt would not be pumped away in ultra-high vacuum since it is a solid. The results are shown in Fig. 23. In this case, an ν(OH) stretch mode at 3500 cm^{-1} is *not* observable either for the film from the 5.0 m*M* or from the 100.0 m*M* emersion; the fact that no ν(OH) peak was observed for the unadsorbed diphenolic salt is unexpected and inexplicable.

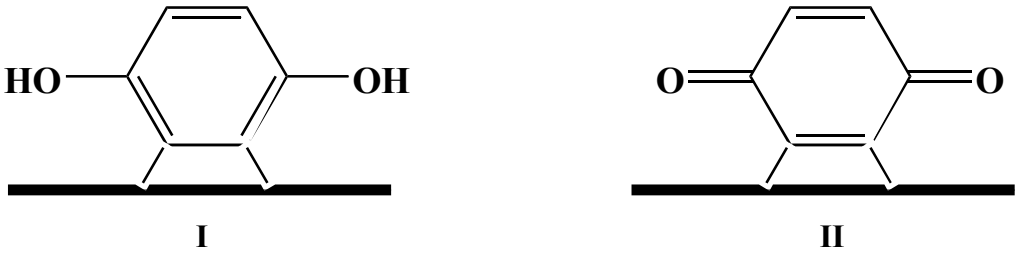

I **II**

Fig. 22. Models for the ortho-di-σ-bonded species in the reduced (**I**) and oxidized (**II**) forms. The bottom black line represents the Pd surface.

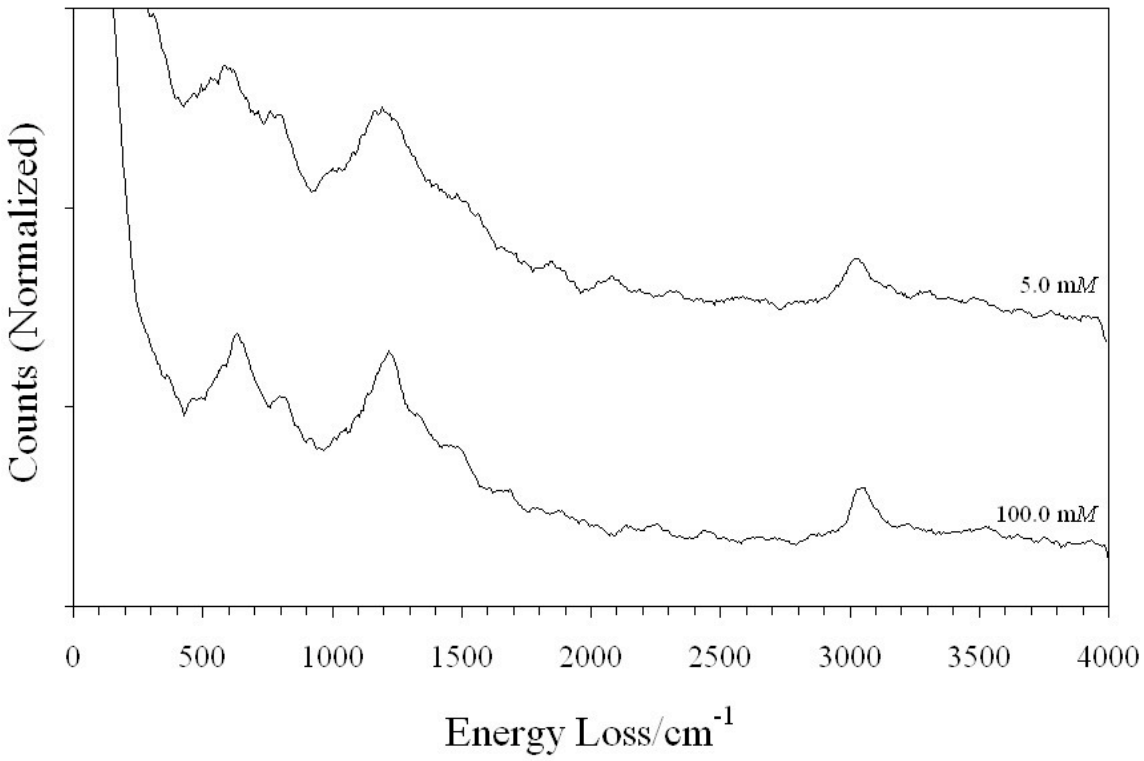

Fig. 23. HREELS spectra of H_2QS^--coated Pd(100) surfaces after emersion from solutions with two different concentrations.

Since HREELS peaks may be deteriorated by the presence of a multilayer film, it was necessary to confirm that an unadsorbed salt film actually exists on the surface. AES measurements were carried out with the layers generated from 5.0 m*M* and 100.0 m*M* emersions. The relevant results are shown in Fig. 24. It is clear that much more than a single layer is present on the surface, especially that emersed from 100.0 m*M* H_2QS salt. It must be emphasized that the multilayer film should consist of intact sulfonate diphenolic as no catalytic surface reaction is possible from the Pd surface passivated by condensed multilayers of organic species. It is not understood at this point why no O-H peaks are observed with HREELS; further information will have to be conducted in this regard. Surface infrared reflection-absorption spectroscopy may have to be employed since, as already mentioned, the ν(OH) mode was observed with this technique for 2,3-η^2-H_2Q on Pt [31].

Electrochemical hydrogenation

Fig. 25a shows the CV of a UHV-prepared Pd(100) surface cycled in 10 m*M* H_2SO_4 solution (black trace) and in 0.10 m*M* H_2Q / 10 m*M* H_2SO_4 solution (blue trace). Only potentials more negative than the double-layer region are shown. The CV of pure supporting electrolyte shows one redox peak; the cathodic part at –0.33 V and the anodic portion at –0.19 V. These features have been ascribed to hydrogen absorption and desorption processes respectively [91]; hydrogen evolution occurs at potentials more negative than -0.33 V and it is also shown in Fig. 25a. The hydrogen absorption-desorption peaks disappear when the Pd electrode is coated with H_2Q or Q.

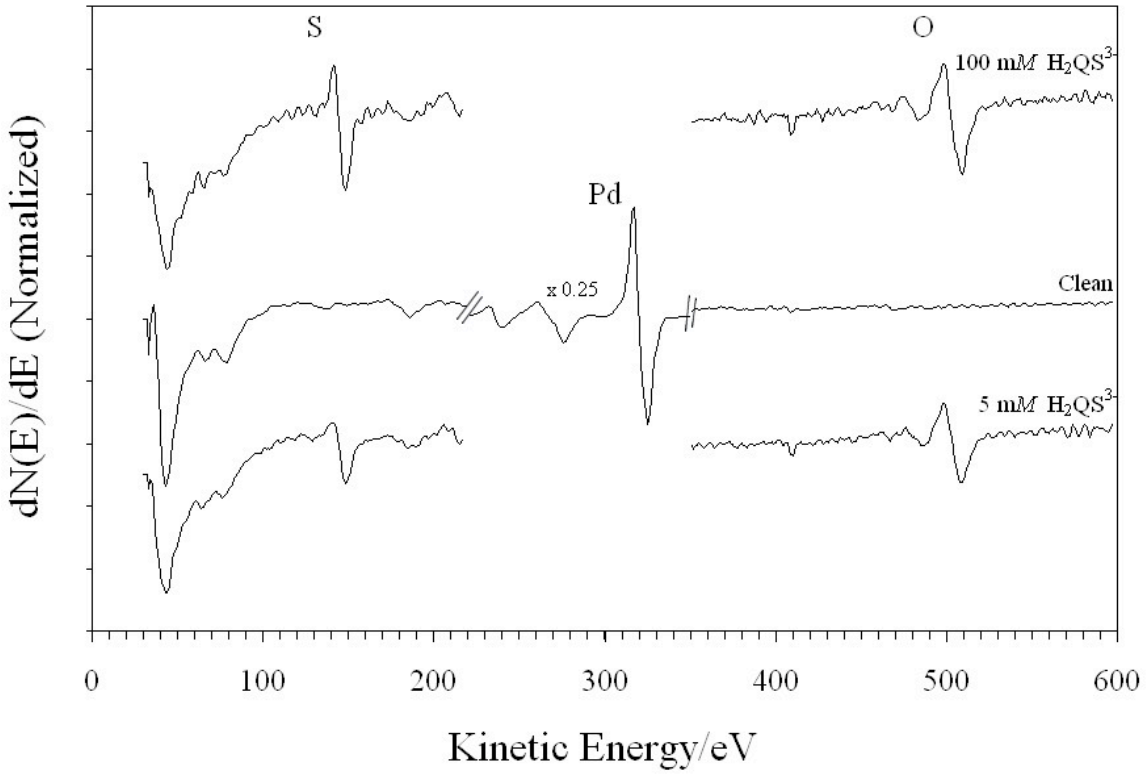

Fig. 24. Auger spectra for H_2QS^--coated Pd(100) electrodes after emersion from solutions with different concentrations. Essentially two-fold increases in the S/Pd and O/Pd Auger peak intensities were observed on going from 5.0 mM to 100 mM H_2QS^-.

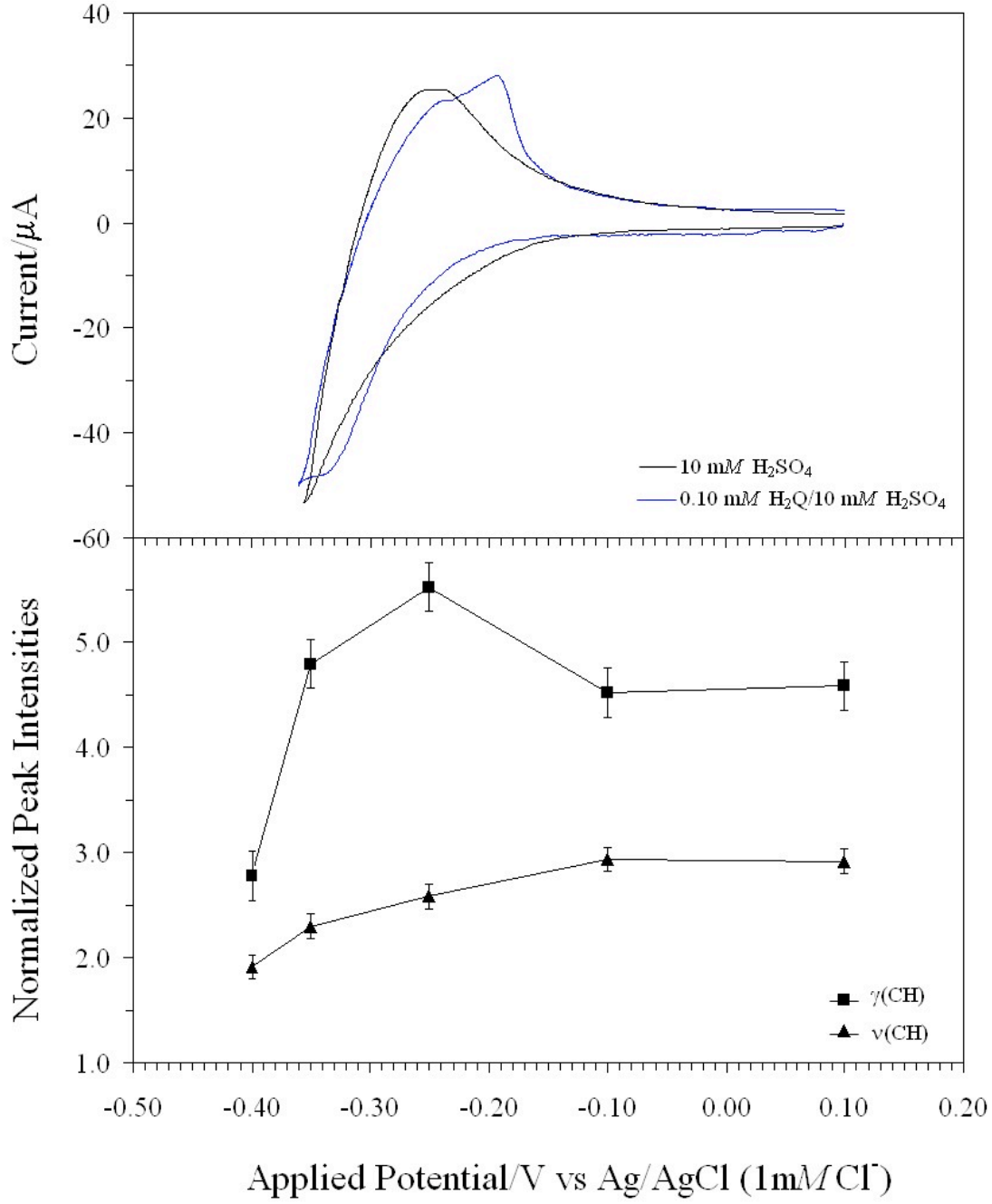

Fig. 25. (a) Current-potential curves of a Pd(100) electrode in supporting electrolyte and in the presence of 0.10 m*M* H_2Q / 10 m*M* H_2SO_4 solution. s.r.: 5 mV/s, A = 1.27 cm^2. (b) Normalized HREELS peak intensities of the out-of-plane γ(CH) mode and the in-plane ν(CH) mode at different applied potentials.

Experiments were performed in which η^6-oriented Q was precoated onto the Pd(100) electrode and subjected to preselected reductive hydrogenation potentials in organic-free supporting electrolyte. The HREEL spectra were obtained after 3 minutes reaction time; the spectrum at 0.10 V represents the reference spectrum for the non-hydrogenated adlayer. The following trends can be observed from Fig. 26: (i) the intensity of the γ(CH) peak increases to a maximum at -0.25V and decreases when the potential is made more negative; (ii) the intensity of the ν(CH) peak decreases progressively as the potential is made more negative; and (iii) a fraction of the starting material survives the excursion to potentials into the hydrogen evolution region.*

Fig. 25b shows the normalized integrated HREELS peak intensities as a function of potential. The decrease in the ν(CH) peak as the hydrogenation potential is made more negative may indicate potential-induced desorption and/or hydrogenative desorption of a fraction of the starting chemisorbed material. However, the maximum in the γ(CH) at -0.25 V requires a more detailed investigation.

Clearly, the maximum in the integrated intensity-vs-potential plot for the γ(CH) peak cannot result from an increase in surface coverage since there is no supply of starting material and catalytic hydrogenation can only lead to desorption. At least two reasons may be invoked for the appearance of the maximum: (i) partial hydrogenation of the chemisorbed aromatic to aliphatic groups to increase the number of γ(CH) wags; and/or (ii) negative-potential-induced increase in the vibrational intensity of the non-hydrogenated (intact) starting material. The first is deemed highly unlikely since earlier work [90] on the anodic oxidation of H_2Q chemisorbed on Pd(100) electrodes suggested that, once oxidation starts for a given molecule, it proceeds to completion until the oxygenated molecule (*e.g.* CO_2) is desorbed; in other words, partially-oxygenated chemisorbed species do not remain on the surface. If the *complete* reductive desorption is also the scenario for electrochemical hydrogenation, partially hydrogenated cycloalkenes should not be formed. The intensity γ(CH)-vs-E maximum at -0.25 V is

* The intensity changes in the other peaks were not considered here since these peaks are envelopes (composites) of at least two vibrational modes

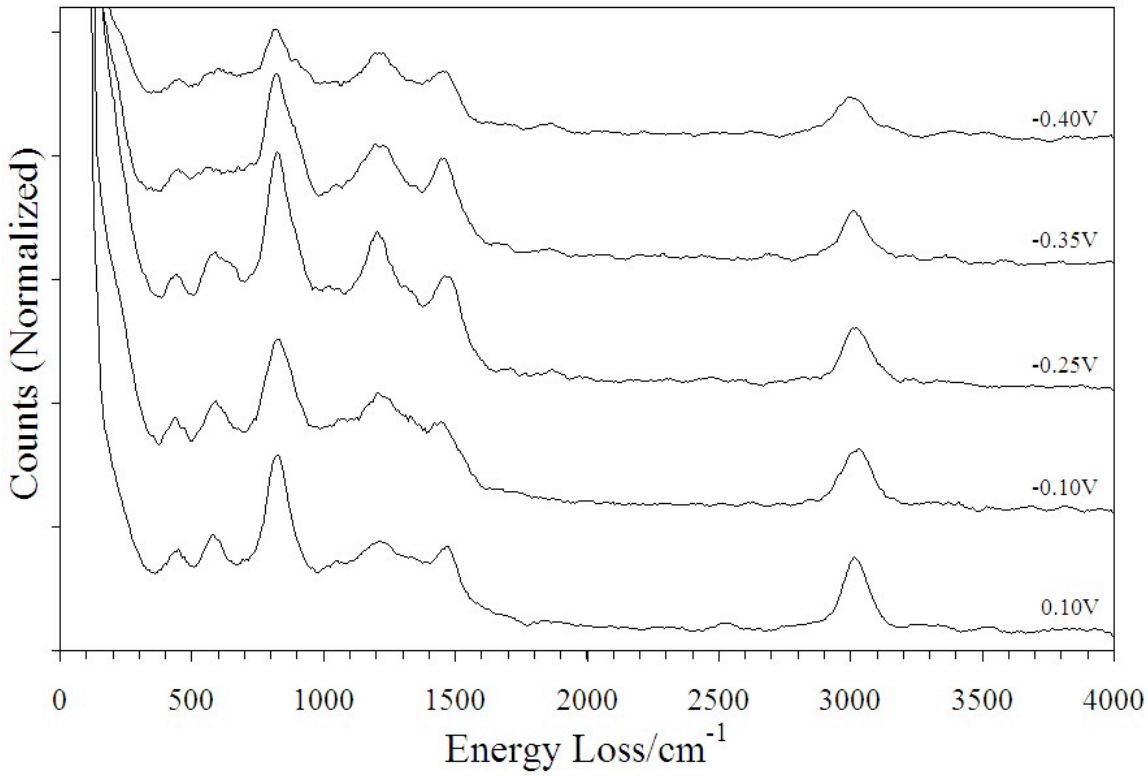

Fig. 26. HREEL spectra of H_2Q-coated Pd(100) surfaces after hydrogenation in H_2Q-free solution at selected applied potentials.

probably due to an electrode–surface-charge effect; that is, an increase in the negative charge density at the electrode surface leads to an intensity increase in the γ(CH) out-of-plane bends. The eventual decrease in coverage, of course, is because, as the potential is made more negative, a greater extent of hydrogenative desorption takes place, and the absorption intensities eventually decreases. Unfortunately, while experimental and theoretical studies [92-97] have been conducted on the effect of electric field on vibrational frequencies (the so-called electrochemical Stark effect), no work has been reported on the effect of applied potential on integrated band intensities.

Sequential incremental hydrogenation

In the above-described experiments, the starting point had always been a UHV-prepared single-crystal surface, that is, H_2Q was always chemisorbed at 0.1 V and then subjected to preselected hydrogenation potentials at 0.0, -0.1, -0.25, -0.35, and -0.40 V. In a variation of this procedure, a set of experiments was also carried out in which the electrode was pretreated with the adsorbate and then hydrogenated incrementally at progressively more negative potentials, but with HREELS measurements in between the hydrogenation reaction. In other words, after electrode pretreatment with H_2Q at 0.1 V, the potential was set for 3 minutes at 0.0 V, following which an HREEL spectrum was obtained; the electrode was then returned to the electrolytic solution and a potential of -0.1 V was applied. This sequence was repeated until a potential of -0.4 V was reached. The results are displayed in Fig. 27. It is of major significance that the data in this figure are essentially identical to that in Fig. 26. This observation helps support the assertion presented above that the hydrogenation reaction occurs completely for each molecule, that is, once hydrogenation is initiated, it does not stop until complete hydrogenative desorption transpired. Hence, as evidenced by the HREEL spectra in Figs. 26 and 27, the molecules that are retained in the surface are (intact) starting material that have resisted initial hydrogenation.

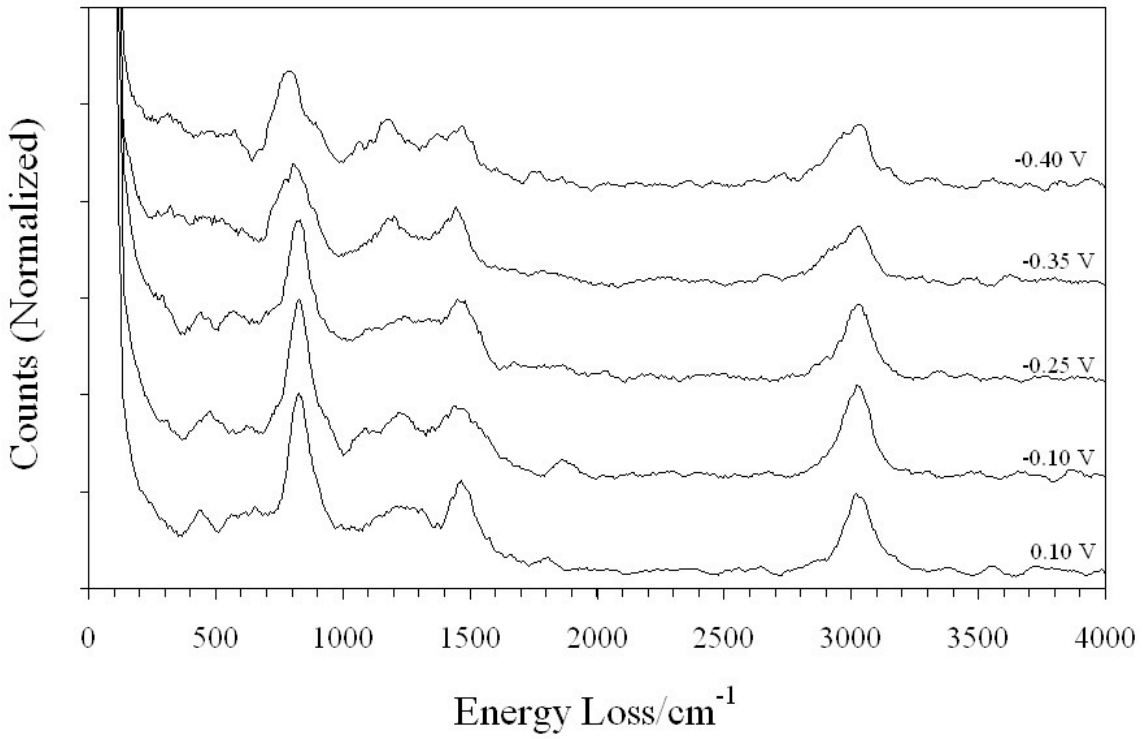

Fig. 27. HREEL spectra of H_2Q-coated Pd(100) surfaces after sequential incremental hydrogenation in H_2Q-free solution at selected applied potentials.

Electrochemical mass spectrometry (EC-MS or DEMS)

Experiments based upon HREELS provided information on species that exist on the electrode surface, prior to and after electrochemical hydrogenation. However, in order to acquire a more complete view of the hydrogenation reaction, the distribution of products that are desorbed into solution also need to be assayed. It is for this purpose that experiments based upon a combination of electrochemistry and mass spectrometry were undertaken.

Investigations with Pt(pc)and well-defined Pt(111) surfaces

No EC-MS investigations on the electrochemical hydrogenation of chemisorbed hydroquinone (or benzoquinone) had been previously carried out on either polycrystalline or monocrystalline platinum electrocatalysts. Hence, the first EC-MS experiments in the present study were devoted to these interfacial systems. The work has already been described in a publication. This manuscript is reproduced in Appendix B and should be read at this juncture.

Ultra-thin Pd films

Hydrogenation reactions on bulk Pd catalysts are invariably assisted by sub-surface hydrogen; however, the role of absorbed hydrogen is not within the scope of the present dissertation. Hence, EC-MS measurements were limited only to ultrathin (monolayer) films of Pd in which hydrogen absorption is absent. In addition, to ensure that the substrate on which the Pd film was formed had no influence on the electrochemical hydrogenation reaction, a well-defined Au substrate was employed.

Au(111) and Au(332): Templates for terrace-dominated and step-dominated Pd Sites

Au(332) is essentially a Au(111) surface with a (111) monoatomic step every six (111) terrace atoms [Au-6(111)x(111)]. Previous work had established that electrodeposition of Pd at low coverages onto a Au(332) surface resulted in the formation of Pd adatoms exclusively on the step sites of the Au substrate; deposition of

Pd at monolayer coverages located the additional Pd atoms onto the terrace sites. Hence, EC-MS experiments were conducted at Au(111) and Au(332), the latter coated at low and high coverages of Pd, in order to determine the differences, if any, in the hydrogenation at terrace and kink (step) sites. The electrochemical properties of the pristine and Pd-coated Au(332) have been described in a publication [79] that is reprinted in Appendix C; it should be perused at this point.

Hydrogenation on step- and terrace-dominated Pd surfaces

In an attempt to identify the hydrogenation products of H_2Q on Pd electrodes, EC-MS experiments were performed at Pd modified Au(111) and Au(332) substrates. The use of thin films facilitates the exploration of surface reactions by avoiding any contribution from the bulk. This is an important aspect, for example, in the study of the electrocatalytic hydrogenation on massive Pd substrates because of the complication of hydrogen *absorption*.

Fig. 28 shows the CV and MSCV for the oxidation of H_2Q adsorbed on ultrathin (0.72 ML) Pd films deposited on a Au(332) surface [hereinafter referred to as Au(332)-0.72ML-Pd]. At this coverage, Pd occupies both terrace and step sites. The data in Fig. 28, therefore, represent a combination of the individual results at the two sites. In Fig. 28a, the first potential scan headed in the anodic direction is characterized by a single prominent peak at 0.64 V. This peak, which corresponds to the anodic oxidation of the chemisorbed H_2Q, is considerably, but not completely, diminished in the second anodic cycle. New, less intense peaks emerge, which are attributed to Pd surface-oxide formation. The cathodic peak at 0.69 V is because of the reduction of Au surface-oxide that is formed above 1.0 V. The cathodic peak at 0.24 V arises from the reduction of the Pd surface-oxide. The reversible peaks at *ca*. -0.26 V are due to the hydrogen adsorption-desorption reactions that transpire only on ultrathin Pd films. After several more current-potential scans, a portion of the oxide film dissolves in the acidic electrolyte, and patches of the Au underlayer are exposed. This is evidenced by the fact

the Pd oxide reduction peak at 0.24 V has decreased while the Au-oxide-reduction peak at 0.69 V has increased.

It is well known that the presence of chemisorbed H_2Q suppresses the oxidation of the Pd surface [52]. The Pd-oxide-formation features, during the anodic scan, (Fig. 28a) are regenerated only after multiple cycles which indicate that the oxidative desorption of H_2Q to CO_2 is not complete after just a single anodic scan. That is, other products that are only partially oxidized are generated after the first scan. Since the incompletely oxidized intermediates remain surface-active, they are re-adsorbed upon reversal of the potential scan into the double-layer region where the oxided Pd surface is reverted to its metallic state. This scenario is confirmed by the MSCV data in Fig. 28b. An intense m/z = 44 spectral band indicative of CO_2 appears in a potential region that coincides with the anodic-oxidation signal in Fig. 28a. The CO_2 mass peak observed in the second cycle provides evidence that *i*) ample quantities of only partially oxidized organic remained in the EC-MS thin-layer cell after the first cycle, either adsorbed or desorbed and dissolved into the supporting electrolyte, and *ii*) these species are re-adsorbed upon reversal of the potential scan into the double layer region (where the oxidized Pd is reverted to its metallic state) and oxidized to CO_2 in a subsequent scan. In fact, oxidation is exhaustive only after the third cycle, as shown in Fig. 29.

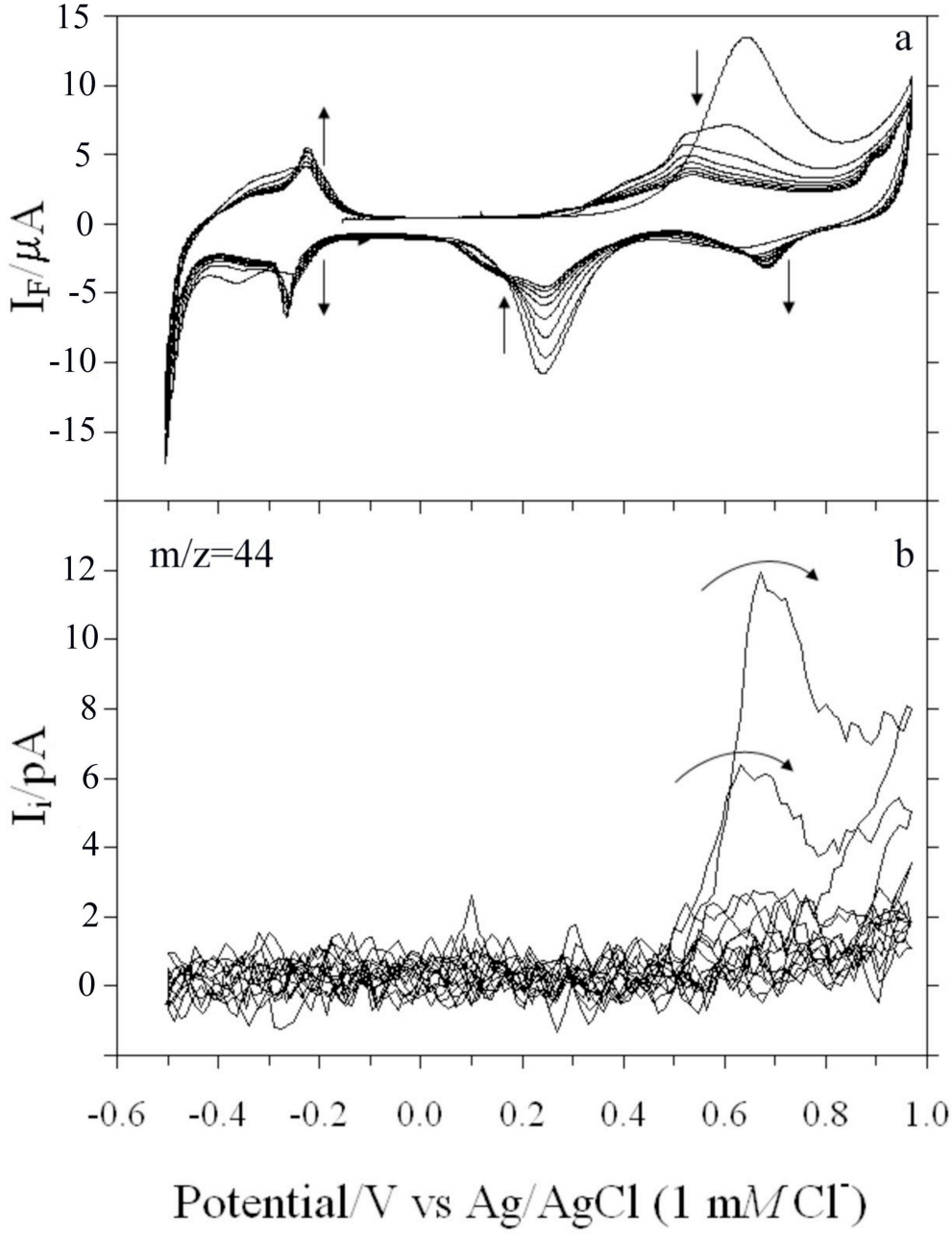

Fig. 28. (a) Thin-layer cyclic current-potential curves, and (b) mass spectrometric cyclic voltammetric (MSCV) curves (m/z = 44, CO_2) for H_2Q chemisorbed on Au(332)-0.72ML-Pd electrodes in H_2Q-free 0.1 *M* H_2SO_4. Scan rate = 10 mV/s. The potential scans were initiated in the anodic direction.

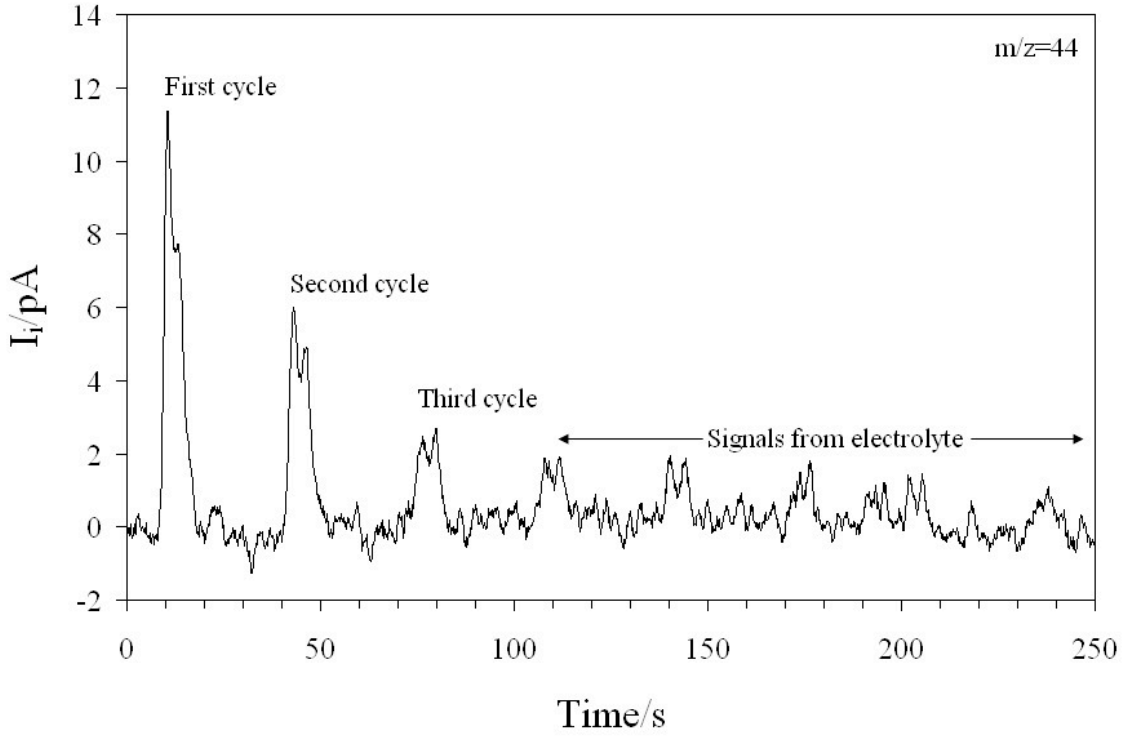

Fig. 29. Ion-current transients of CO_2 (m/z = 44) evolved during the anodic oxidation of H_2Q at Au(332)-0.72ML-Pd (see Fig. 28). Only the areas of the first three peaks were used to calculate the CO_2 yields. The subsequent peaks were identical to those from pure supporting electrolyte. The average area of the latter was taken as background and subtracted from the areas of the first three cycles.

It should be noted that, regardless of the direction of the potential sweep, only CO_2 was detected by EC-MS. In other words, either no other products were formed upon anodic oxidation or reductive hydrogenation of H_2Q or that products are non-volatile and undetectable by EC-MS.

Fig. 30 shows CV and MSCV data for the same Au(332)-0.72ML-Pd electrode after H_2Q chemisorption except that the potential scan is initiated in the cathodic direction. During the initial cathodic excursion, a unique feature is present in the hydrogen adsorption region: a cathodic peak at -0.37 V with a counterpart at -0.34 V during the anodic sweep. Similar features have been observed with chemisorbed benzene on Pt(111) and have been associated with the potential-induced desorption and readsorption of the adsorbate on the packed (111) surface [98]. Because of the presence of this index plane at the terraces of the Pd-modified Au(332) surface and because the structural similarity of benzene with H_2Q, the peak at -0.37 V can be assigned to desorption of H_2Q and the one at -0.34 V to its readsorption on the Pd thin films. No species were detected by EC-MS in this potential region. By continuing the scan in the anodic direction, a prominent peak is observed at 0.63 V. This feature is associated with the anodic oxidation of the adlayer. CO_2 was the only product detected by EC-MS in this potential region (Fig. 30b).

Comparison between Figs. 28 and 30 leaves the following noteworthy features: (i) No MSCV signals can be found in the hydrogen-evolution region regardless of the number of reductive scans. That is, either no hydrogenation has taken place or the reduction products are non-volatile. (ii) Oxidation is exhaustive only after a third scan; 70% of the total CO_2 was generated in the first cycle, and only 10% was produced in the third sweep [Fig. 30b]. (iii) While the *cycle-dependent* relative CO_2 yields were essentially independent of the initial potential-sweep direction, the *total* CO_2 yield was significantly smaller (0.39 nmol/cm^2 *versus* 0.48 nmol/cm^2) if a cathodic scan was first initiated. This last result clearly indicates that part of the organic adlayer is hydrogenated when the potential is scanned in the hydrogen adsorption/evolution region. The fact that no species were detected by EC-MS during the excursion into this potential region only

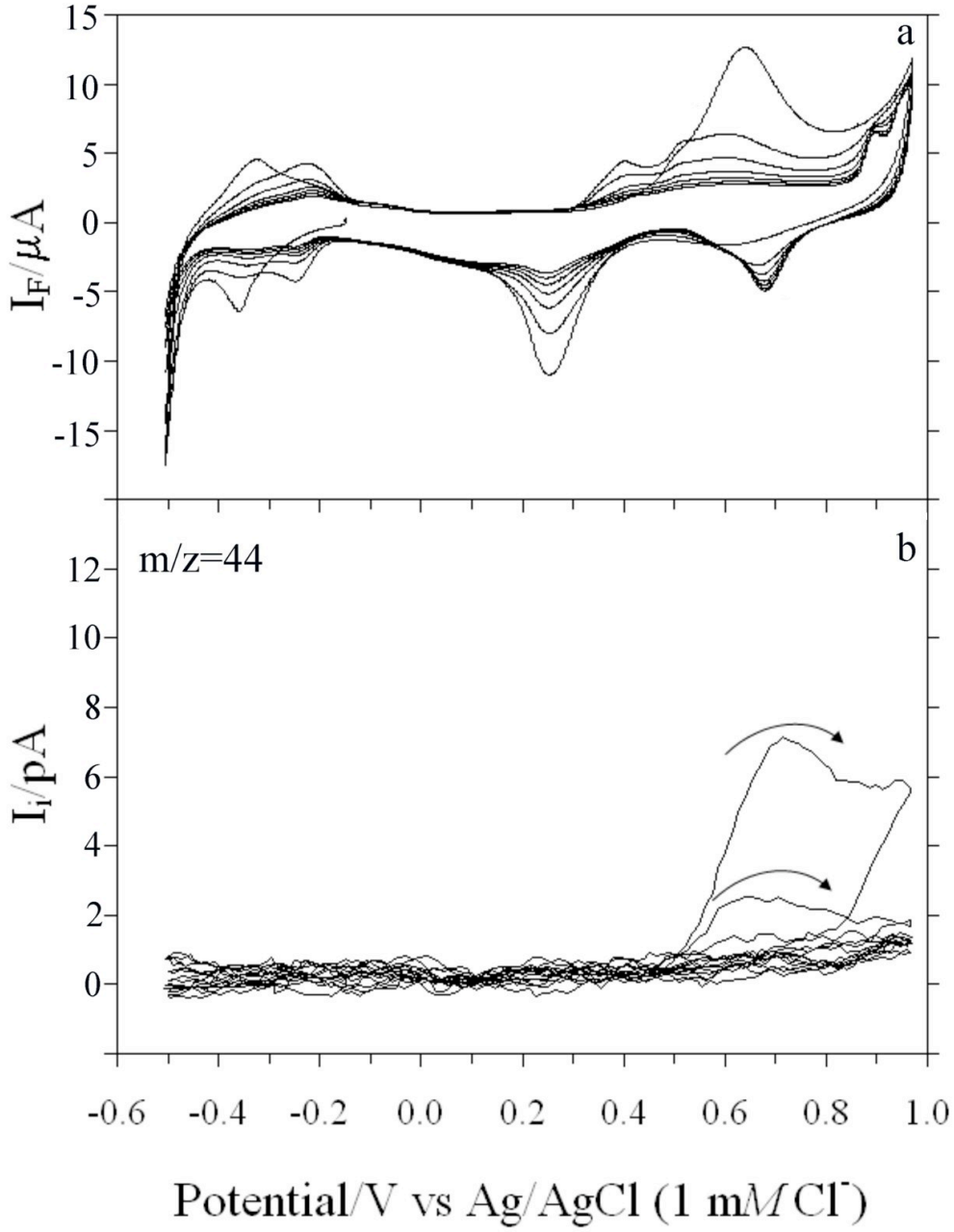

Fig. 30. a) Thin-layer cyclic current-potential curves, and b) mass spectrometric cyclic voltammetric (MSCV) curves (m/z = 44, CO_2) for H_2Q chemisorbed on Au(332)-0.72ML-Pd electrodes in H_2Q-free 0.1 *M* H_2SO_4. Scan rate = 10 mV/s. The potential scans were initiated in the cathodic direction.

confirms the belief that, under the present experimental conditions, the hydrogenation products are either no-volatile enough or they are soluble enough to remain in the aqueous phase. It is noteworthy to mention that an earlier work has documented the formation of 1,4-cyclohexanediol, a non-volatile surface-inactive material, when H_2Q chemisorbed on platinum is electrochemically hydrogenated [38].

An additional experiment was carried out to verify the above postulate that species, which could be oxidized, are desorbed in the hydrogen evolution region. Here, the EC-MS thin-layer cell is rinsed with pure supporting electrolyte while the potential is briefly paused at -0.51 V. CV and MSCV measurements were then undertaken for the ensuing anodic scans. The results are shown in Fig. 31. As in the previous cases, exhaustive oxidation is not attained in only one oxidation cycle. More importantly, there is considerable loss of oxidizable species after the cathodic rinse. This is evident in the morphological changes in the first anodic-oxidation scan (Fig. 31a), as well as in the pronounced decrease in the total CO_2 yield when the electrode was rinsed. It is not known whether desorption is due to hydrogenation or simply to the effect of electrode potential (electro-desorption).

A recent study has shown that electrodeposition of Pd at coverages no higher than 0.2 ML yields an interfacial structure in which the Pd ad-atoms are preferentially located at the step sites of the Au(332) substrate [79,86]. The interfacial properties of Pd adsorbed only at the step sites were investigated at Au(332) modified with 0.14 ML of Pd [Au(332)-0.14ML-Pd] (Fig. 32). The total amount of CO_2 produced is considerably lower; this is to be expected because the coverage of Pd has been decreased, and although H_2Q weakly interacts with roughened Au electrodes when present in solution as demonstrated by surface enhanced Raman spectroscopy [99], H_2Q does not irreversibly chemisorb on pure Au surfaces. As with the results for Au(332)-0.72ML-Pd, exhaustive anodic oxidation was achieved only after multiple anodic cycles. This result may seem to run counter to expectations based solely on the general trend that step sites are more reactive than terrace sites. The similarity of the results for Au(332)-0.14ML-Pd

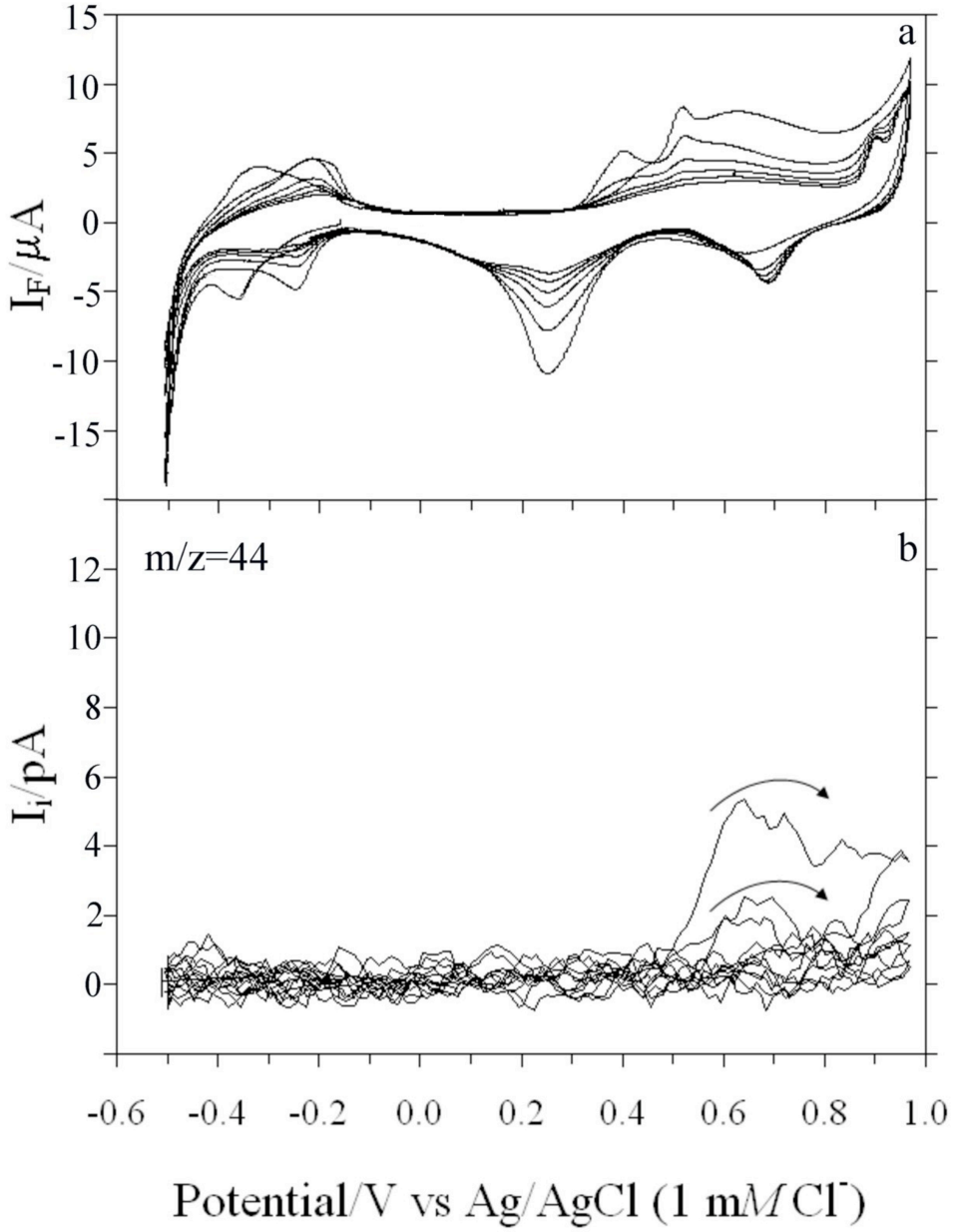

Fig. 31. (a) Thin-layer cyclic current-potential curves, and (b) mass spectrometric cyclic voltammetric (MSCV) curves (m/z = 44, CO_2) for H_2Q chemisorbed on Au(332)-0.72ML-Pd electrodes in H_2Q-free 0.1 *M* H_2SO_4. The potential scan was initiated in the cathodic direction and the EC-MS cell was rinsed at 0.0 V prior to the anodic scans. All other experimental conditions were as in Fig. 28.

and Au(332)-0.72ML-Pd can only signify that the anodic oxidation of aromatic molecules is not a strongly structure-sensitive reaction. Such weak structure-sensitivity may be due to the fact that exhaustive oxidation involves multiple-electron chemical steps that require the participation of surface oxides.

To further investigate the structure sensitivity of the oxidation and hydrogenation reactions, the above experiments were replicated on a Au(111) electrode surface electrodeposited with 0.6 ML of Pd [Au(111)-0.6ML-Pd]. For such a partial Pd coverage, STM images demonstrate that Pd forms large two-dimensional islands [100].

The CV and MSCV results for experiments performed on Au(111) substrates are shown in Figs. 33 and 34. There are close similarities as well as stark differences with the data from the Au(332)-Pd surfaces. The similarities are (i) The H_2Q coverage, as indicated by the total CO_2 yield, closely correlates with the Pd coverage. (ii) CO_2 is the only oxidation product detected by EC-MS. (iii) When the first scan is in the cathodic direction (Fig. 34), no species are detected by EC-MS in the hydrogen evolution region. The differences are (i) The extent of first-anodic-scan oxidation is higher (80 % CO_2) for the Au(111)-Pd electrode than for the Au(332)-Pd electrode (72%). (ii) The cycle-dependent CO_2 yields for the cathodically initiated scans are dramatically lower (56 %) than for the anodically initiated sweeps (80 %). (iii) The cathodic-sweep-induced decrease in total CO_2 yield is slightly higher for Au(332)-Pd (25 %) than for Au(111)-Pd (20 %). Although the anodic oxidation reaction is only weakly structure-sensitive, a possible hydrogenation and desorption reaction in the cathodic sweep is very structure sensitive, leaving a different coverage when the oxidation is started. A further cause may be topographic differences. The Au(111)-Pd surface is much smoother and more compact than the Au(332)-Pd surface; that is, there may be more contiguous uniform sites on the Au(111)-Pd electrode surface.

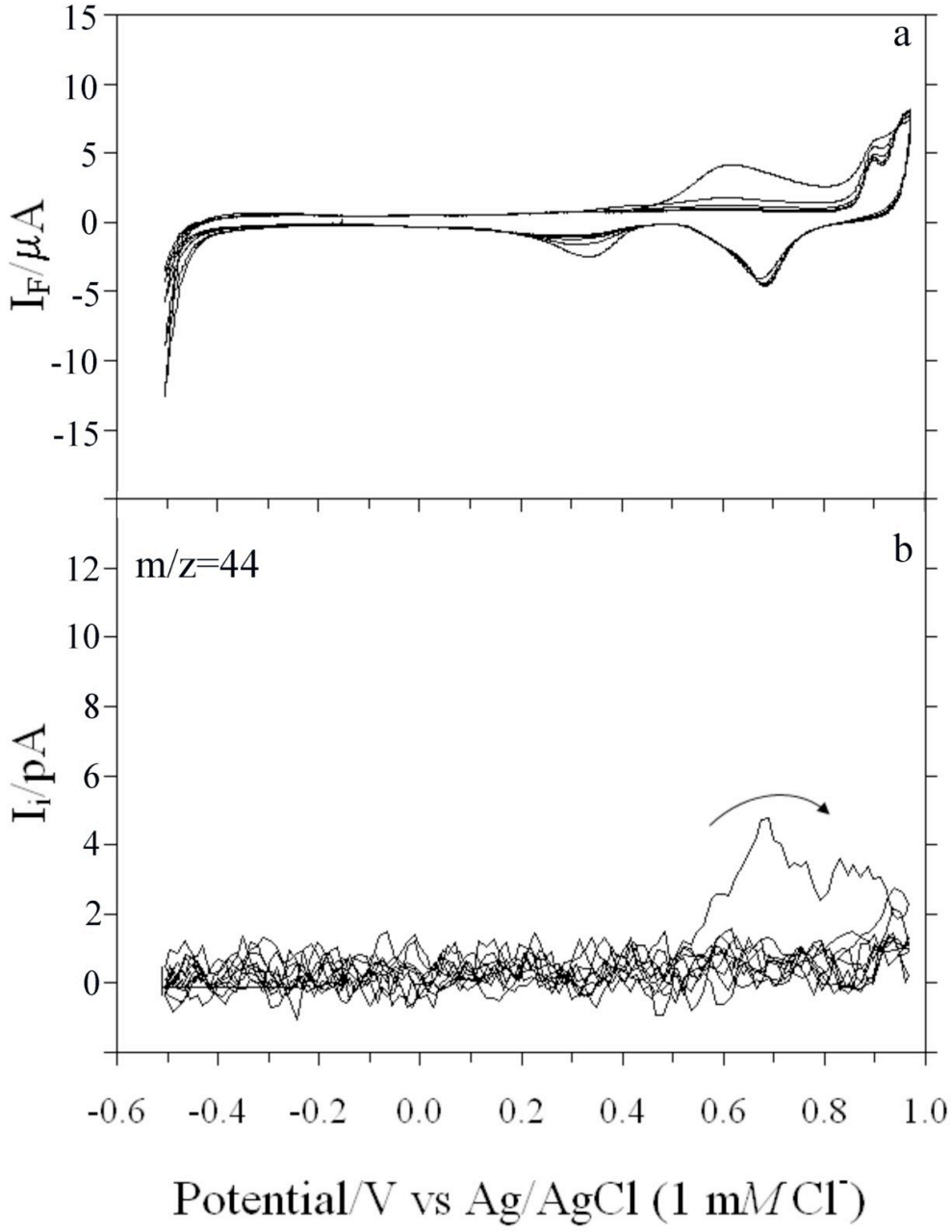

Fig. 32. (a) Thin-layer cyclic current-potential curves, and (b) mass spectrometric cyclic voltammetric (MSCV) curves (m/z = 44, CO_2) for H_2Q chemisorbed on Au(332)-0.17ML-Pd electrodes in H_2Q-free 0.1 *M* H_2SO_4. The potential scan was initiated in the cathodic direction. All other experimental conditions were as in Fig. 28.

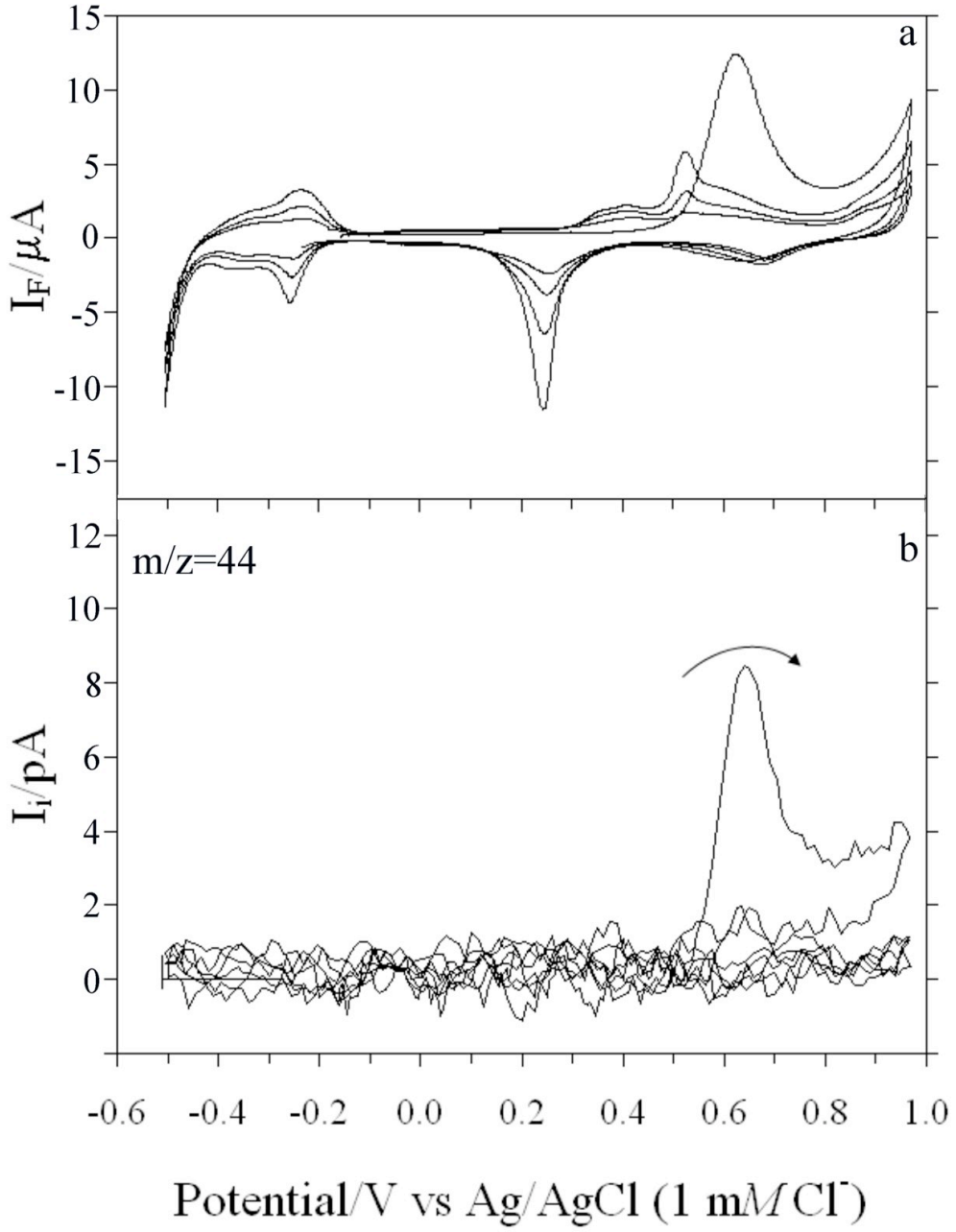

Fig. 33. (a) Thin-layer cyclic current-potential curves, and (b) mass spectrometric cyclic voltammetric (MSCV) curves (m/z = 44, CO_2) for H_2Q chemisorbed on Au(111)-0.60ML-Pd electrodes in H_2Q-free 0.1 *M* H_2SO_4. The potential scan was initiated in the anodic direction. All other experimental conditions were as in Fig. 28.

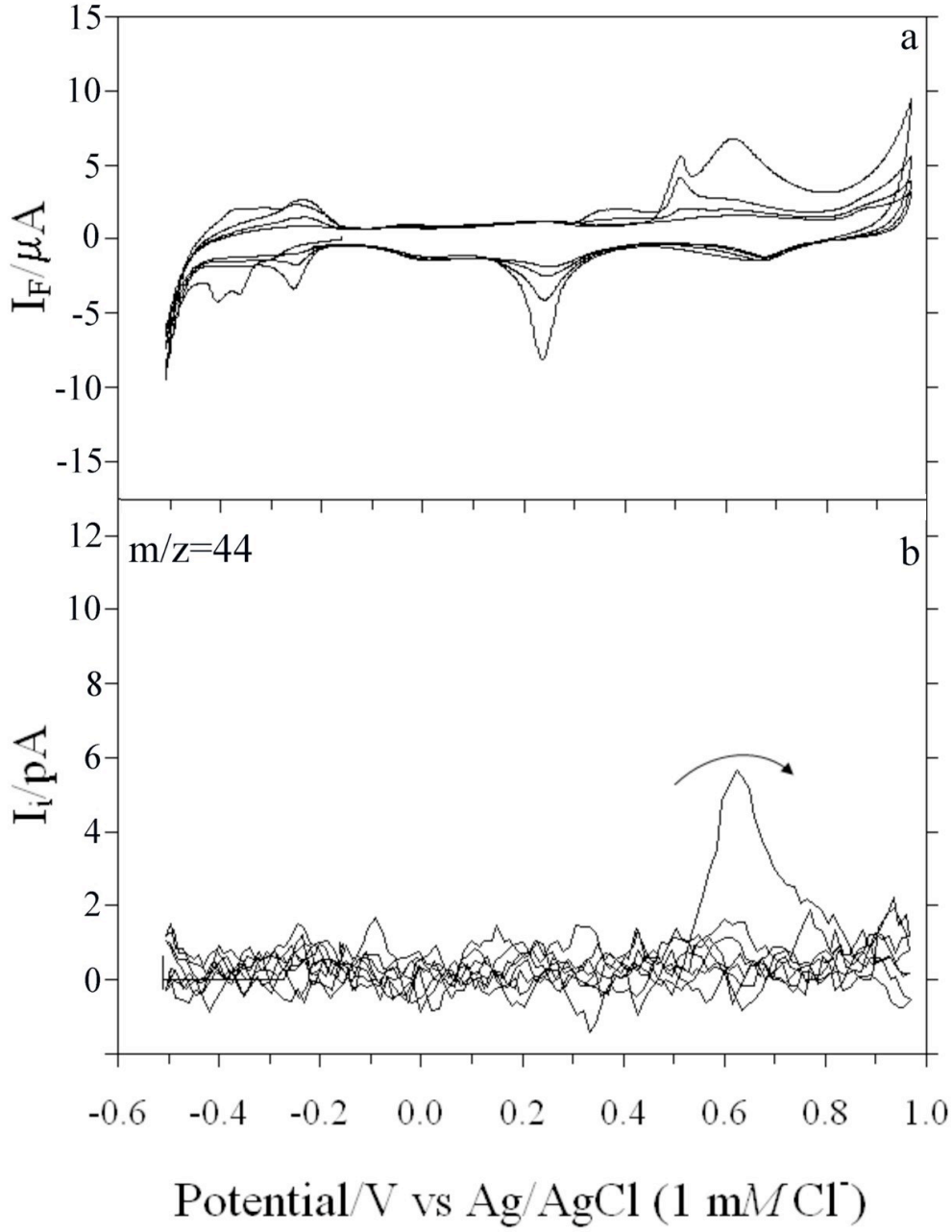

Fig. 34. (a) Thin-layer cyclic current-potential curves, and (b) mass spectrometric cyclic voltammetric (MSCV) curves (m/z = 44, CO_2) for H_2Q chemisorbed on Au(111)-0.60ML-Pd electrodes in H_2Q-free 0.1 *M* H_2SO_4. The potential scan was initiated in the cathodic direction. All other experimental conditions were as in Fig. 28.

Benzene hydrogenation

Benzene is volatile enough to be detectable by EC-MS. Hence, experiments with benzene, similar to those for H_2Q, may shed light into the nature of the desorbed non-CO_2 products. For example, it would be important to know if the original adsorbate can be desorbed, either anodically or cathodically, without damage. Caution with respect to extrapolation of results from benzene to hydroquinone must be practiced. However, adsorbate displacement (substitution) reactions at polycrystalline platinum electrodes have indicated that hydroquinone is more strongly chemisorbed than benzene [17,37]. In other words, just because benzene can be desorbed does not necessarily translate that hydroquinone would behave similarly.

Fig. 35 gives the CV and MSCV curves for benzene at Au(332) modified with 0.82 ML of Pd [Au(332)-0.82ML-Pd]. The only commonality in the voltammetric features for benzene and H_2Q is the prominent anodic-oxidation peak at *ca.* 0.64 V. For benzene, a pronounced anodic peak appears at 0.49 V, which can be attributed to oxidation of bare Pd at terrace sites. The existence of the terrace sites is due to the desorption of benzene itself in the initial cathodic scan. This is indicated by the MSCV data in Fig. 35b which shows m/z = 78 (benzene) spectral peaks in both the cathodic and anodic regions; the benzene mass peak at 0.62 V is approximately 50 % smaller than the peak at -0.46 V (Table 2). No other hydrogenation products were detected by EC-MS, but CO_2 was found at essentially the same potential where benzene is desorbed. At 0.64 V, the anodic oxidation of benzene is accompanied by benzene electro-desorption. It can be inferred from the MSCV for CO_2 and benzene that a greater fraction of benzene is electro-desorbed rather than oxidized; such a conclusion is determined after expressing the MSCV signals for CO_2 in terms of C_6H_6 using the stoichiometric factor $1C_6H_6/6CO_2$. As with hydroquinone, exhaustive oxidation of benzene required at least two anodic cycles; since no species other than CO_2 and benzene were detected by EC-MS, this signifies that partially oxidized, non-volatile materials were produced in the first oxidation cycle of benzene.

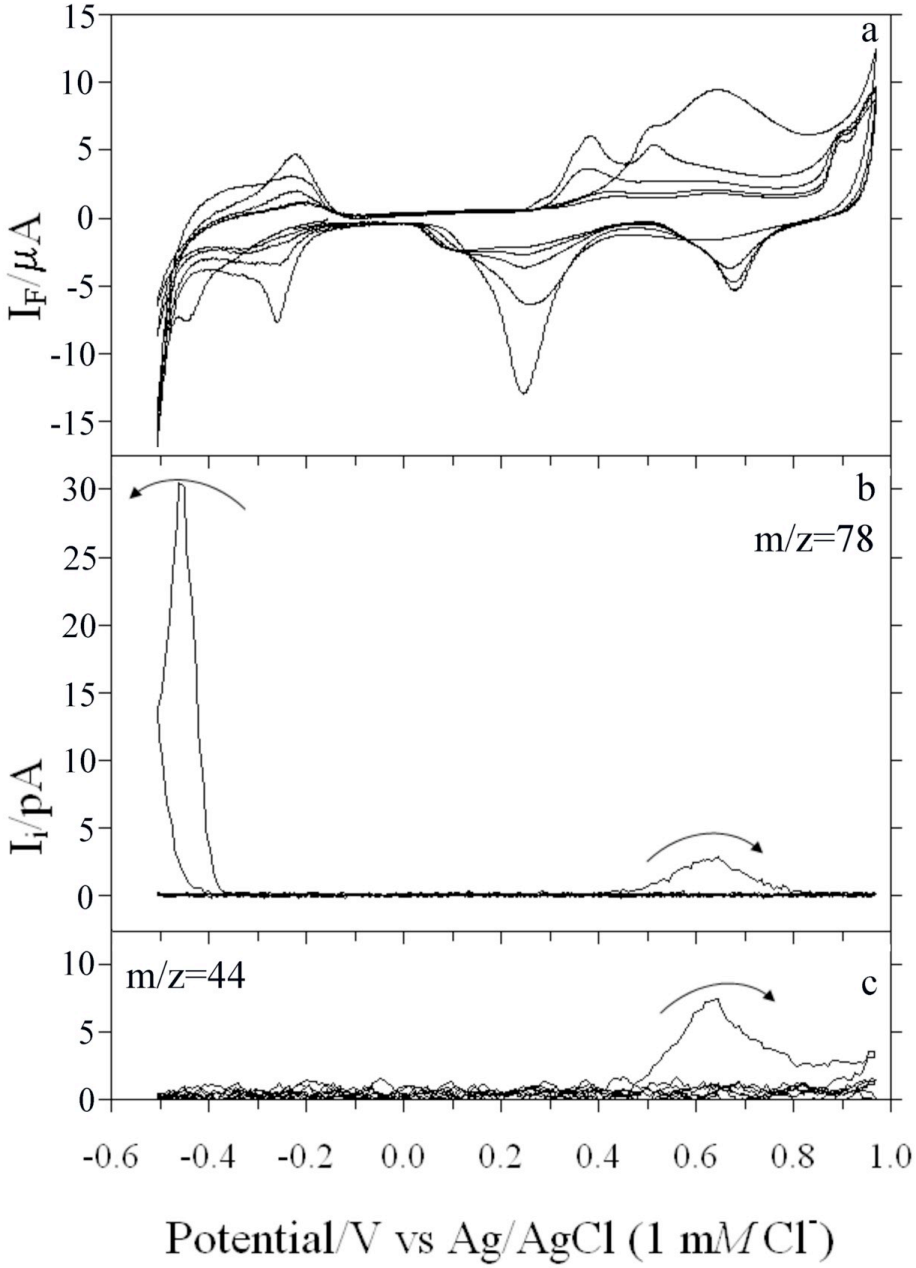

Fig. 35. (a) Thin-layer cyclic current-potential curves, and mass spectrometric cyclic voltammetric (MSCV) curves of (b) benzene (m/z = 78) and (c) CO_2 (m/z = 44) for benzene chemisorbed on Au(332)-0.82ML-Pd electrodes in benzene-free 0.1 *M* H_2SO_4. The potential scan was initiated in the cathodic direction. All other experimental conditions were as in Fig. 28.

The above experiments were repeated with Au(332)-0.14ML-Pd, in which the Pd ad-atoms are exclusively at the step sites. The CV and MSCV results are shown in Fig. 36. The same trends as above are observed for this surface, except for the relative intensities between the benzene mass peaks at -0.46 V and at 0.62 V. With Au(332)-0.82ML-Pd, the ratio of the area under the benzene peak at 0.62 V to that at -0.46 V is 0.65. With Au(332)-0.14ML-Pd, the reverse is true; the ratio of the peak areas is 5.0. This result suggests that electro-desorption of benzene at the lower potential is easier from the terrace sites than from the step sites, but the electro-desorption of benzene at the higher potential is easier from the step sites than from the terrace sites.

Fig. 37 shows CV and MSCV plots for Au(111)-0.6ML-Pd. The results are not too different from those for Au(332)-0.82ML-Pd; in other words, under these two conditions, reactions at the terrace sites predominate. As with the hydroquinone studies, the differences may arise from topographic differences as the smoother Au(111)-Pd contains more contiguous uniform sites than the Au(332)-Pd electrode surface. On all surfaces studied, the amount of CO_2 formed is larger for H_2Q than for benzene, showing that desorption (due to hydrogenation or displacement by either hydrogen or oxygen) is less relevant for H_2Q.

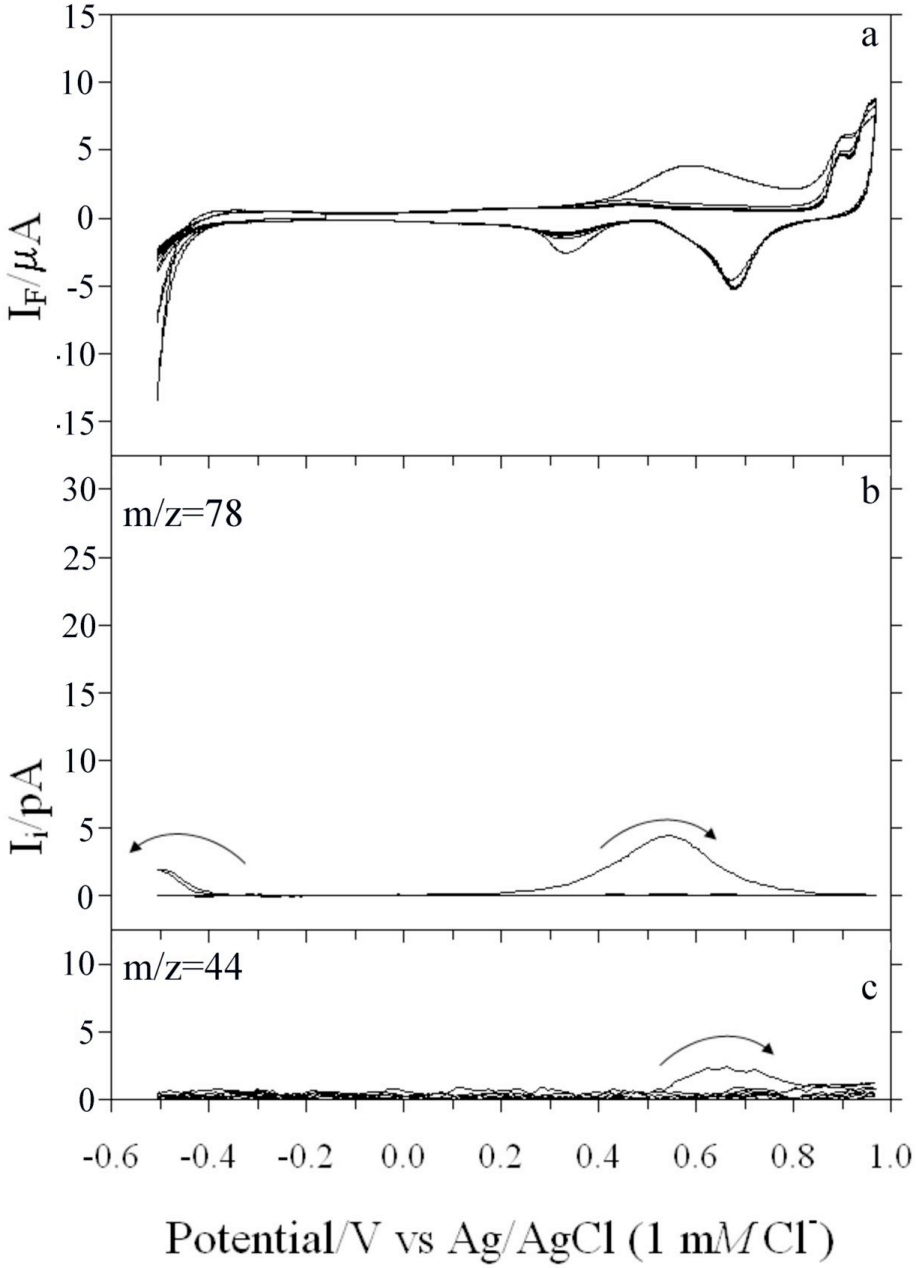

Fig. 36. (a) Thin-layer cyclic current-potential curves, and mass spectrometric cyclic voltammetric (MSCV) curves of (b) benzene (m/z = 78) and (c) CO_2 (m/z = 44) for benzene chemisorbed on Au(332)-0.14ML-Pd electrodes in benzene-free 0.1 *M* H_2SO_4. The potential scan was initiated in the cathodic direction. All other experimental conditions were as in Fig. 28.

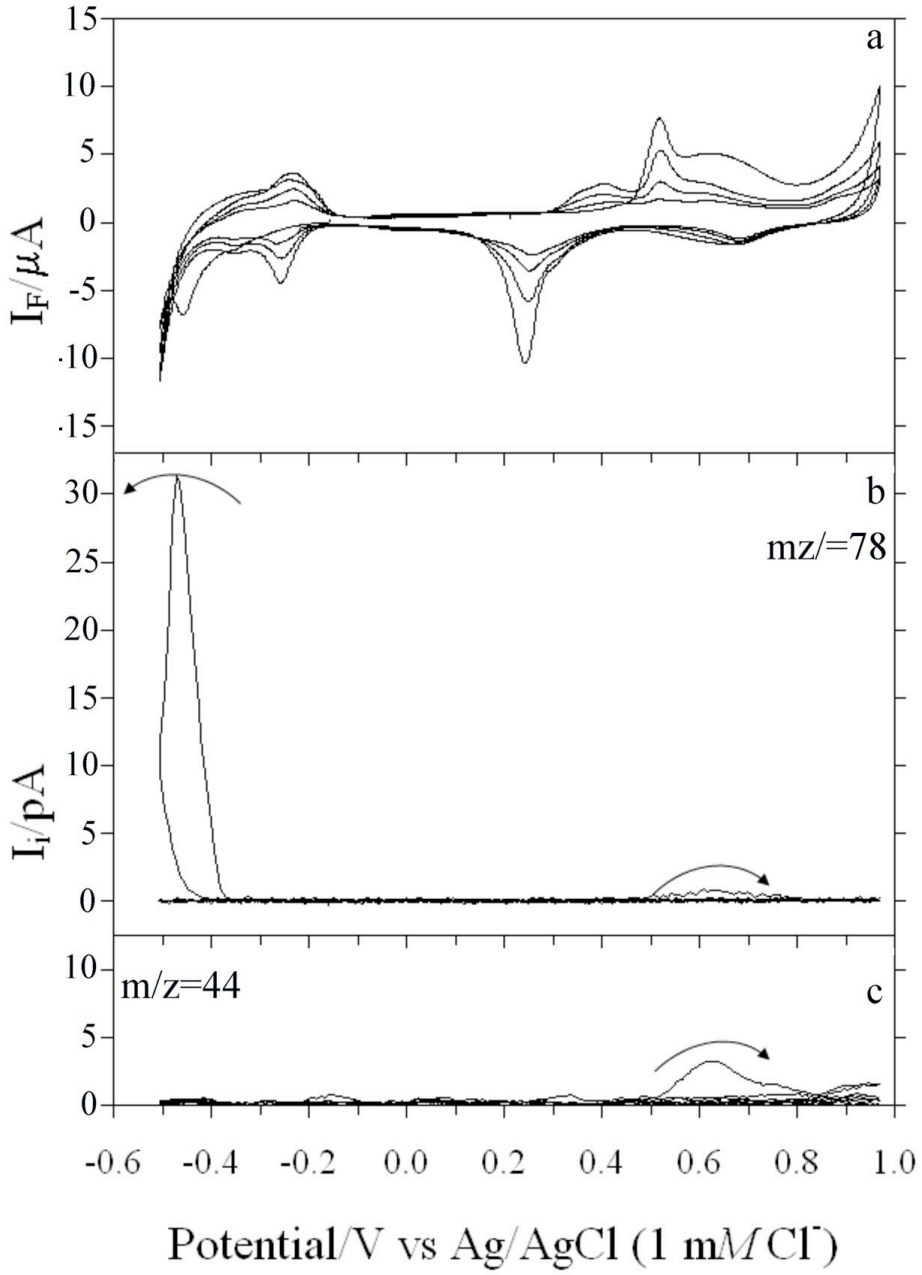

Fig. 37. (a) Thin-layer cyclic current-potential curves, and mass spectrometric cyclic voltammetric (MSCV) curves of (b) benzene (m/z = 78) and (c) CO_2 (m/z = 44) for benzene chemisorbed on Au(111)-0.60ML-Pd electrodes in benzene-free 0.1 *M* H_2SO_4. The potential scan was initiated in the cathodic direction. All other experimental conditions were as in Fig. 28.

CONCLUSIONS

Traditional and thin-layer electrochemistry, ultrahigh vacuum surface spectroscopy, and mass spectrometry were combined to investigate the chemisorption and electrochemical hydrogenation of compounds surface immobilized from dilute aqueous solutions of hydroquinone and benzene onto polycrystalline Pd, well-defined Pd(111), and ultrathin Pd films on Au(111) and Au(332) [Au-6(111)x(111)]; the latter film electrodes mitigated the participation of sub-surface hydrogen and the underlying foreign-metal substrate.

Thin-layer electrochemistry made possible the measurement of absolute surface coverages. Surface vibrational spectroscopy, via normalized integrated band intensities, afforded an independent measure of the relative surface concentrations; more critically, it provided a means by which the molecular identity of the chemisorbed species, prior to and after hydrogenation, could be determined. Mass spectrometry was the basis for the identification of (volatile and hydrophobic) reaction products.

Detailed analysis of the experimental results yielded the following trends and conclusions with respect only to the principal objectives of this dissertation:

Hydroquinone is oxidatively chemisorbed on palladium; at ambient temperatures, it is neither desorbed in ultrahigh vacuum nor rinsed away with pure water. Its mode of chemisorption is a function of aqueous-solution concentration: At concentrations less than 0.1 mM, it is adsorbed as benzoquinone, oriented flat but with a slight tilt; at much higher concentrations, it is chemisorbed in the vertical (edgewise) orientation, most likely as the ortho-di-σ-bonded diphenol.

As in anodic oxidation, the extent of electrochemical hydrogenation is dependent upon the initial orientation. Hydrogenation occurred to a greater extent when the organic was chemisorbed in the flat orientation relative to when it was surface-bonded in the vertical configuration. The degree of electrochemical hydrogenation, as anticipated, was also a function of the applied potential: It increased as the potential was made more negative. Unexpectedly, however, an appreciable fraction of intact starting material

remained on the surface even after potential excursions into the hydrogen evolution region. Neither benzene nor cyclohexane was detected as products of the hydrogenation reaction; chemisorbed benzene itself did not undergo hydrogenation but only potential-induced desorption. Dihydroxycyclohexane, a water-soluble species undetectable by electrochemical mass spectrometry, is most likely the major product; it had earlier been detected in the hydrogenation of hydroquinone chemisorbed on platinum.

The species that remained on the surface after hydrogenation retained its original molecular identity. This indicates that once the hydrogenation of a molecule is initiated, it goes to completion; at least to the extent that the hydrogenation product loses surface activity and is desorbed into solution. This suggests that hydrogenative desorption transpires one molecule at a time. Unreacted diphenol-derived species remain anchored on the surface even in the presence of copious amounts of electrochemically generated hydrogen.

REFERENCES

[1] G. A. Somorjai, Introduction to Surface Chemistry and Catalysis, Wiley, New York (1994).

[2] M.P. Soriaga, Y.-G. Kim, J.E. Soto, in A. Wieckowski (Ed.), Interfacial Electrochemistry: Theory, Experiment, and Applications, Marcel Dekker, New York, 1999.

[3] J. Tsuji, Palladium Reagents and Catalysis: New Perspectives for the 21st Century, second ed., John Wiley & Sons, Chichester, England 2004.

[4] R.A. Sheldon, H. van Bekkum (Eds.), Fine Chemicals through Heterogeneous Catalysis, Wiley-VCH, Weinheim, Germany 2001.

[5] H. Lund, O. Hammerich (Eds.), Organic Electrochemistry, fourth ed., Marcel Dekker, New York 2001.

[6] J.M. Chapuzet, A. Lasia, J. Lessard in: J. Lipkowski, P.N. Ross (Eds.), Electrocatalysis, Wiley-VCH, New York, 1998.

[7] L.L. Miller, L. Christensen, J. Org. Chem. 43 (1978) 2059-2061.

[8] A.M. Couper, D. Pletcher, F.C. Walch, Chem. Rev. 90 (1990) 837-865.

[9] T.Ya. Safonova, N.S. Gulyukina, Yu.V. Novakovskaya, E.A. Astaf'ev, G.N. Bondarenko, O.A. Petrii, G.A. Tsirlina, I.P. Beletskaya, Russ. J. Electrochem. 38 (2002) 515-525.

[10] A. Chagnes, F. Laplante, F. Kerdouss, P. Proulx, H. Ménard, Can. J. Chem. 82 (2004) 641-648.

[11] G.V. Smith, F. Notheisz, Heterogeneous Catalysis in Organic Chemistry, Academic Press, San Diego, CA 1999.

[12] S.J.C. Cleghorn, D. Pletcher, Electrochim. Acta 38 (1993) 425-430.

[13] M.A. Casadei, D. Pletcher, Electrochim. Acta 33 (1988) 117-120.

[14] M.A. Quiroz, F. Córdoba, E. Lamy-Pitara, J. Barbier, Electrochim. Acta 45 (2001) 4291-4298.

[15] T. Mebrahtu, G.M. Berry, M.P. Soriaga, J. Electroanal. Chem. 247 (1988) 241-251.

[16] M.P. Soriaga, A.T. Hubbard, J. Am. Chem. Soc. 104 (1982) 2735-2742.

[17] M.P. Soriaga, E. Binamira-Soriaga, A.T. Hubbard, J.B. Bezinger, K.-W. P. Pang, Inorg. Chem. 24 (1985) 65-73.

[18] A.T. Hubbard, Chem. Rev. 88 (1988) 633-656.

[19] M.P. Soriaga, Chem. Rev. 90 (1990) 771-793.

[20] M.P. Soriaga, P.H. Wilson, A.T. Hubbard, J. Electroanal. Chem. 142 (1982) 317-336.

[21] M.P. Soriaga, A.T. Hubbard, J. Am. Chem. Soc. 104 (1982) 3937-3945.

[22] M.P. Soriaga, J.H. White A.T. Hubbard, J. Phys. Chem. 87 (1983) 3048-3054.

[23] M.P. Soriaga, A.T. Hubbard, J. Phys. Chem. 88 (1984) 1089-1094.

[24] M.P. Soriaga, V.K.F. Chia, J.H. White, D. Song, A.T. Hubbard, J. Electroanal. Chem. 162 (1984) 143-152.

[25] V.K.F. Chia, M.P. Soriaga, A.T. Hubbard, J. Electroanal. Chem. 167 (1984) 97-106.

[26] M.P. Soriaga, J.H. White, D. Song, A.T. Hubbard, J. Electroanal. Chem. 171 (1984) 359-363.

[27] J.H. White, M.P. Soriaga, A.T. Hubbard, J. Electroanal. Chem. 177 (1984) 89-96.

[28] M.P. Soriaga, D. Song, A.T. Hubbard, J. Phys. Chem. 89 (1985) 285-289.

[29] M.P. Soriaga, D. Song, D.C. Zapien, A.T. Hubbard, Langmuir 1 (1985) 123-127.

[30] L.C. Pauling, The Nature of the Chemical Bond, third ed., Ithaca, NY, Cornell University, 1960.

[31] K.P. Pang, J.B. Benziger, M.P. Soriaga, A.T. Hubbard, J. Phys. Chem. 88 (1984) 4583-4586.

[32] E.K. Krauskopf, A. Wieckowski, J. Electroanal. Chem. 296 (1990) 159-169.

[33] M.P. Soriaga, J.L. Stickney, A.T. Hubbard, J. Mol. Cat. 21 (1983) 211-221.

[34] M.P. Soriaga, J.L. Stickney, A.T. Hubbard, J. Electroanal. Chem. 144 (1983) 207-215.

[35] T. Mebrahtu, G.M. Berry, M.P. Soriaga, J. Electroanal. Chem. 239 (1988) 375-386.

[36] B. Bravo, S.L. Michelhaugh, T. Mebrahtu, M.P. Soriaga, Electrochim. Acta 11 (1988) 1507-1511.

[37] M.P. Soriaga, J.H. White, D. Song, V.K. Chia, P.O. Arrhenius, A.T. Hubbard, Inorg. Chem. 24 (1985) 73-79.

[38] Y-P. Gui, T. Kuwana, Langmuir 2 (1986) 471-476.

[39] G.N. Salaita, L. Laguren-Davidson, F. Lu, N. Walton, E. Wellner, D.A. Stern, N. Batina, D.G. Frank, C.-H. Lin, C.S. Benton, A.T. Hubbard, J. Electroanal. Chem. 245 (1988) 253-273.

[40] F. Lu, G.N. Salaita, L. Laguren-Davidson, D.A. Stern, E. Wellner, D.G. Frank, N. Batina, D.C. Zapien, N. Walton, A.T. Hubbard, Langmuir 4 (1988) 637-646.

[41] J.Y. Gui, B.E. Kahn, L. Laguren-Davidson, C.-H. Lin, F. Lu, G.N. Salaita, D.A. Stern, A.T. Hubbard, Langmuir 5 (1989) 819-828.

[42] N. Batina, D.G. Frank, J.Y. Gui, B.E. Kahn, C.-H. Lin, F. Lu, J.W. McCargar, G.N. Salaita, D.A. Stern, D.C. Zapien, A.T. Hubbard, Electrochim. Acta 34 (1989) 1031-1044.

[43] G.N. Salaita, C.-H. Lin, P. Gao, A.T. Hubbard, Arb. J. Sci. Eng. 15 (1990) 319-335.

[44] D. Ren, A.T. Hubbard, J. Colloid. Interace Sci. 209 (1999) 435-441.

[45] J. Inukai, M. Kawisaka, M. Yamagishi, K. Itaya, Langmuir 20 (2004) 7507-7511.

[46] J. Inukai, M. Kawisaka, M. Yamagishi, K. Itaya, J. Electrochem. Soc. 152 (2005) E35-E39.

[47] S.L. Michelhaugh, C. Bhardwaj, G.J. Cali, B.G. Bravo, M.E. Bothwell, G.M. Berry, M.P. Soriaga, Corrosion 47 (1991) 322-328.

[48] Y.-G. Kim, X. Chen, Y.-S. Park, J.H. Baricuatro, J. Sanabria-Chinchilla, M.P. Soriaga, J. Arg. Chem Soc. 91 (2003) 1-22.

[49] Y.-G. Kim, M.P. Soriaga, J. Colloid. Interace Sci. 236 (2001) 197-199.

[50] J.E. Soto, Y.-G. Kim, X. Chen, Y.-S. Park, M.P. Soriaga, J. Electroanal. Chem. 500 (2001) 374-378.

[51] Y.-G. Kim, M.P. Soriaga, Phys. Chem. Chem. Phys. 3 (2001) 3303-3306.

[52] X. Chen, J. Sanabria-Chinchilla, M.P. Soriaga, Electroanalysis 17 (2005) 2121-2127.

[53] J.E. Soto, Y.-G. Kim, M.P. Soriaga, Electrochem. Commun. 1 (1999) 135-138.

[54] A.T. Hubbard, F.C. Anson, in A.J. Bard (Ed.) Electroanalytical Chemistry, A Series of Advances, vol. 4, Marcel Dekker, Inc., New York, 1970.

[55] A.T. Hubbard, D.G. Peters, CRC Crit. Rev. Anal. Chem. 3 (1973) 201-242.

[56] J.F. Rodriguez, T. Mebrahtu, M.P. Soriaga, J. Electroanal. Chem. 233 (1987) 283-289.

[57] A.J. Bard, L.R. Faulkner, Electrochemical Methods: Fundamentals and Applications, second ed., John Wiley & Sons, New York, 2001.

[58] M.P. Soriaga, Prog. Surf. Sci. 39 (1992) 325-443.

[59] D.G. Frank, in: A.T. Hubbard (Ed.), The Handbook of Surface Imaging and Visualization, CRC Press, Boca Raton, FL, 1995, pp. 289-354.

[60] D. Lin-Vien, N.B. Colthup, W.G. Fately, J.G. Grasselli, The Handbook of Infrared and Raman Characteristic Frequencies of Organic Molecules, Academic Press, San Diego, CA, 1991.

[61] E. Maslowski, Vibrational Spectra of Organometallic Compounds, Wiley, New York, 1977.

[62] J. Jungwirthova, L.L. Kesmodel, J. Phys. Chem. B 105 (2001) 674-680.

[63] L.E. Davis, N.C. MacDonald, P.W. Palmberg, G.E. Riach, R.E. Weber (Eds.), Handbook of Auger Electron Spectroscopy, A Reference Book of Standard Data for Identification and Interpretation of Auger Electron Spectroscopy Data, second ed., Physical Electronics Industries, Inc., Eden Prairie, MN, 1976.

[64] J.T. Grant, T.W. Haas, Surf. Sci. 42 (1974) 1-11.

[65] H. Baltruschat, in A. Wieckowski (Ed.), Interfacial Electrochemistry: Theory, Experiment, and Applications, Marcel Dekker, New York, 1999.

[66] H. Baltruschat, J. Am. Soc. Mass Spectrom. 15 (2004) 1693-1706.

[67] O. Wolter, J. Heitbaum, Ber. Bunsenges. Phys. Chem. 88 (1984) 2-6.

[68] O. Wolter, J. Heitbaum, Ber. Bunsenges. Phys. Chem. 88 (1984) 6-10.

[69] T. Hartung, H. Baltruschat, Langmuir. 6 (1990) 953-957.

[70] T. Hartung, U. Schmiemann, I. Kamphausen, H. Baltruschat, Anal. Chem. 63 (1991) 44-48.

[71] U. Schmiemann, H. Baltruschat, J. Electroanal. Chem. 347 (1993) 93-109.

[72] Th. Löffler, R. Bussar, E. Drbalkova, P. Janderka, H. Baltruschat, Electrochim. Acta, 48 (2003) 3829-3839.

[73] U. Schmiemann, Z. Jusys, H. Baltruschat, Electrochim. Acta. 39 (1994) 561-576.

[74] Th. Löffler, E. Drbalkova, P. Janderka, P. Konigshoven, H. Baltruschat, J. Electroanal. Chem. 550-551 (2003) 81-92.

[75] J. Vestral, Th. Löffler, U. Müller, H. Baltruschat, J. Electroanal. Chem. 461 (1999) 90-93.

[76] J. L. Rodríguez, R. M. Souto, S. González and E. Pastor, Electrochim. Acta 44 (1998) 1415-1422.

[77] R. M. Souto, J. L. Rodríguez, L. Fernández-Mérida, E. Pastor, J. Electroanal. Chem. 494 (2000) 127-135.

[78] R. M. Souto, J. L. Rodríguez, G. Pastor, E. Pastor, Electrochim. Acta 45 (2000) 1645-1653.

[79] F. Hernandez, J. Sanabria-Chinchilla, M.P. Soriaga, H. Baltruschat, Proc. Electrochem. Soc. 18 (2005) 15-24.

[80] J. Sanabria-Chinchilla, M.P. Soriaga, R. Bussar, H. Baltruschat, J. Appl. Electrochem. (2005) accepted.

[81] J. Willsau, J. Heitbaum, Electrochim. Acta 31 (1986) 943-948.

[82] J. Clavilier, R. Albalat, R. Gomez, J.M. Orts, F.M. Feliu, A. Aldaz, J. Electroanal. Chem. 330 (1992) 489-497.

[83] A. Hamelin, J. Electroanal. Chem. 407 (1996) 1-11.

[84] A. Hamelin, A. M. Martins, J. Electroanal. Chem. 407 (1996) 13-21.

[85] U. Schmiemann, Z. Jusys, H. Baltruschat, Electrochim. Acta. 39 (1994) 561-576.

[86] F. Hernandez, H. Baltruschat, Langmuir 22 (2006) 4877-4884.

[87] K. Sashikata, Y. Matsui, K. Itaya, M. P. Soriaga, J. Phys. Chem. 100 (1996) 20027-20034.

[88] W. Alcalay, Helv. Chim. Acta 30 (1947) 578-584.

[89] M.E. Bothwell, Ph.D. dissertation, Texas A&M University, 1991.

[90] X. Chen, Ph.D. dissertation, Texas A&M University, 2004.

[91] F.C. Henn, A.L. Diaz, M.E. Bussell, M.B. Hugenschmidt, M.E. Domagala, C.T. Campbell, J. Phys. Chem. 96 (1992) 5965-5974.

[92] J.S. Luo, R.G. Tobin, D.K. Lambert, Chemical Physics Letters 204 (1993) 445-450.

[93] D.K. Lambert, Electrochim. Acta 41 (1996) 623-630.

[94] D.K. Lambert, Solid State Communications 51 (1984) 297-300.

[95] J.S. Luo, R.G. Tobin, D.K. Lambert, G.B. Fisher, C.L. DiMaggio, Surface Science 274 (1992) 53-62.

[96] H. Wang, R.G. Tobin, D.K. Lambert, G.B. Fisher, C.L. DiMaggio, J. Chem. Phys. 103 (1995) 2711-2718.

[97] K. Hermansson, J. Chem. Phys. 99 (1993) 861-868.

[98] M. DeBlois, J. Lessard, G. Jerkiewicz, Electrochim. Acta 50 (2005) 3517-3523.

[99] H. Baltruschat, N. Staud, J. Heitbaum, J. Electroanal. Chem. 239 (1988) 361-374.

[100] L.A. Kibler, M. Kleinert, R. Randler, D.M. Kolb, Surf. Sci. 443 (1999) 19-30.

APPENDIX A
THE USE OF THIN-LAYER ELECTROANALYSIS IN THE STUDY OF THE CHEMISORPTION AND ANODIC OXIDATION OF AROMATIC MOLECULES AT SMOOTH POLYCRYSTALLINE PALLADIUM*

Xiaole Chen, Jean Sanabria-Chinchilla, Manuel P. Soriaga†
Department of Chemistry, Texas A&M University, College Station, TX 77843, USA
†e-mail: M-Soriaga@tamu.edu

Received: April 17, 2004
Accepted: November 15, 2004

Abstract

Thin-layer electroanalytical chemistry has been used in the study of the chemisorption and anodic oxidation of hydroquinone and benzoquinone at smooth polycrystalline palladium electrode surfaces in aqueous sulfuric acid solutions. The results were reminiscent of those obtained previously on smooth polycrystalline platinum: i) At low aqueous-solution concentrations, the diphenol is oxidatively chemisorbed to form surface-coordinated benzoquinone oriented parallel to the surface. ii) At higher concentrations, the oxidative chemisorption occurs via C-H activation to yield an edge-oriented diphenolic species. iii) Chemisorption from benzoquinone solutions leads to species identical to those from hydroquinone solutions. iv) The extent of anodic oxidation of the chemisorbed organic depends upon the initial adsorbed-molecule orientation: the flat-adsorbed species are oxidized completely to carbon

* Reprinted from Electroanalysis, vol. 17, no. 23, X. Chen, J. Sanabria-Chinchilla, M.P. Soriaga, The Use of Thin-Layer Electroanalysis in the Study of the Chemisorption and Anodic Oxidation of Aromatic Molecules at Smooth Polycrystalline Palladium, pp. 2121-2127.

dioxide, whereas oxidation of the edge-chemisorbed species yields other (unidentified) products that are chemisorbed upon regeneration of the oxide-free surface.

Keywords: Chemisorption of aromatic molecules, Electrocatalytic oxidation, Palladium electrodes, Electrochemical surface science, Surface science of electrocatalysis

Introduction

We have long been interested in the chemistry of homogeneous molecular and cluster organometallic compounds or coordination complexes as models for the interactions of organic molecules with pure and mixed-metal surfaces [A1,A2]. In this regard, we have examined the surface-coordination properties of noble-metal electrodes when exposed to aqueous solutions that typical preselected surface-active functional groups; such groups range from simple halides [A3] to more complex aromatic molecules [A4,A5]. Indeed, at least in terms of modes of binding and strengths of chemisorption, we found a distinct correlation between the homogeneous and the interfacial systems [A5,A6]. For example, benzene was found to be inert towards Au but was quite strongly chemisorbed on the platinum metals [A7]; such behavior is identical to what have been reported in the organometallic literature [A8]. In addition, the chemisorption of catechols and hydroquinones from low concentrations in aqueous solutions occurred oxidatively to form surface-coordinated quinones [A2,A5]; the latter are exactly the same as when benzoquinone is coordinated to zerovalent Pt [A9].

With direct relevance to electrocatalysis [A10-A12], we then sought to investigate the anodic oxidation [A13] and cathodic hydrogenation [A14] of the aromatic compounds at polycrystalline Pt [A15]. One intriguing result was that the product distributions were strongly dependent on the initial adsorbate orientation. For instance, anodic oxidation of edge-adsorbed diphenols yielded products less oxygenated than CO_2; in comparison, only CO_2 was generated from the oxidation of flat-adsorbed analogues [A13].

It will be mentioned that, whereas copious amounts of work have been reported on the anodic oxidation of small organic molecules such as carbon monoxide, formic acid and methanol [A10-A12,A16], studies by other investigators [A17] similar to the present work on the more complex organic molecules are rather limited. In addition, while the use of thin-layer electroanalytical techniques [A18] to characterize solution species is not novel, its adoption as a tool in electrochemical surface science, specifically in the study of electrocatalytic reactions, is not conventional. We describe such utility in this manuscript.

Thin-Layer Electroanalysis in Surface Electrochemistry

Measurement of Absolute Surface Concentrations and Adsorbed-Molecule Orientations [A19,A20]

Such measurement takes advantage of the fact that the redox (quinone-diphenol) chemistry of the unadsorbed H_2Q (or BQ) is vastly different from that of the irreversibly adsorbed species [A4,A5,A9,A21]. Hence, the difference between the H_2Q (or BQ) concentration in the bulk solution and inside the thin-layer cell (immediately after chemisorption) is a measure of the amount of organic that is coordinated to the surface.

Introduction of a single aliquot of sample solution into the thin-layer cell introduces a precise amount of solute. If the bulk solute concentration (C^o) were low, a major fraction of the solute would be chemisorbed onto the clean surface; as a result, there is a substantial decrease in the solute concentration (C) inside the thin-layer cavity:

$$VC = VC^o - A\Gamma \qquad \text{(A1)}$$

where Γ (mol/cm^2) is the absolute surface concentration of the chemisorbed organic. If (Q1-Q1b) is the background corrected electrolytic charge for the diphenol-to-quinone (or quinone-to-diphenol) reaction after only one aliquot. Faraday's Law can be written as:

$$Q - Q_{1b} = 2FVC = 2F(VC^o - A\Gamma) \quad \text{(A2)}$$

If the thin-layer cavity is then flushed and refilled with a second (fresh) aliquot, the solute concentration inside the cell should equal that in the bulk, provided the electrode surface had been saturated with organic after the first aliquot. Faraday's Law, under these conditions, is given by:

$$Q - Q_b = nFVC^o \quad \text{(A3)}$$

An expression for the surface coverage is derived when Eq. A2 is subtracted from Eq. A3:

$$\Gamma = \frac{(Q - Q_b) - (Q_1 - Q_{1b})}{nFA} \quad \text{(A4)}$$

In general, Q_b and Q_{1b} are identical since, in both cases, the electrode surface contains the same amount of chemisorbed material and no unadsorbed species exist in solution.

If Γ is known, the adsorbed-molecule orientation can be deduced from a comparison of the measured molecular cross sections (σ) with those calculated for all possible orientations. Γ is inversely proportional σ.

$$\sigma = \frac{10^{16}}{N_A\Gamma} \quad \text{(A5)}$$

where σ is in units of $Å^2$ and N_A is Avogadro's number.

In order to vault from σ data to conclusions about molecular orientation, the surface area occupied by a single adsorbed molecule must be calculated for each possible orientation; the calculated value σ_{calc} closest to the measured σ would then

indicate the most probable adsorbed-molecule orientation. Applicable σ-calculation methods have been described and tested by numerous workers [A22]. The approach adopted in this study is based upon molecular models, constructed from tabulated [A23] covalent and van der Waals radii; it has long been noted that the cross-section of the rectangular parallelepiped, which just encloses the model closely approximates the actual area occupied by an adsorbed molecule [A24]. Details on this approach can be found elsewhere [A20].

Characterization of the Anodic Oxidation of Chemisorbed Species [A25,A26]

The extent of the anodic oxidation may be monitored in terms of n_{ox}, the average number of electrons transferred during electrocatalytic oxidation; this parameter can be identified with an effective stoichiometry of the oxidation reaction,

$$\text{Organic}_{(\text{ads})} \rightarrow \text{Oxidation products} + n_{ox}\text{e}^- \qquad \text{(A6)}$$

The n_{ox} value can be determined if the surface coverage and the background-corrected anodic oxidation charge $(Q_{ox} - Q_{ox,\,b})$ are known:

$$n_{ox} = \frac{(Q_{ox}-Q_{ox,\,b})}{FA\tilde{A}} \qquad \text{(A7)}$$

In Eq. A7, Q_{ox} is the Faradaic charge for the anodic oxidation of the adsorbed organic, and $Q_{ox,\,b}$ is the background charge due only to surface-oxide formation. On polycrystalline Pt, the value of n_{ox} has been shown to be orientation-dependent: Aromatic molecules chemisorbed in the flat orientation yield n_{ox} values indicative of complete oxidation to CO_2; lower values are indicated by molecules chemisorbed vertically [A25,A26].

An additional advantage in the use of thin-layer electrochemistry in the study of electrocatalysis is the fact that products generated from the reaction are retained inside

the thin-layer cell. We have utilized this advantage as an independent probe of the extent of anodic oxidation. If only CO_2 were produced from the reaction, a subsequent voltammetric scan (after reduction of the oxidized metal surface) would indicate a clean (organic-free) electrode surface since CO_2 is a surface-inert material; if the extent of oxidation were lower, an anodic-oxidation peak would be observed due to the re-adsorption of the oxidatively unsaturated (non-CO_2) products.

Experimental

The fabrication and utilization of thin-layer electrochemical cells have been described in detail elsewhere [A27]. In such cells, the electrolyte solution resides inside the thin (ca. 40 mm) space between a cylindrical electrode and the glass wall that surrounds it; the volume of the cavity, as calibrated by coulometry with an Fe^{2+} solution of known concentration, was 3.56 mL. Located near the tip of the cell are two tiny pinholes through which the spent solution is removed when pressurized gas (N_2) is passed through it. The thin-layer cavity is refilled with fresh solution by capillary action after the N_2 flow is stopped.

The Pd electrode used in this study was fabricated from a 99.99%-pure Pd rod (Wilkinson Co., WestlakeVillage, CA). The surface was metallographically polished with successive finer grades of diamond paste (Beuhler Ltd., Evanston, IL) to a near-mirror finish. The electrode billet was thermally annealed to redness in a hydrogen-oxygen flame, and then quenched in Milli-Q Plus water (Millipore Systems, Houston, TX). This preparative procedure renders the surface “atomically smooth”, with less than 5% surface roughness [A28]. In this study, the surface area of the Pd electrode (1.26 cm^2) was taken from its geometric area with an allowance for a surface roughness factor of 1.05. A more accurate determination is hampered by the facts that, unlike Pt, there is no hydrogen chemisorption on Pd, and surface-area quantization by adsorbed-iodine oxidation [A28] results in the anodic dissolution of Pd [A29].

The experiments were performed with a commercial potentiostat, BAS CV-27 (Bioanalytical Systems Inc.,West Lafayette, IN). Unless otherwise stated, electrode

potentials are reported against a Ag/AgCl (1.0 M Cl^-) reference electrode; a Pt wire was used as the auxiliary electrode. The supporting electrolyte was 1 M H_2SO_4, prepared from fuming sulfuric acid (Aldrich Chemicals, Milwaukee, WI). Analytical-grade hydroquinone (Aldrich Chemicals, Milwaukee, WI) was employed as received; benzoquinone was sublimed prior to its use. All solutions were prepared with Milli-Q Plus water.

Results and Discussion

Chemisorption

The cyclic voltammogram of a clean, thermally annealed Pd electrode in organic-free 1 M H_2SO_4 solution was as expected from previous studies: Surface oxidation was initiated at 0.47 V and the oxide-reduction peak was at 0.44 V; the hydrogen evolution reaction occurred below 0.1 V. The current – potential curves for a polycrystalline Pd electrode after single and multiple aliquots of 0.1 mM H_2Q + 1 M H_2SO_4 were introduced into the thin-layer cavity are shown in Fig. A-1. The peak at 0.46 V arises from the two-electron, two-proton oxidation of the unadsorbed H_2Q to unadsorbed BQ (see Scheme A1).

The oxidation peak obtained after introduction of only a single aliquot of diluteH_2Q is dramatically smaller than that obtained after multiple aliquots (after the electrode surface was saturated with organic). The diminution of the peak after only one aliquot is, as previously indicated, due to formation of redox-inert chemisorbed species.

Surface coverage (Γ) measurements, based upon Eq. A4 and the data in Fig. A-1, for various H_2Q or BQ solution concentrations are expressed in Fig. A-2 in terms of chemisorption isotherms (Γ vs. log C plots). The near identity of the plots for H_2Q and BQ is obvious. Although similar results were obtained previously on polycrystalline Pt [A13,A15], there are nonsubtle differences in the morphologies of the isotherms for Pt and for Pd: i) In Fig. A-2, the existence of a Γ-plateau at concentrations below 0.1 mM is not clearly defined for Pd as it is for Pt. ii) For Pt, the transition between the lower and upper Γ-plateaus is rather sharp; that for Pd is not as abrupt.

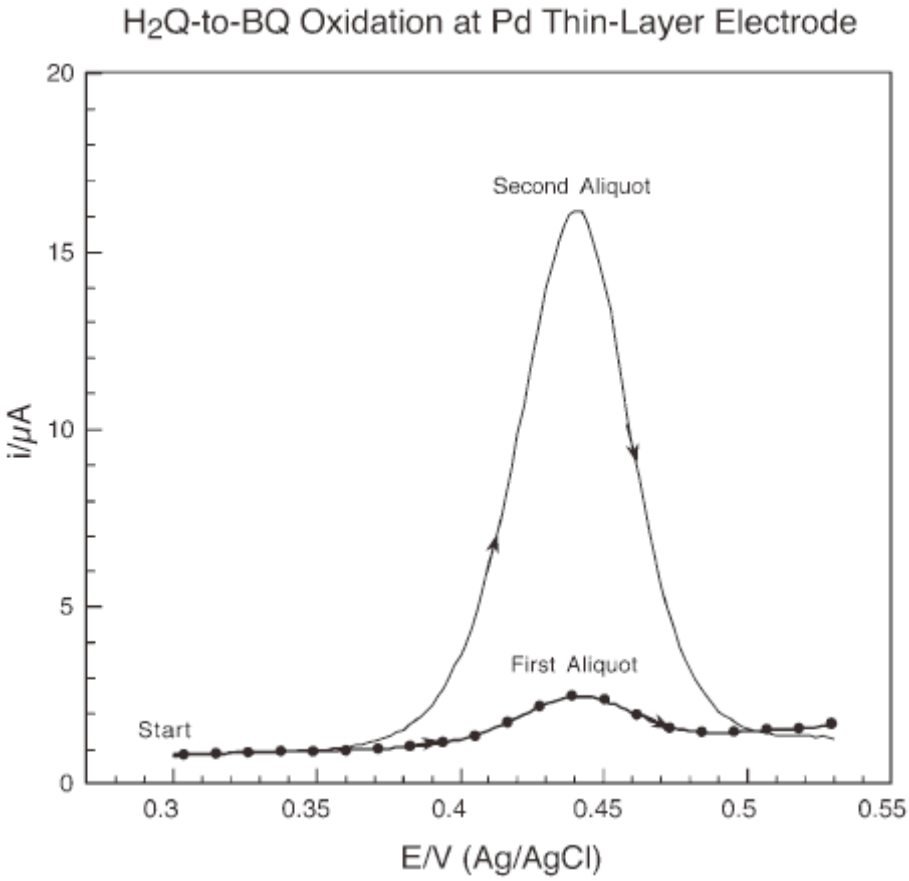

Fig. A-1. Current – potential curves for a smooth polycrystalline Pd electrode in a thin-layer cell for i) the first, and ii) the second aliquot (filling) of 0.1 mM H_2Q in 1M H_2SO_4. Volume of thin layer cell, V = 3.56 μL, electrode surface area, A = 1.26 cm^2, scan rate, r = 2 mV s^{-1}, and temperature, T = 298 K.

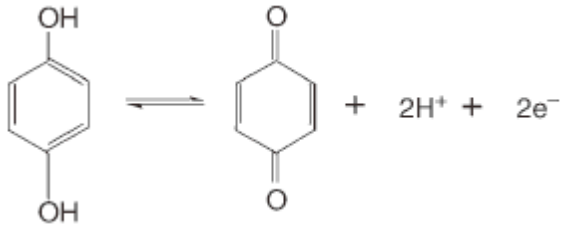

Scheme A1.

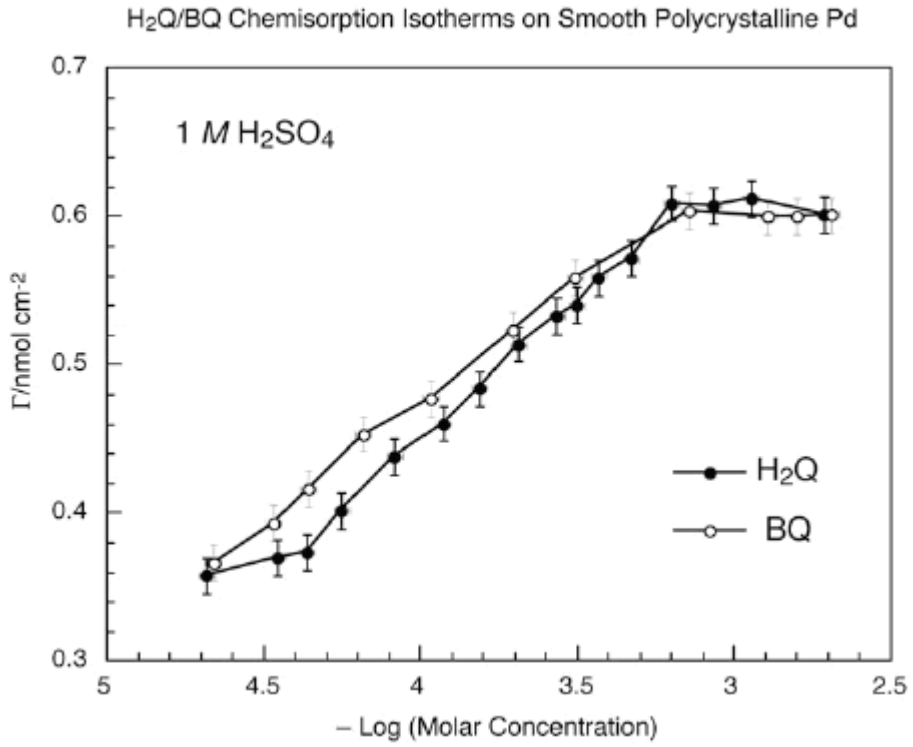

Fig. A-2. Chemisorption isotherms, Γ vs. log C plots, for H_2Q and BQ solutions at a smooth polycrystalline Pd electrode. The solid lines merely interconnect the data points and do not imply any theoretical fit. Experimental conditions were as described in the text and in Fig. A-1.

Nevertheless, as with Pt, the two plateaus in the chemisorption isotherm can be rationalized in terms of the orientations of the molecules in the chemisorbed layer. Earlier studies based upon surface-coverage measurements and infrared reflection-absorption spectroscopy of H_2Q chemisorbed on Pt had demonstrated that, in the low concentration region, the molecules are surface-attached in a parallel (η^6) orientation, whereas at much high-concentrations, the aromatic is adsorbed in an edge-vertical (η^2) orientation [A13,A15,A25,A26].

The experimental cross-section s obtained in the high concentration plateau, 27.5 $Å^2$ [cf., Eq. A5] is suggestive of an edge-vertical (2,3-η^2) orientation, σ_{calc} = 28.6 $Å^2$, in which the 2,3-C-H bonds are activated to form two C-Pt bonds and gaseous H_2. These observations are in agreement with published results on Pt [A13,A15,A25,A26]. Since the plateau at the lower-concentration region is not sharply defined, only the lowest Γ value obtained was used to extract σ, 46.5 $Å^2$. The latter is smaller than that obtained for Pt (52.7 $Å^2$) as well as that calculated for a completely flat (η^6)-oriented species (53.8 $Å^2$). Such deviation suggests that the species chemisorbed from low concentrations are not fully parallel to the surface but are slightly tilted. Support for this claim can be gleaned from high-resolution electron energy loss spectroscopy (HREELS) of H_2Q and BQ chemisorbed on Pd(111) and Pd(100) surfaces: the spectra showed an in-plane C–H stretch mode which, if the molecules were completely parallel to the surface, would have been inactive [A30]. Apropos to this issue is the fact that detailed analysis of the HREELS spectra points to the existence of benzoquinone (not hydroquinone) in the η^6 orientation, regardless of whether H_2Q or BQ was the starting material [A31]; that is, chemisorption of H_2Q occurs oxidatively to yield chemisorbed BQ in which adsorbate–substrate interactions occur through the π-system of the quinonoid ring [A13,A15,A25,A26].

No vibrational data are available for the η^2-oriented aromatic on Pd. However, i) the surface IR spectra for the η^2 species on Pt [A32] indicated that the adsorbed species is diphenolic with the (activated) 2,3-carbons bound to the surface, and ii) the chemisorption-induced rest-potential shifts observed for Pd were virtually identical to

those for Pt. Hence, the same oxidative chemisorption processes on Pt were deemed to occur also on Pd; that is, 2,3-η^2-HQ is formed at higher concentrations on either Pd or Pt.

Anodic Oxidation

Earlier studies on Pt electrodes revealed that the anodic oxidation of aromatic molecules is strongly dependent upon the initial (preoxidation) orientations of the chemisorbed organic [A13,A15,A25,A26]. Identical experiments were conducted to ascertain whether or not the same phenomenon transpires on Pd.

Fig. A-3 shows the current – potential curves for the irreversible electrochemical oxidation of η^2-H_2Q at a Pd thin-layer electrode. The solid curve is for Pd presaturated with η^2-oriented species, in the presence of unadsorbed H_2Q; the existence of the latter is indicated by the H_2Q-to-BQ anodic peak at 0.42 V. The dotted curve is for adsorbed (η^2) material only. The large anodic band peaked at 0.85 V is due to the irreversible oxidation of the chemisorbed organic accompanied by the formation of surface oxides on sites vacated by the oxidation products. Since the solid and dotted curves are identical above 0.55 V, the indication is that electrocatalytic oxidation does not occur unless the organic is surface-coordinated to the pure-metal surface and no organic chemisorption takes place at an oxide-coated surface.

In Fig. A-4, Γ and n_{ox} are plotted simultaneously as functions of the concentration at which chemisorption was carried out. As it is obvious in Fig. A-4, n_{ox} is closely correlated with Γ; that is, transitions in n_{ox} occur at the same concentrations where the transitions in Γ take place. Evidence is thus provided that the extent of the anodic oxidation is profoundly linked to the initial adsorbed molecule orientation.

For η^6-BQ, n_{ox} was measured to be 22.2 ± 0.3, a value not too different from that expected for complete oxidation to CO_2 (n_{ox} = 24):

$$\eta^6\text{-}C_6H_4O_2 + 10H_2O \rightarrow 6CO_2 + 24H^+ + 24e^- \qquad \text{(A9)}$$

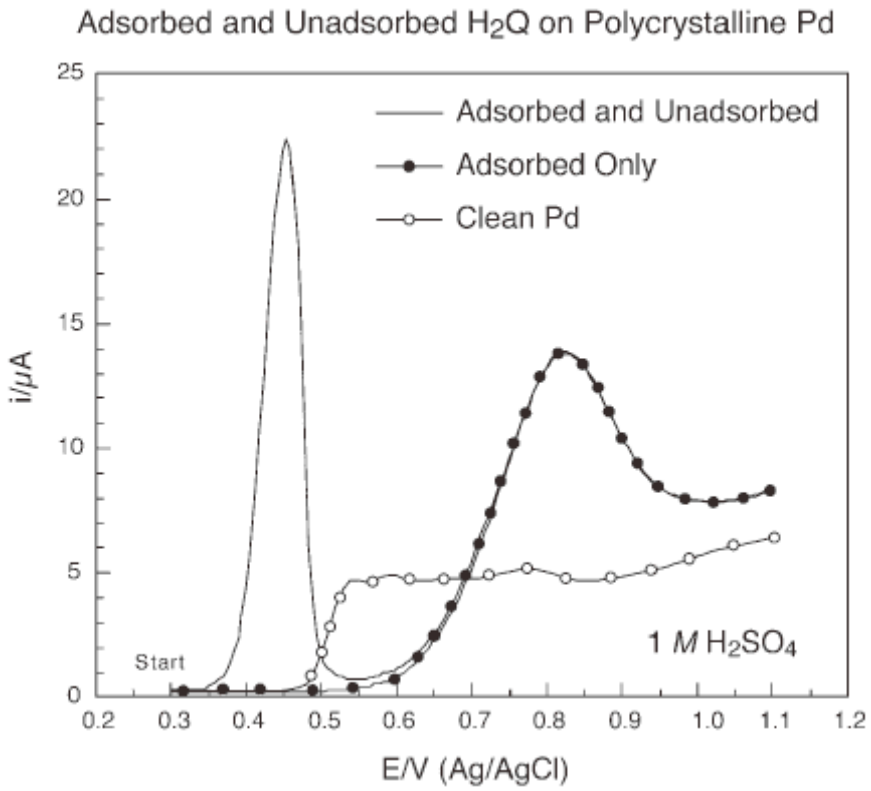

Fig. A-3. Thin-layer current–potential curves for the anodic oxidation of species chemisorbed from a 1 mM H_2Q + 1 M H_2SO_4 solution at a Pd thin-layer electrode in the presence (solid line) and absence (dotted line) of unadsorbed H_2Q. Experimental conditions were as described in the text and in Fig. A-1.

In comparison, the n_{ox} for 2,3-η^2-H_2Q was found to be 15±0.2. Based upon earlier studies on Pt [A13,A15,A25,A26], the lower n_{ox} value for η^2-H_2Q relative to η^6-BQ is taken here to signify that only those carbons directly bonded to the electrode surface undergo complete conversion to CO_2. An n_{ox} value of 15 for 2,3-η^2-H_2Q is consistent with complete oxidation of the 2,3-carbons directly attached to the surface (to CO_2) and milder oxidation of the remaining four-carbon fragment. Possible (but yet to be proven) anodic oxidation products are tartaric acid (n_{ox} = 14) and maleic acid (n_{ox} = 12):

$$\eta^2\text{-}C_6H_4O_2 + 6H_2O \rightarrow 2CO_2 + C_4H_4O_4 + 12H^+ + 12e^- \quad \text{(A10a)}$$

$$\eta^2\text{-}C_6H_4O_2 + 8H_2O \rightarrow 2CO_2 + C_4H_4O_4 + 14H^+ + 14e^- \quad \text{(A10b)}$$

It may be mentioned that maleic acid was found to be one of the products in the anodic oxidation of 2,3-η^2-H_2Q on Pt [A15,A33].

Two additional sets of experiments were conducted with the η^2-adsorbed species to determine if products other than CO_2 are actually generated; such partially oxidized products (which are retained inside an unrinsed thin-layer cell) would have enough surface activity to be re-adsorbed when the oxided Pd surface is reduced back to the pure metal. In one set, the electrode surface was saturated with η^2-H_2Q and subjected to anodic-oxidation potentials in the range from 0.30 V to 1.00 V. After 180 seconds, the thin-layer cavity was rinsed with organic-free electrolyte while the electrode was maintained at the same potential. After the rinse, the potential was switched to 0.30 V and held for 180 seconds ensure complete reduction of the oxidized surface back to the metal; a current–potential curve was then obtained. In this set of experiments, the anodic-oxidation products are flushed out of the thin-layer cavity prior to equilibration at 0.3 V; hence, if oxidation products other than CO_2 are formed, they are rinsed away and are unavailable for re-adsorption at 0.3 V. The results are shown in Fig. A-5.

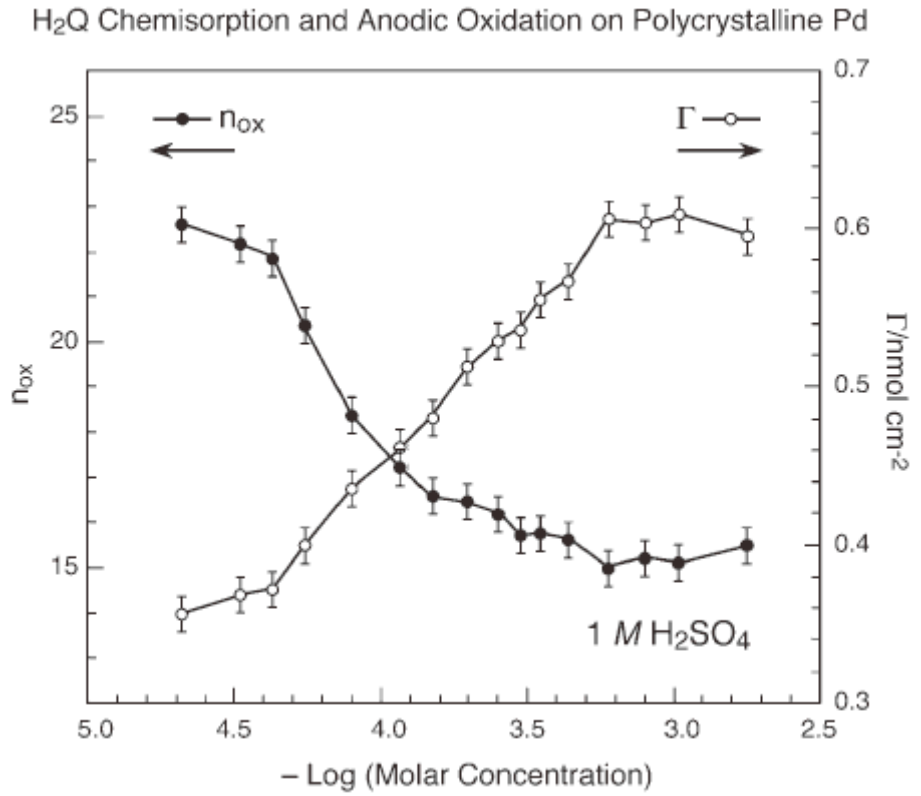

Fig. A-4. Simultaneous plots of the surface concentration (Γ) and the number of electrons (n_{ox}) for the oxidative-desorption as functions of the H_2Q solution concentration. Experimental conditions were as described in the text and in Fig. A-1.

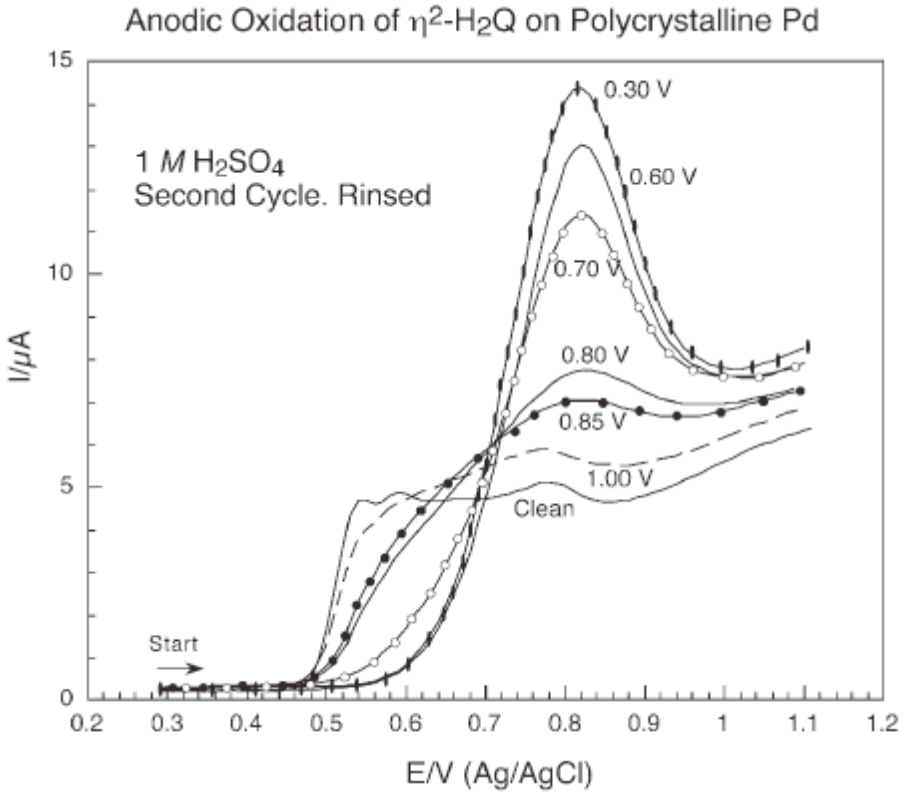

Fig. A-5. Post-oxidation voltammetric curves for η^2-H_2Q-coated Pd after the thin-layer cell was rinsed at the potential (0.3, 0.6, 0.7, 0.8, 0.85 or 1.0 V) where the anodic oxidation was carried out; under these conditions, all oxidation products were flushed out of the cell prior to the voltammetric scans. Experimental conditions were as described in the text and in Fig. A-1.

In Fig. A-5, the trend is clear that the magnitude of the anodic-oxidation peak decreases as the anodic-oxidation potential was increased; such trend proves the expected result that the extent of oxidative desorption is increased if the oxidation potential is made more positive. For example, the peak labeled 0.3 V is the largest since, at 0.3 V (which lies in the double-layer region), no oxidative desorption takes place. The band labeled 1.0 V is smallest since complete oxidative desorption transpires at 1.0 V, and all (CO_2 and other) products are flushed out of the thin-layer cell.

The data in Fig. A-5 are to be compared with the results from the second set of experiments (Fig. A-6). In this case, the thin-layer cell was not rinsed at the anodic-oxidation potential prior to re-equilibration at 0.3 V. In other words, surface-active (non-CO_2) oxidation products will remain inside the thin-layer cell to be re-adsorbed at 0.3 V.

From the results in Fig. A-6, it can be concluded that oxidation of η^2-H_2Q yields surface-active (non-CO_2) products that are re-adsorbed at 0.3 V, when an oxide-free Pd surface is regenerated; the subsequent anodic-oxidation scan thus shows a substantial oxidation peak. For example, an examination of the magnitude of the anodic-oxidation peak labeled 1.0 V shows that it is much larger in Fig. A-6 than in Fig. A-5. This is, of course, because, in Fig. A-6, surface-active (non-CO_2) products that were kept inside the thin-layer cell were re-adsorbed at 0.3 V; in Fig. A-5, the same products were flushed out of the cell and, hence, were not available for re-adsorption prior to the voltammetric scan.

Reactions such as those typified in Eq. A10 are thus proven, although the actual non-CO_2 products have not (yet) been identified.

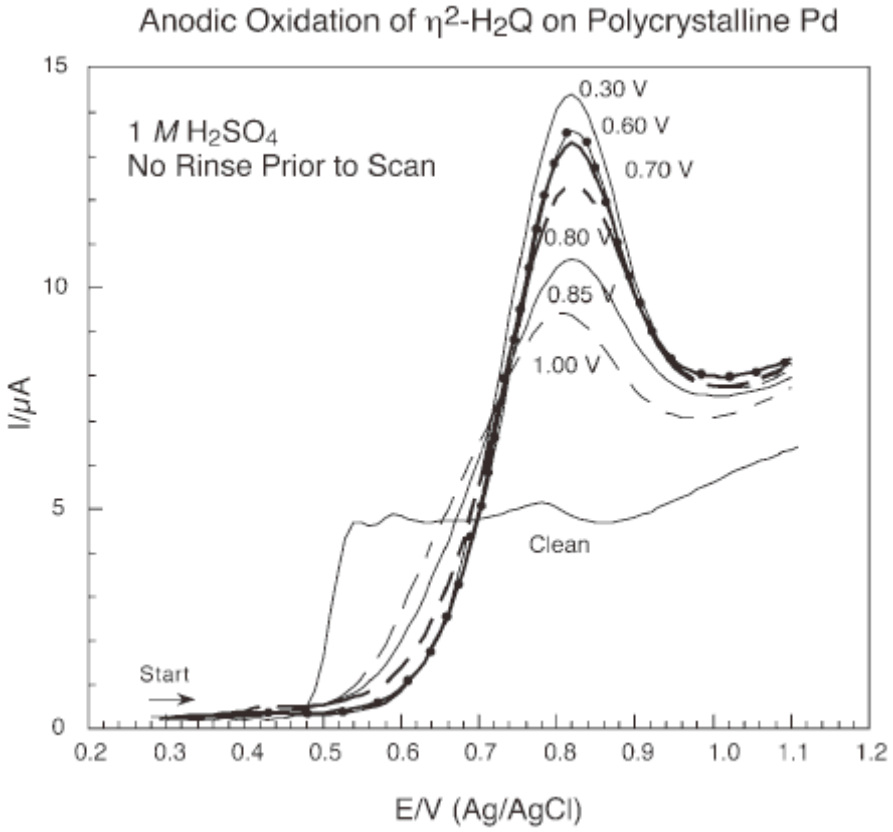

Fig. A-6. Post-oxidation voltammetric curves for η^2-H_2Q-coated Pd. In contrast to the experiments in Fig. A-5, the thin-layer cell here was not rinsed at the potential (0.3, 0.6, 0.7, 0.8, 0.85 or 1.0 V) where the anodic oxidation was carried out; that is, oxidation products were retained inside the cell which, if not CO_2, are re-adsorbed onto the surface prior to the voltammetric scans. Experimental conditions were as described in the text and in Fig. A-1.

Conclusions

The chemisorption and anodic oxidation of hydroquinone and benzoquinone at smooth polycrystalline palladium electrode surfaces in aqueous sulfuric acid solutions have been studied by thin-layer voltammetry and coulometry. The results, similar to those obtained previously on smooth polycrystalline platinum were as follows: i) At low aqueous solution concentrations, the diphenol is oxidatively chemisorbed to form surface-coordinated benzoquinone oriented parallel to the surface. ii) At higher concentrations, the oxidative chemisorption (via C-H activation) forms an edge-oriented diphenolic species. iii) Chemisorption from benzoquinone solutions leads to species identical to those from hydroquinone solutions. iv) The extent of anodic oxidation of the chemisorbed organic depends upon the initial adsorbed-molecule orientation: the flat-adsorbed species are oxidized completely to carbon dioxide, whereas oxidation of the edge-chemisorbed species yields other (unidentified) products that are chemisorbed upon regeneration of the oxide-free surface.

These trends form the basis for future work; three critical aspects that need to pursued are: a) The use of well-defined electrode surfaces; b) the adoption of surface-specific analytical methods for a better and more direct characterization of the chemisorbed species; and c) quantitative analysis of the product distributions.

Acknowledgements

Acknowledgement is made to The Welch Foundation for support of this work. J. S.-C. would also like to acknowledge the scholarship provided by the Deutscher Akademischer Austausch Dienst.

References

[A1] a) C. M. Friend, E. L. Muetterties, *J. Am. Chem. Soc.* **1981**, *103*, 773; b) J. Y. Saillard, R. Hoffman, *J. Am. Chem. Soc.* **1984**, *106*, 2006; c) M. R. Albert, J. T. Yates, Jr., *A Surface Scientist's Guide to Organometallic Chemistry*, American Chemical Society, Washington DC **1987**; d) R. Hoffman, *Surfaces and Solids*, VCH, New York, NY **1989**; e)T. N. Rhodin, G. Ertl, *The Nature of the Surface Chemical Bond*, North Holland Publishing, New York, NY **1979**; f) E. L. Muetterties, in *The Chemistry and Physics of Electrocatalysis* (Eds: J. D. McIntyre, J. D, M. J. Weaver, E. B. Yeager), The Electrochemical Society, Pennington, NJ **1984**; g) P. M. Cook, L. F. Dahl, D.W. Dickerhoof, *J. Am. Chem. Soc.* **1972**, *94*, 5511.

[A2] M. P. Soriaga, E. Binamira-Soriaga, A. T. Hubbard, J. B. Benziger, K.W. P. Pang, *Inorg. Chem.* **1985**, *24*, 65.

[A3] A. Carrasquillo, J.-J. Jeng, R. J. Barriga, W. F. Temesghen, M. P. Soriaga, *Inorg. Chim. Acta.* **1997**, *255*, 249.

[A4] B. C. Schardt, J. L. Stickney, D. A. Stern, D. G. Frank, J. Y. Katekaru, S. D. Rosasco, G. N. Salaita, M. P. Soriaga, A. T. Hubbard, *Inorg. Chem.* **1985**, *24*, 1419.

[A5] M. P. Soriaga. *Chem. Rev.* **1990**, *90*, 771.

[A6] Y.-G. Kim, M. P. Soriaga, in *Interfacial Electrochemistry* (Ed: A. Wieckowski), Marcel Dekker, New York **1999**.

[A7] a) J. L. Stickney, M. P. Soriaga, A. T. Hubbard, S. E. Anderson. *J. Electroanal. Chem*. **1981**, *125*, 73; b) S. L. Michelhaugh, G. J. Cali, B. G. Bravo, M. E. Bothwell, C. Bhardwaj, G. M. Berry, M. P. Soriaga, *Corrosion* **1991**, *47*, 322.

[A8] a) F. A. Cotton, G. Wilkinson, *Advanced Inorganic Chemistry*, Wiley, New York, NY **1988**; b) R. A. Crabtree, *The Organometallic Chemistry of the Transition Metals*, Wiley, New York, NY **1988**.

[A9] a) U. Belluco, *Organometallic and Corodination Chemistry of Platinum*, Academic press, New York, NY **1974**; b)F. R. Hartley, *The Chemistry of Platinum and Palladium*, Wiley, New York, NY **1973**.

[A10] *Structural Effects in Electrocatalysis*, (Eds: D. Scherson, D. Tryk, M. Daroux, X. Xing), The Electrochemical Society, Penniington, NJ **1991**.

[A11] *Electrode Processes* (Eds: A. Wieckowski, K. Itaya), The Electrochemical Society, Penniington, NJ **1996**.

[A12] *Electrocatalysis* (Eds: J. Lipkowski, P. N. Ross), Wiley-VCH, New York, NY **1998**.

[A13] M. P. Soriaga, J. L. Stickney, A. T. Hubbard, *J. Mol. Catal.* **1983**, *21*, 211.

[A14] T. Mebrahtu, G. M. Berry, M. P. Soriaga, *J. Electroanal. Chem.* **1988**, *239*, 375.

[A15] M. P. Soriaga, J. H. White, V. K. F. Chia, D. Song, P. O. Arrhenius, A. T. Hubbard, *Inorg. Chem.* **1985**, *24*, 73.

[A16] T. D. Jarvi, E. M. Stuve, in *Electrocatalysis*, Wiley-VCH, New York, NY **1998**.

[A17] Y. P. Gui, T. Kuwana, *Langmuir* **1986**, *2*, 471.

[A18] A. T. Hubbard, F. C. Anson, in *Electroanalytical Chemistry* (Ed: A. J. Bard), Marcel Dekker, New York, NY **1970**.

[A19] M. P. Soriaga, A. T. Hubbard. *J. Am. Chem. Soc.* **1982**, *104*, 2735.

APPENDIX B
CHEMISORPTION, ELECTROCHEMICAL OXIDATION AND HYDROGENATION OF BENZENE AND HYDROQUINONE ON POLYCRYSTALLINE, DISORDERED, AND WELL-DEFINED Pt SUBSTRATES: A DEMS STUDY*

J. Sanabria-Chinchilla and M. P. Soriaga
Department of Chemistry
Texas A&M University
College Station, TX 77843 USA

R. Bussar and H. Baltruschat
Institut für Physikalische und Theoretische Chemie
Universität Bonn
D–53117 Bonn, Germany

Abstract

The electrochemical hydrogenation and oxidation of *p*-dihydroxybenzene (hydroquinone) chemisorbed at polycrystalline Pt, well-ordered Pt(111) and disordered Pt(111) electrodes were studied by differential electrochemical mass spectrometry (DEMS). For comparative purposes, benzene was investigated at polycrystalline Pt. Anodic oxidation yielded only CO_2 as the volatile (DEMS-detectable) product. However, at least three oxidation cycles were necessary for exhaustive oxidation; this indicates that: (i) non-volatile products were generated in the first cycle, (ii) these products either stayed adsorbed or, in part, were re-adsorbed during a cathodic scan into the double-layer potential region, and (iii) these species were further oxidized on

* Reprinted from J. Appl. Electrochem., accepted, J. Sanabria-Chinchilla, M.P. Soriaga, R. Bussar, H. Baltruschat, A DEMS Study of the Electrocatalytic Hydrogenation and Oxidation of p-Dihydroxybenzene at Polycrystalline and Monocrystalline Platinum Electrodes.

subsequent anodic scans. Electrocatalytic hydrogenation of hydroquinone at polycrystalline Pt followed two parallel (not sequential) paths to generate benzene and cyclohexane: the "branching ratio" was heavily in favor of the latter product. The adsorbate can be displaced by CO at potentials in the double layer region. Since no volatile species was observed during this process, the adsorbate is not already reduced; e.g., to benzene. On well-ordered Pt(111), no cyclohexane was produced and only a minuscule fraction of benzene was observed; however, quantitative desorption of (unidentified) non-volatile organic material took place at the negative potential. The disordered Pt(111) surface behaved more like the polycrystalline rather than the monocrystalline surface. The H_2Q-hydrogenation reaction proceeds more readily on Pt with surface steps and kinks.

Introduction

Studies on the chemisorption of organic compounds at catalytic surfaces have been aided by a proliferation of surface analytical methods [B1-B3] that can be applied to electrochemical systems. The extension of such studies to electrocatalytic reactions such as hydrogenation or oxidation is less straightforward because of the paucity of techniques that are able to provide qualitative and quantitative analysis of the (low-level) product distributions. The difficulty arises primarily from the fact that organic compounds do not undergo electrocatalytic reactions unless they are chemisorbed at the electrode surface. Unless ultrahigh-area surfaces such as porous or finely divided powder electrodes are used, the amounts of products generated are not only minuscule (*ca.* pmol cm^{-2}), they are also swamped by a huge excess of supporting electrolyte. The drawback in the employment of such surfaces is that they are ill-defined; hence, it is virtually impossible to obtain fundamental mechanistic information such as correlations between catalytic reactivities, surface sites and modes of chemisorption.

Studies on the orientation of chemisorbed molecules and its influence in electrochemical oxidation or reduction reactions were first attempted by indirect measurements using thin-layer electrochemistry (TLE) by Hubbard and coworkers [B4,

B5]. Central to the molecular orientation studies was the measurement of the surface coverage or packing density (Γ, mol/cm^2) of the intact chemisorbed molecules [B6, B7]. Dihydroxy substituted benzene compounds were popular subject molecules because of the well-characterized electrochemistry [B8-B17]. The chemisorption isotherm of H_2Q on Pt(pc) surfaces has demonstrated that H_2Q chemisorption is a nonrandom, irreversible process in which chemisorbed species adopts specific orientations depending of the bulk organic solution. When chemisorption proceeds from diluted H_2Q solutions ($C < 0.10$ m*M*) flat-oriented species (η^6) is formed; whereas for solution with concentrations higher than 1.0 m*M*, edgewise-oriented species (η^2) are formed. These orientational assignments have been verified using independent techniques such as infrared reflection-adsorption spectroscopy (IRAS) [B18] and radiochemistry [B19]. Studies on H_2Q chemisorption at well-defined Pt(111) surfaces have been reported as well [B25,B39].

The effects of adsorbed-molecule orientation on the electrochemical oxidation and reduction of aromatic compounds were first studied on Pt electrodes [B20-B24]. The initial work involved a direct measurement of the number of electrons transferred during the oxidation (n_{ox}) or reduction (n_H) of adsorbed material by TLE. Gas chromatography (GC) with derivatization by silylation was employed to confirm oxidation products such as maleic acid [B25]. Long optical path length thin-layer spectroelectrochemistry was employed to identify 1,4-cyclohexandiol as the product of the electrochemical reduction of H_2Q [B26]. The use of the long optical path length and the large ratio of electrode area-to-solution volume were meaningful aspects in the detection of these species.

The development of differential electrochemical mass spectrometry (DEMS) has provided a major boost in the research area of electrochemical surface science. DEMS allows the identification and quantification of reaction product distributions. Equally critical is the fact that the product analysis can be directly linked to prominent features in a current-potential measurement: it is possible to record the electrochemical currents simultaneously with the mass spectrometer ion currents [B27,B28]. DEMS has been successfully applied in the study of electrocatalytic hydrogenation of aromatic molecules. Examples are benzene on polycrystalline Pt [B29], Pt(111) [B30], Pt(110)

and Pt(100) [B31], and Pt(332) [B32]; aniline and pyridine on polycrystalline and single-crystal Pt, Ru and Pd electrodes [B33]; biphenyl, naphthalene and t-butylbenzene on Pt electrodes [B34,B35]; benzyl alcohol [B36]; and benzoic acid [B37,B38] on Pd and Pt electrodes.

The present paper describes the application of DEMS on the electrocatalytic hydrogenation and oxidation of H_2Q at polycrystalline Pt(pc), well-ordered Pt(111) and disordered Pt(111). The former consists predominantly of surface terrace sites, whereas the disordered Pt(111) electrode would have an appreciable amount of surface defects (steps and kinks [B1, B40-B43]).

Experimental

The fabrication and utilization of a DEMS instrument has been described in detail elsewhere [B27,B28]. In this study, a differentially pumped Balzers QMG 422 quadrupole mass spectrometer was employed; this set-up allows the simultaneous detection of up to sixty-four ion fragments. Electrochemistry was done in a one-compartment thin-layer cell.

Disc-shaped (polycrystalline and single-crystal) platinum electrodes were initially treated by immersion by in 10 *M* HNO_3 (Merck) for at least ten minutes. The Pt(pc) electrode was briefly flame-annealed to render it uniformly smooth. The Pt(111) single crystal was annealed for 3 minutes and quenched in an H-cell that contained 0.1 *M* H_2SO_4 under a stream of ultrapure argon (Air Products). The Pt(111) surface was disordered by multiple potential cycles between the hydrogen and oxygen evolution regions until a steady-state current-potential curve, devoid of the "butterfly peaks" characteristic of the well-ordered surface, was obtained. The electrodes were emersed and, with a protective drop of Ar-saturated supporting electrolyte, transferred into the DEMS thin-layer cell. The integrity of the electrode surfaces was always monitored prior to the adsorption experiments. The active surface areas of the working electrodes were determined from the hydrogen-adsorption (or desorption) faradaic charges [B2,B3,B5,B25]. A standard hydrogen electrode (SHE) in 0.1 *M* H_2SO_4 was used as the

reference electrode.

Milli-Q® Plus water (Millipore Systems) was utilized to prepare all solutions which were deaerated with ultrapure argon. Hydroquinone (Merck) and benzene (Riedel-de Haën) solutions were prepared in 0.1 *M* H_2SO_4 at millimolar concentrations. Adsorption was performed by introduction of fresh adsorbate solution into the DEMS cell, at potentials in the double-layer region (0.35 V), followed by a three-minute equilibration. The cell was then rinsed copiously with pure supporting electrolyte to remove the unadsorbed material. The potential was scanned either in the anodic or cathodic direction without electrolyte flow. Multiple potential cycles were obtained until no more changes were observed in both the cyclic voltammograms and the mass spectra.

Calibration of the DEMS system was achieved as described elsewhere [B27,B28]. Surface coverage data were estimated from integrated ion currents. (Note that the calibration constant, relating the ion current to the number of molecules entering the vacuum system, contains both the ionization probability and the fragmentation ratio of the corresponding ion).

Results and discussion

Figure B-1 shows simultaneous electrochemical cyclic voltammograms (CV) and mass spectrometric cyclic voltammograms (MSCV) for H_2Q chemisorbed on Pt(pc) in a potential regime well above the hydrogen-evolution region. A potential-dependent intensity was found only for mass m/z = 44, which corresponds to CO_2. Although the second-cycle anodic-oxidation currents are only slightly larger than the background (Pt-surface-oxide-formation) currents, an appreciable amount of CO_2 was still detected by DEMS up to the third anodic scan. This result can only mean that: (a) there actually are non-volatile oxidation products that are retained in the DEMS thin-layer cell, (b) these non-CO_2 products are chemisorbed on the surface after the oxidized Pt is reverted to its metallic form, and (c) the adsorbed products are eventually oxidized exhaustively (to CO_2) on subsequent anodic cycles, consuming a lower number of electrons per CO_2

formed than in the first sweep which results in a smaller faradaic-to-ion-current ratio. A similar behavior had been observed previously for other aromatic systems such as toluene, benzene and biphenyl [B30,B32,B44].

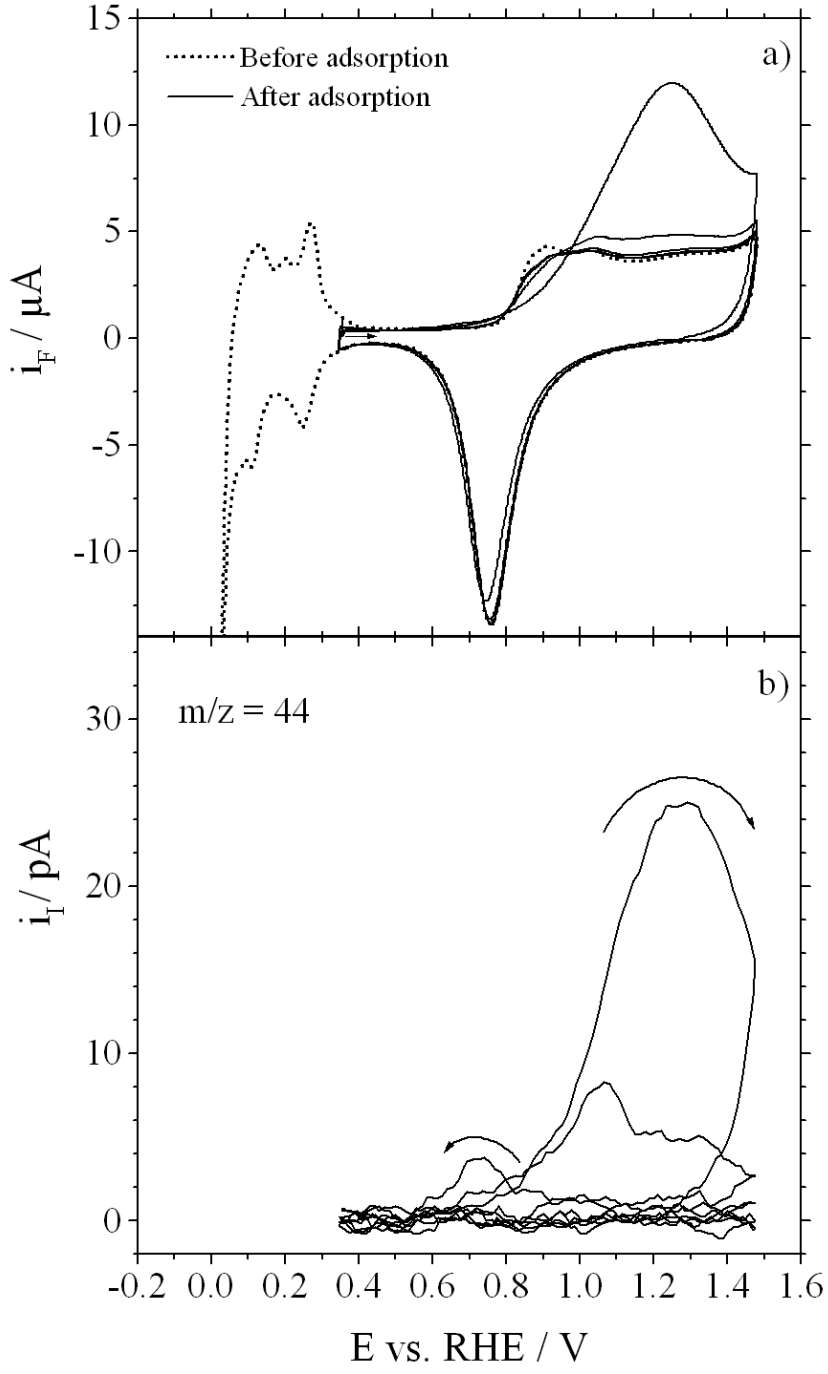

Figure B-1. (a) Cyclic voltammetric (CV) curve and (b) mass spectrometric cyclic voltammetric (MSCV) curve (m/z = 44, CO_2) for the anodic oxidation of a H_2Q-coated Pt(pc) electrode in H_2Q-free 0.1 *M* H_2SO_4. H_2Q was chemisorbed at 0.35 V. Scan rate = 10 mV/s.

The cycle-dependent percent yields of CO_2 were determined from the areas under the CO_2 mass peaks in Figure B-1. (It will be mentioned that the currents beyond the third sweep are identical to those obtained from the pure supporting electrolyte; hence, they were used for the background correction.)

Eighty percent of the total CO_2 yield was generated in the first anodic scan, 17 % in the second sweep, and 3 % in the third cycle (Table B-1). No information is available that would permit the identification of the non-volatile species that remained in the DEMS thin-layer cell after the first cycle. The possibility exists that 20% of the organic may have been partially oxidized to a shorter-chain unsaturated species; for example, maleic acid was detected in the anodic oxidation of hydroquinone on polycrystalline Pt [B5,B25]. On the other hand, for benzene and toluene, a similar behavior has been observed in the "classical" DEMS cell [B44] where a porous electrode is used at the bottom of a cylindric cell with a height of several centimeters; dissolved products are therefore free to diffuse away into the bulk of the electrolyte. It has been concluded that some carbonaceous species stay absorbed (and, possibly, are buried below the PtO during the place exchange between Pt and O) [B44]. This may also be true for H_2Q.

Figure B-2 shows CV and MSCV data for the hydrogenation of H_2Q; here, the potential sweep was initiated in the negative direction. Only two hydrogenation products, cyclohexane (m/z = 56) and benzene (m/z = 78), were detected by DEMS. It is important to note that the two mass peaks occur at almost the same potential, a result that suggests that the hydrogenation of H_2Q to cyclohexane and benzene involves two *parallel* mechanistic paths. In other words, the reaction is *not sequential* as in:

$$H_2Q_{(ads)} \not\rightarrow C_6H_{6(ads)} \not\rightarrow C_6H_{12(ads)} \qquad \text{(B1)}$$

Table B-1. Amounts of desorption products from hydroquinone and benzene adsorbates on Pt(pc)

Detected species	Γ / nmol cm^{-2} (cath sweep)				Γ / nmol cm^{-2} (anodic sweep)	n_{ox}
Adsorbate/surface	Cyclohexane	Benzene	CO_2	Total C_6	(total, from CO_2)	(anodic sweep)
H_2Q/Pt(pc)	0.095	0.004	0.063*6	0.16	0.28	5.2
H_2Q/Pt(111)	0	0.002	0.175*6	0.18	0.19	5.3
H_2Q/ rough Pt(111)	0.07	0.003	0.092*6	0.17		
Benzene/Pt(pc)	0.11	0.043	0.064*6	0.22	0.30	5.2

This does not exclude the possibility that, in the reaction path leading to cyclohexane, adsorbed benzene is formed as a short-lived intermediate which does not desorb. The hydrogenation "branching ratio" is heavily in favor of the saturated product as the cyclohexane:benzene ratio (taking into account the differing sensitivities) is approximately 26:1 (Figures B-2-b and B-2-c and Table B-1). The likelihood of two parallel mechanisms is further supported by the fact that, in order for benzene to be hydrogenated, it must remain chemisorbed on the surface [B5, B23, B25, B39].

It can be seen from Figure B-2-d that a small but noticeable CO_2 peak appears in the MSCV curve in the first post-hydrogenation anodic scan. This is an indication that there is a small fraction of organic that remains on the surface and/or in the solution during the hydrogenation reaction; these species are the ones that undergo anodic oxidation to CO_2 on the ensuing anodic scan. That both surface and unadsorbed materials exist is confirmed by an experiment that, if the DEMS thin-layer cell is rinsed with pure supporting electrolyte at -0.1V (to remove any non-surface-attached species), a CO_2 mass peak is still observed, albeit at a smaller quantity (*cf.,* dotted line in Figure B-2-d). Therefore, a small part of the adsorbate might desorb as a non volatile species, possibly H_2Q itself or 1,4-cyclohexanediol; it has also been reported that hydrogenation of chemisorbed H_2Q at thermally smoothened Pt(pc) with a copious amount of $H_{2(g)}$ yields 1,4-cyclohexanediol [B23]. That part of the adsorbate which is not desorbed at low potentials might be due to molecules bound strongly to sites of a particular surface orientation. For comparison, whereas benzene is completely desorbed from most surfaces at low potentials, either under hydrogenation or without, from Pt(100) less than half of the adsorbate can be desorbed [B31].

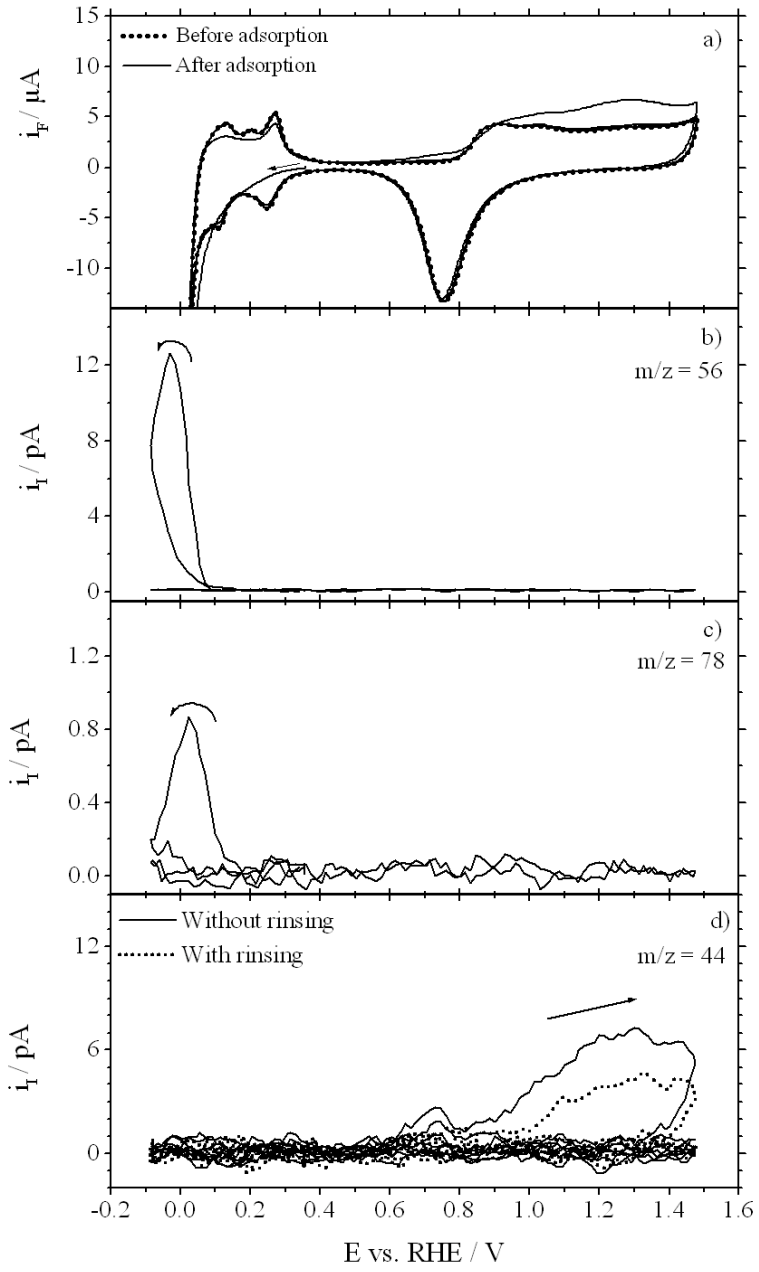

Figure B-2. (a) Cyclic voltammetric (CV) curve, (b) mass spectrometric cyclic voltammetric (MSCV) curve (m/z = 56, cyclohexane), (c) MSCV curve (m/z = 78, benzene), and (d) MSCV curve (m/z = 44, CO_2) for the electrochemical hydrogenation of a H_2Q-coated Pt(pc) electrode in H_2Q-free 0.1 *M* H_2SO_4. All other experimental conditions were as in Figure B-1.

For comparative purposes, the electrocatalytic hydrogenation of benzene chemisorbed on Pt(pc) was also investigated in the identical cell and under identical conditions. The results, in terms of CV and MSCV data, are shown in Figure B-3. When scrutinized in relation to the observations in Figure B-2, three major differences emerge: (i) The MSCV peak for cyclohexane has not only increased, but is also of a different morphology. (ii) The benzene mass peak has increased substantially; its onset is shifted to 0.3V. The cyclohexane-to-benzene peak-area ratio obtained from the hydrogenation of H_2Q is approximately ten-fold larger than that measured from the hydrogenation of benzene. (iii) The time (or potential) lag for cyclohexane production relative to the benzene desorption is much more pronounced. In [B32], it was described an experiment, where after adsorption of benzene on Pt(332) the potential was held at 70 mV for 5 min, only m/z=78 was observed. After continuation of the sweep in the negative direction, mostly cyclohexane and only traces of benzene were observed. The total amounts of benzene and cyclohexane were identical to those observed during a continuous sweep. Therefore, the original adsorption site determines which species is formed at low potentials. Since in the case of H_2Q, benzene and cyclohexane are formed at nearly identical potentials, this is further evidence that the H_2Q hydrogenation to cyclohexane and benzene transpires along two parallel, not sequential, pathways:

$$H_2Q_{(ads)} \xrightarrow[Pt(pc)]{\text{Hydrogenation}} \text{Cyclohexane}_{(aq)} + \text{Benzene}_{(aq)} + \text{Non-volatile Products} \quad \text{(B2)}$$

It may be noted in Figure B-3-d that a small but measurable CO_2 mass peak appears in a subsequent anodic scan; since possible hydrogenated products of benzene are volatile, incomplete desorption is thus indicated for benzene.

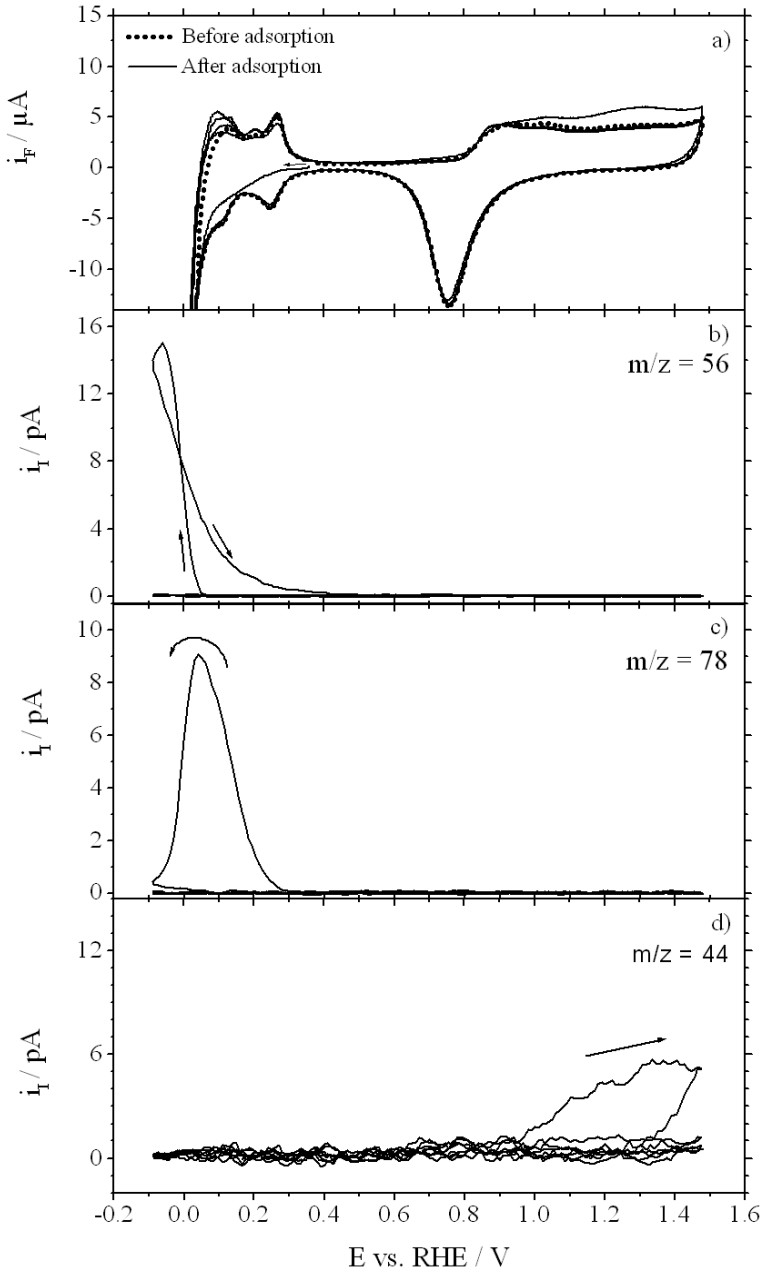

Figure B-3. (a) Cyclic voltammetric (CV) curve, (b) mass spectrometric cyclic voltammetric (MSCV) curve (m/z = 56, cyclohexane), (c) MSCV curve (m/z = 78, benzene), and (d) MSCV curve (m/z = 44, CO_2) for the electrochemical hydrogenation of a benzene-coated Pt(pc) electrode in benzene-free 0.1 *M* H_2SO_4. All other experimental conditions were as in Figure B-1.

A comparison of the amounts of desorbing species, calculated from the integrated ion currents, is given in Table B-1. Values obtained from cathodic desorption experiments are lower than those obtained from the amount of CO_2 when the first sweep was in the anodic direction. For benzene, it has been observed that several sweeps, restricted to the hydrogen region, are necessary for a complete hydrogenation of the adsorbate; up to 30% of the total cyclohexane are desorbed only in those subsequent sweeps [B29]. In the case of H_2Q, this relative amount may even be larger. Even without an electrolyte exchange at the negative potential limit, some of the species may be lost due to a constant, small flow of electrolyte and diffusion into the capillaries of the cell, and thus not oxidized to CO_2.

A priori, one cannot exclude that H_2Q is already reduced to adsorbed benzene upon adsorption, in particular on polycrystalline Pt.. From the different morphology of the ion current transient for cyclohexane formed after adsorption of H_2Q and benzene, one may already exclude this possibility. To further prove that this is not the case, displacement experiments were carried out using CO. After H_2Q adsorption at 0.35V, a CO-saturated 0.1M H_2SO_4 solution was passed through the cell under potential control (0.25V) using a flow rate of 0.70μL/s. Such a slow flow rate was used to guarantee that the desorbed species have enough time to diffuse from the electrode surface to the membrane and reach the mass spectrometer instead of leaving the cell with the solution. As was expected, no active signals were detected during the displacement since it is not possible to detect H_2Q using DEMS.

Control experiments were performed displacing pre-adsorbed benzene at the same H_2Q experimental conditions. Figure B-4 summarizes the results of the H_2Q and benzene displacement experiments. The ion-current transient in Figure B-4-a shows benzene (m/z = 78) during the introduction of the CO-saturated solution into the thin-layer DEMS cell. Figures B-4-b and B-4-c show the CV and MSCV recorded after the displacement experiments and electrolyte exchange. The CV shows the suppression of the hydrogen region at 0.25V due to CO adsorption. The voltammetric feature at 0.70 V corresponds to the CO oxidation as can be extracted from the MSCV. In addition, a

small contribution of aromatic-like species was observed in the region between 1.00 V and 1.40 V indicating the oxidation of the remaining aromatic adsorbate. The amount of displaced adsorbate by CO was estimated to be 90% for H_2Q; in comparison, 97% of the original benzene adlayer was displaced in the second experiment. The surface coverage of benzene was calculated to be 0.26 nmol/cm^2.

Figure B-5 shows CV and MSCV results for the H_2Q hydrogenation, initiated by a cathodic scan, and subsequent anodic oxidation of the chemisorbed adlayer on a well-ordered Pt(111) surface. The two most significant observations are: (i) No cyclohexane was produced; only benzene, in minuscule quantities, was detected by DEMS. (ii) A large amount of CO_2, essentially as much as that for H_2Q on Pt(pc) without prior hydrogenation (*cf.*, Figure B-1-d), was generated. These results both point to the relative inactivity of the well-ordered Pt(111) surface towards electrocatalytic hydrogenation of H_2Q to cyclohexane and/or benzene. Presumably, because the polycrystalline surface contains an appreciable amount of steps and/or kinks [B1], it is much more aggressive towards H_2Q hydrogenation than a well-ordered hexagonally close-packed surface.

The fact that, in the experiment of Figure B-5-b cyclohexane is not produced, or that benzene is generated only to an almost negligible extent, does not necessarily mean that the well-ordered Pt(111) surface is totally devoid of interfacial reactions, whether it is hydrogenation or simple electro-desorption. This may be inferred from the data in Figure B-6, where the DEMS thin-layer cell was rinsed with pure supporting electrolyte at -0.1V. Since no CO_2 mass peak appears on the subsequent anodic scan, it is clear that non-volatile material was quantitatively desorbed from the surface, and rinsed away, at the negative potential. Furthermore, the cathodic peak around 0.40 V in Figures B-5 and B-6 indicates displacement of the original H_2Q adsorbate by adsorbed hydrogen. It must be noted that, contrary to the experiments at Pt(pc), no CO_2 was formed in the subsequent anodic sweep; desorption therefore was complete.

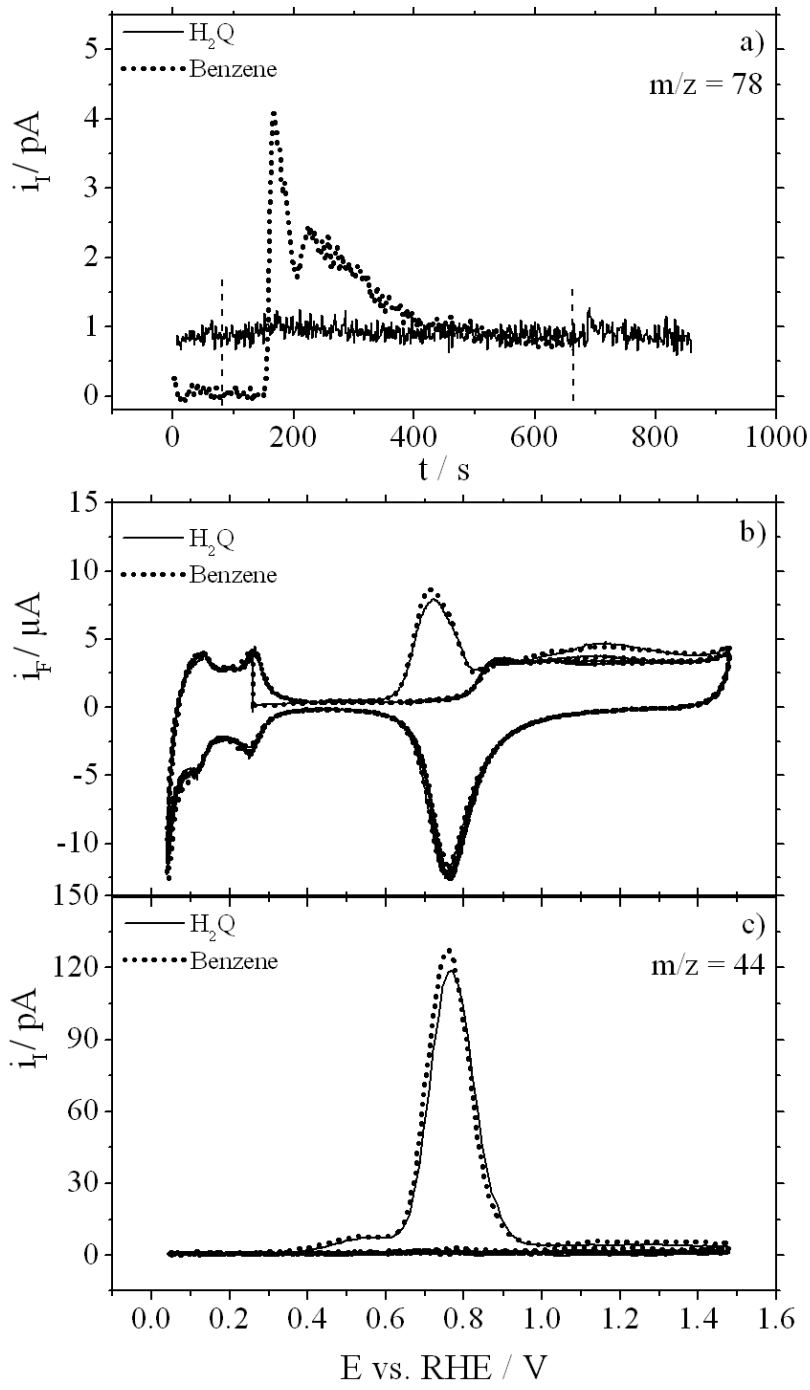

Figure B-4. (a) Ion current transients of m/z = 78 during the displacement of H_2Q- and benzene-coated Pt(pc) electrodes by CO adsorption, (m/z = 78, benzene). (b) CV after CO adsorption, same conditions as in Figure B-1. (c) MSCV (m/z = 44, CO_2).

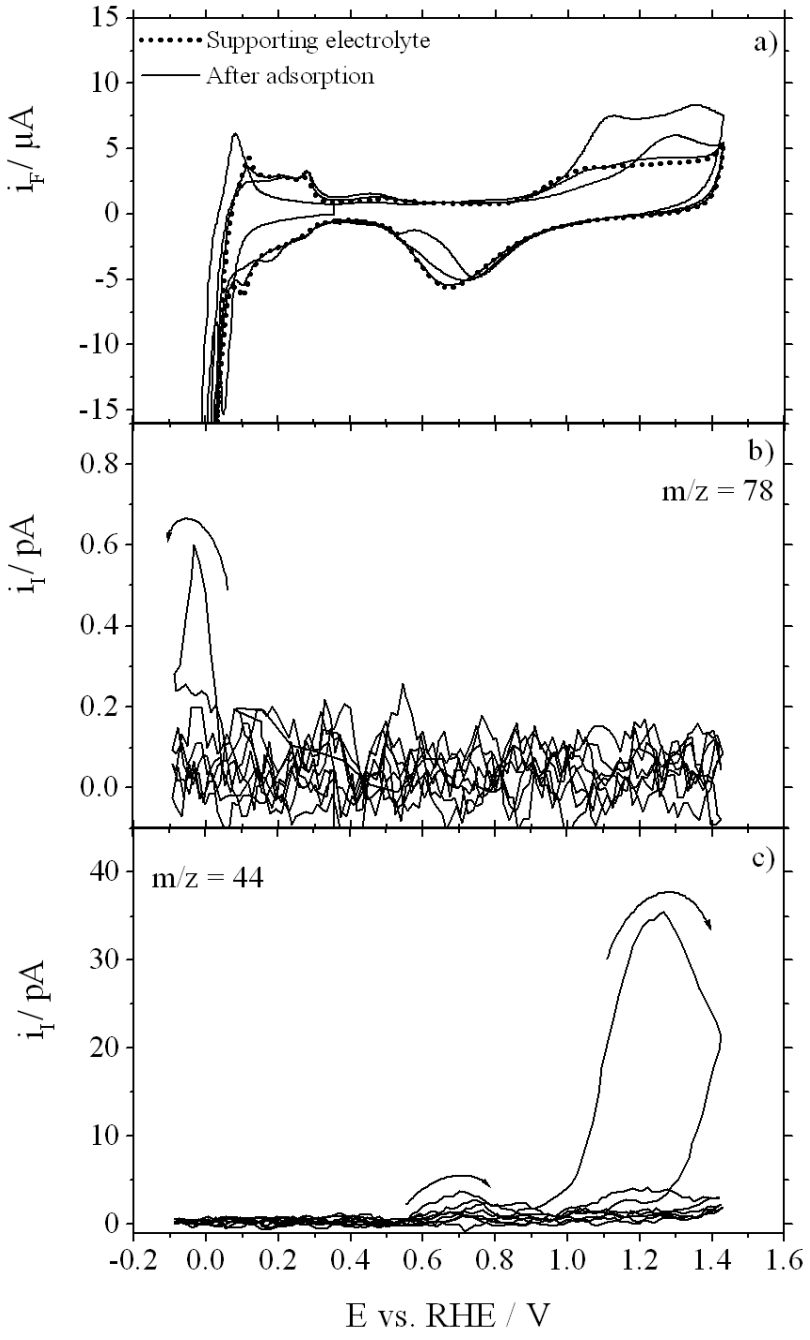

Figure B-5. (a) Cyclic voltammetric (CV) curve, (b) mass spectrometric cyclic voltammetric (MSCV) (m/z = 78, benzene), and (c) MSCV curve (m/z = 44, CO_2) for the electrochemical hydrogenation of a H_2Q-coated Pt(111) electrode in H_2Q-free 0.1 *M* H_2SO_4. All other experimental conditions were as in Figure B-1.

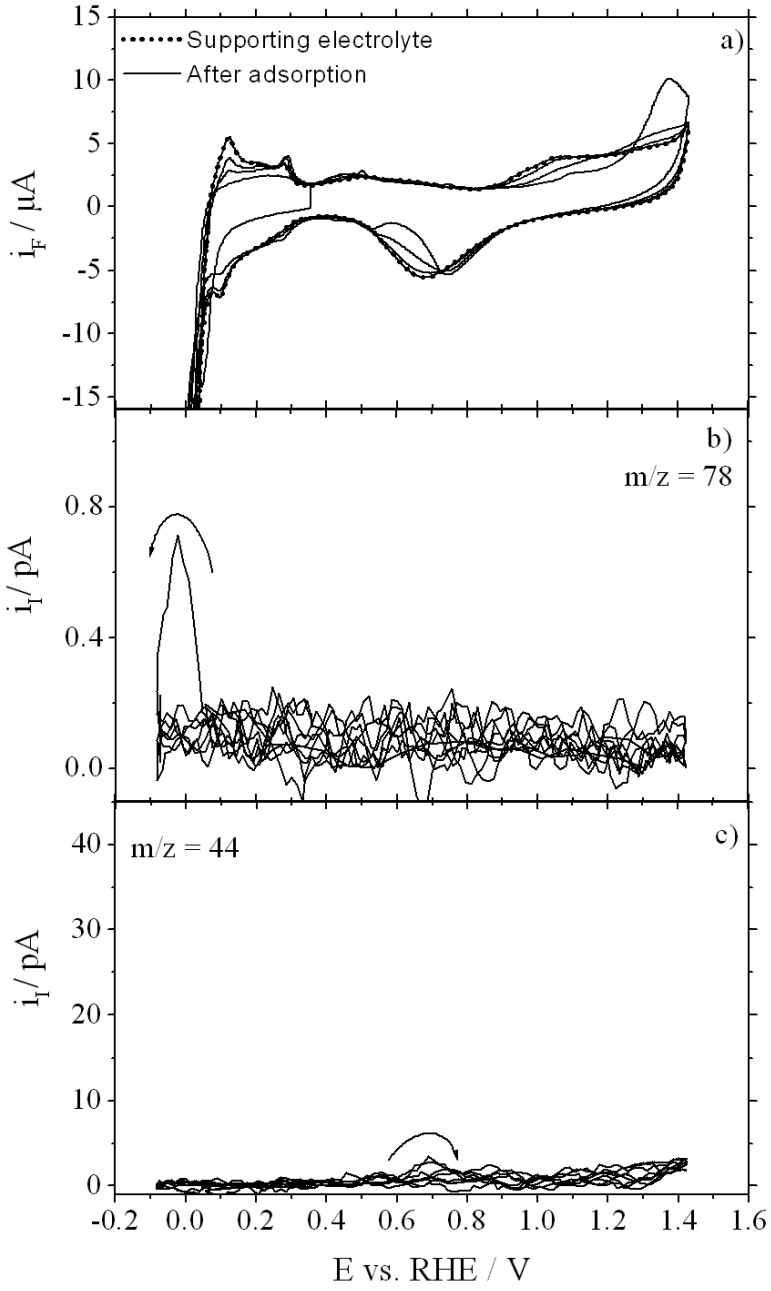

Figure B-6. (a) Cyclic voltammetric (CV) curve, (b) mass spectrometric cyclic voltammetric (MSCV) (m/z = 78, benzene), and (c) MSCV curve (m/z = 44, CO_2) for the electrochemical hydrogenation of a H_2Q-coated Pt(111) electrode in H_2Q-free 0.1 *M* H_2SO_4. The DEMS thin-layer cell was rinsed at -0.10V prior to the anodic scan. All other experimental conditions were as in Figure B-1.

In comparison, oxidation of benzene adsorbed at Pt(111) proceeds in two steps, only the second of which is paralleled by CO_2 formation [B30]. From the oxidation-charge values, it is suggested that adsorbed hydroquinone/quinone species are formed in the first step, which, upon reversal of the sweep in the cathodic direction, are desorbed in a sharp peak prior to hydrogen evolution. The similar desorption behavior and peak shape in the present study corroborate this interpretation.

The above experiments were repeated with a Pt(111) surface that had been disordered by multiple electrochemical oxidation and reduction cycles; the aim was to introduce (mild) surface disorder and ascertain its effect on H_2Q hydrogenation. The CV and MSCV results are given in Figure B-7. It is not difficult to note that the features in this Figure are quite similar to those at Pt(pc) (*cf.*, Figure B-2), but profoundly different from those at well-ordered Pt(111); specifically, both cyclohexane and benzene are generated on the disordered surface but not on the well-ordered single-crystal electrode. Evidently, a slightly roughened Pt(111) behaves more like a polycrystalline rather than a monocrystalline platinum surface, at least in terms of H_2Q hydrogenation. It also appears that the latter reaction proceeds more readily at Pt surfaces that contain surface defects such as steps and kinks. A similar effect was earlier observed for the hydrogenative desorption of ethene from a roughened Pt(111) [B42] and of benzene from a stepped Pt(332) [B32]. The different shape of the cyclohexane signal (majority of the species is detected only in the subsequent anodic scan) may indicate a slower desorption of cyclohexane than on Pt(pc). However, the desorption starts at potentials where hydrogen evolution is strong; since the resulting iR-drop in the thin layer cell is considerable, the actual potential at the negative potential limit (on which the desorption rate strongly depends) is not well defined.

The amount of species detected upon desorption from Pt(111) is also included in Table B-1. It is smaller than that observed for Pt(pc) or roughened Pt(111), in accordance with the previous observations [B39]. The corresponding coverage is lower than that obtained from Auger electron spectroscopy (0.3 nmol cm^{-2} [39]) and much lower than that calculated from the structure observed by STM (0.38 nmol cm^{-2}, [B45]).

Although this difference may partly be caused by losses due to desorption and experimental errors, changes in pH, differences in supporting electrolyte and, in particular, the presence of H_2Q may also lead to variable surface coverages. Moreover, it must be noted that coverages extracted from structure determinations are ideal values which, on real surfaces, are lowered due to domain boundaries and other imperfections.

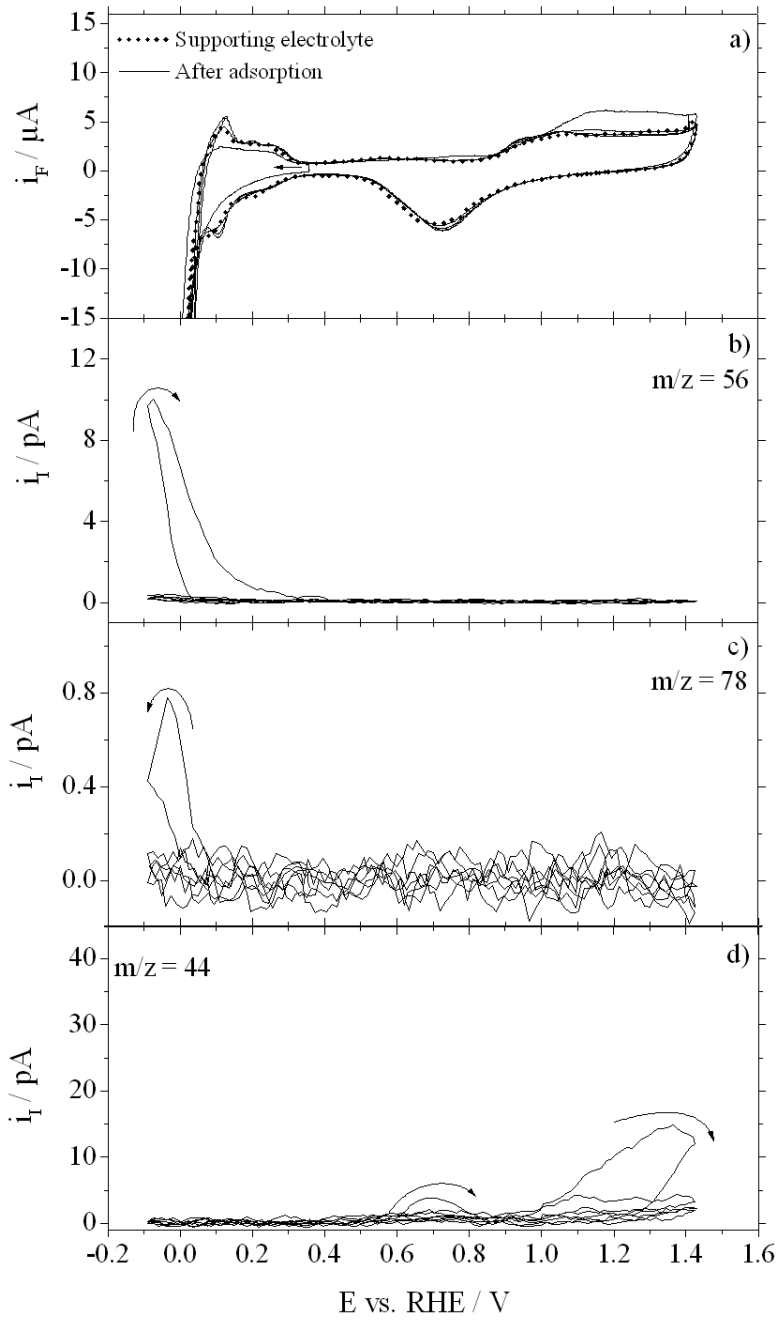

Figure B-7. (a) Cyclic voltammetric (CV) curve, (b) mass spectrometric cyclic voltammetric (MSCV) (m/z = 78, benzene), and (c) MSCV curve (m/z = 44, CO_2) for the electrochemical hydrogenation of H_2Q-coated disordered Pt(111) electrode in H_2Q-free 0.1 *M* H_2SO_4. All other experimental conditions were as in Figure B-1.

Conclusions

The electrocatalytic hydrogenation and oxidation of hydroquinone chemisorbed on polycrystalline Pt, well-ordered Pt(111), and disordered Pt(111) surfaces were studied by DEMS. For comparative purposes, benzene was investigated at polycrystalline Pt. Anodic oxidation yielded only CO_2 as the volatile (DEMS-detectable) product. However, at least three oxidation cycles were necessary for exhaustive oxidation; this indicates that: (i) non-volatile products were generated in the first cycle, (ii) these products were re-adsorbed during a cathodic scan into the double-layer potential region, and (iii) the re-chemisorbed species were further oxidized on subsequent anodic scans. Electrocatalytic hydrogenation of H_2Q at Pt(pc) followed two parallel (not sequential) paths to generate benzene and cyclohexane: the "branching ratio" was heavily in favor of the latter product. On well-ordered Pt(111), no cyclohexane was produced and only a minuscule fraction of benzene was observed; however, quantitative desorption of (unidentified) non-volatile organic material took place at the negative potential. The disordered Pt(111) surface behaved more like the polycrystalline rather than the monocrystalline surface. The H_2Q-hydrogenation reaction proceeds more readily on Pt with surface steps and kinks.

It is interesting to note that, whereas H_2Q is irreversibly reduced to benzene and cyclohexane on polycrystalline Pt, there is strong indication that, on Pt(111), benzene can be (irreversibly) oxidized to adsorbed H_2Q [B30].

Acknowledgments

The present project was funded by the Deustche Forschungsgemeinschaft (DFG). MPS would like to acknowledge the Welch Foundation for additional support. JSC thanks the German Academic Exchange Service (DAAD) for a research fellowship to conduct DEMS experiments in the laboratories of HB.

References

B1. G. A. Somorjai. “Introduction to Surface Chemistry and Catalysis.” Wiley, New York (1994).

B2. M. P. Soriaga, D. A. Harrington, J. L. Stickney and A. Wieckowski. In “Modern Aspects of Electrochemistry.” B. E. Conway, R. E. White and J. O’M. Bockris. Eds. Plenum, New York (1966).

B3. A. J. Bard, H. D. Abruña, C. E. Chidsey, L. R. Faulkner, S. Feldberg, K. Itaya, O. Melroy, R. W. Murray, M. D. Porter, M. P. Soriaga and H. S. White, *J. Phys. Chem.* **97** (1993) 7147.

B4. M. P. Soriaga, A. T. Hubbard, *J. Am. Chem. Soc.* **104** (1982) 2735.

B5. M. P. Soriaga, E. Binamira-Soriaga, A. T. Hubbard, J. B. Bezinger, K.-W. P. Pang, *Inorg. Chem*. **24** (1985) 65.

B6. A. T. Hubbard, *Chem. Rev.* **88** (1988) 633.

B7. M. P. Soriaga, *Chem. Rev.* **90** (1990) 771.

B8. M. P. Soriaga, P.H. Wilson, A. T. Hubbard, *J. Electroanal. Chem*. **142** (1982) 317.

B9. M. P. Soriaga, A. T. Hubbard, *J. Am. Chem. Soc.* **104** (1982) 3937.

B10. M. P. Soriaga, J. H. White A. T. Hubbard, *J. Phys. Chem.* **87** (1983) 3048.

B11. M. P. Soriaga, A. T. Hubbard, *J. Phys. Chem.* **88** (1984) 1089.

B12. M. P. Soriaga, V. K. F. Chia, J. H. White, D. Song, A. T. Hubbard, *J. Electroanal. Chem.* **162** (1984) 143.

B13. V. K. F. Chia, M. P. Soriaga, A. T. Hubbard, *J. Electroanal. Chem.* **167** (1984) 97.

B14. M. P. Soriaga, J. H. White, D. Song, A. T. Hubbard, *J. Electroanal. Chem.* **171** (1984) 359.

B15. J. H. White, M. P. Soriaga, A. T. Hubbard, *J. Electroanal. Chem.* **177** (1984) 89.

B16. M. P. Soriaga, D. Song, A. T. Hubbard, *J. Phys. Chem.* **89** (1985) 285.

B17. M. P. Soriaga, D. Song, D. C. Zapien, A.T. Hubbard, *Langmuir* **1** (1985) 123.

B18. K. P. Pang, J. B. Benziger, M. P. Soriaga, A. T. Hubbard, *J. Phys. Chem.* **88** (1984) 4583.

B19. E. K. Krauskopf, A. Wieckowski, *J. Electroanal. Chem.* **296** (1990) 159.

B20. T. Mebrahtu, G. M. Berry, M. P. Soriaga, *J. Electroanal. Chem.* **247** (1988) 241.

B21. M. P. Soriaga, J. L. Stickney, A. T. Hubbard, *J. Mol. Cat.* **21** (1983) 211.

B22. M. P. Soriaga, J. L. Stickney, A. T. Hubbard, *J. Electroanal. Chem.* **144** (1983) 207.

B23. T. Mebrahtu, G. M. Berry, M. P. Soriaga, *J. Electroanal. Chem.* **239** (1988) 375.

B24. B. Bravo, S. L. Michelhaugh, T. Mebrahtu, M. P. Soriaga, *Electrochim. Acta* **11** (1988) 1507.

B25. M.P. Soriaga, J. H. White, D. Song, V. K. Chia, P. O. Arrhenius, A. T. Hubbard, *Inorg. Chem.* **24** (1985) 73.

B26. Y-P. Gui, T. Kuwana, *Langmuir* **2** (1986) 471.

B27. H. Baltruschat. 'Differential Electrochemical Mass Spectrometry as a Tool for Interfacial Studies' in: A. Wieckowski (Ed.) "Interfacial Electrochemistry".

Marcel Dekker, New York (1999).

B28. H. Baltruschat, *J. Am. Soc. Mass Spectrom.* **15** (2004) 1693.

B29. T. Hartung and H. Baltruschat, *Langmuir* **6** (1990) 953

B30. T. Hartung, U. Schmiemann, I. Kamphausen and H. Baltruschat, *Anal. Chem.* **63** (1991) 44.

B31. U. Schmiemann and H. Baltruschat, *J. Electroanal. Chem.* **347** (1993) 93.

B32. T. Löffler, R. Bussar, E. Drbalkova, P. Janderka and H. Baltruschat, *Electrochim. Acta* **48** (2003) 3829.

B33. U. Schmiemann, Z. Jusys and H. Baltruschat, *Electrochim. Acta* **39** (1994) 561.

B34. J. Vestral, Th. Lofflër, U. Müller and H. Baltruschat, *J. Electroanal. Chem.* **461** (1999) 90.

B35. T. Löffler, E. Drbalkova, P. Janderka, P. Königshoven and H. Baltruschat, *J. Electroanal. Chem.* **550** (2003) 81.

B36. J. L. Rodríguez, R. M. Souto, S. González and E. Pastor, *Electrochim. Acta* **44** (1998) 1415.

B37. R. M. Souto, J. L. Rodríguez, L. Fernández-Mérida and E. Pastor, *J. Electroanal. Chem.* **494** (2000) 127.

B38. R. M. Souto, J. L. Rodríguez, G. Pastor and E. Pastor, *Electrochim. Acta* **45** (2000) 1645.

B39. J. Y. Gui, B. E. Kahn, L. Laguren-Davidson, C.-H. Lin, F. Lu, G. N. Salaita, D. A. Stern and A. T. Hubbard, *Langmuir* **5** (1989) 819.

B40. F. T. Wagner and P. N. Ross, *J. Electroanal. Chem.* **150** (1983) 141.

B41. J. Clavilier, A. Rodes, K. E. Achi and M. A. Zamakhchari, *J. Chim. Phys.* **88** (1991) 1291.

B42. T. Löffler and H. Baltruschat, *J. Electroanal. Chem.* **554-555** (2003) 333.

B43. K. Sashikata, N. Furuya and K. Itaya, *J. Vac. Sci. Technol.* **B 9** (1991) 457.

B44. J. M. Zhu, T. Hartung, D. Tegtmeyer, H. Baltruschat and J. Heitbaum, *J. Electroanal. Chem.* **244** (1988) 273.

B45. J. Inukai, M. Wakisaka; M. Yamagishi and K. Itaya, *Langmuir* **20** *(2004)* 7507.

APPENDIX C

STEP DECORATION AT Au SINGLE CRYSTAL ELECTRODES-IMPACT ON ADSORPTION AND CATALYSIS*

Fernando Hernandez[(1)], Jean Sanabria-Chinchilla[(1)(2)], Manuel P. Soriaga[(2)], Helmut Baltruschat[(1)†]

(1) University of Bonn, Roemerstrasse 164, D-53117 Bonn, Germany

(2) Electrochemical Surface Science Laboratory, Chemistry Department, Texas A&M University, USA

Abstract

Surfaces of regularly stepped single crystals can be decorated with foreign metals in order to change their physicochemical properties. Step decoration of vicinally stepped platinum single crystals was achieved for many metals and can be easily monitored by cyclic voltammetry due to the suppression of the corresponding hydrogen adsorption at step sites. By using the system Pd/Au(hkl) reactive bonding sites are introduced at regular spacings. Here step decoration is more difficult to prove. Au(111) and Au(332) were used as the substrate for palladium deposition in the UPD-regime. Preparation and Pd deposition were checked by STM. Cyclic voltammetry shows two Pd-oxidation peaks, the first one being almost independent of coverage; it is therefore ascribed to Pd decorating steps. Hydrogen adsorption on the modified stepped surfaces, but not on Pd/Au(111), takes place only when more than a critical amount of Pd has been deposited. A voltammetric peak at ca. 0.3 V vs. RHE is related to the adsorption of hydrogen at palladium terraces, at this potential the adsorption of hydrogen on steps is negligible. A quantitative evaluation supports the assumption of step decoration by Pd.

* Reprinted from Proc. Electrochem. Soc., vol. 18, F. Hernandez, J. Sanabria-Chinchilla, M.P. Soriaga, H. Baltruschat, Step Decoration at Au Single Crystal Electrodes-Impact on Adsorption and Catalysis, pp. 15-24.

† Corresponding author: baltruschat@uni-bonn.de

Using differential electrochemical mass spectrometry (DEMS), CO and benzene adsorbing at step sites was distinguished from that adsorbing at terraces.

Introduction

When studying bimetallic catalysts it is advantageous to use surfaces with an ordered arrangement of the two elements in order to get a fundamental insight into the manner of action of such systems. While for studies of the metal/gas interface often ordered bimetallic alloys are used, for studies at the metal/electrolyte interface such alloy systems require a UHV-transfer system in order to control the surface composition and order (C1,C2). An alternative is the use of vicinally stepped single crystal electrodes, after step decoration with a second metal. In this way bimetallic metal surfaces are obtained, on which striped domains of the substrate alternate with monoatomic rows of the second component. In the case of stepped Pt single crystal electrodes with (111) terraces, step decoration can be easily controlled by monitoring the suppression of the corresponding peaks in the cyclic voltammogramm for hydrogen adsorption (C3).

Decorating the steps of a Pt(332) electrode with Sn thus leads to a surface which is much more catalytically active for CO oxidation than a Pt(111) electrode modified by submonolayer amounts of Sn, because in the latter case Sn forms 2D islands after adsorption of CO, whereas on the (332) surface, due to step decoration, the Sn atoms are better and more homogeneously distributed (C4-C6). Up to 50% of the adsorbed CO is oxidizable at 0.3 V, the oxidation potential of the residual adsorbate is hardly shifted with respect to the pure Pt surface. Assuming that surface diffusion of CO is fast, a bifunctional effect of Sn on the CO oxidation on this surface can thus be excluded, because then all adsorbed CO should be oxidized at a lower potential. Instead, Sn exerts an electronic effect on CO and forces part of it into a weakly adsorbed state, which is more easily oxidized.

We have also demonstrated that decoration of steps with Ru is possible as well (C7,C8). The oxidation of adsorbed CO at such a surface proceeds in only one oxidation peak (around 0.5 V as compared to 0.7 V on pure Pt), when the steps, and thus the rows of Ru, are not more separated than by a 5 atom wide terrace. When the distance between

the rows of Ru is larger (e.g. 10 Pt atoms) a further oxidation peak is observed at 0.6 V. We concluded that this is due to CO adsorbed at some distance from the Ru, which is not subject to an electronic effect of Ru. The first oxidation peak, however, corresponds to CO adsorbed in close vicinity of Ru where it is subject to such an electronic effect (decreased adsorption enthalpy). The more positive oxidation peak is still located at a much lower potential than at pure Pt due to a bifunctional effect of Ru; assuming again fast diffusion of adsorbed CO to Ru sites, the activation barrier is decreased for both. In this way, also ternary surfaces can be prepared; further decoration of the Ru/Pt(332) system, e.g. with Mo, led to a surface which is catalytically more active than Ru/Pt(332) or Pt(332) (C9).

Step decoration by catalytically inactive metals confirmed the importance of steps for hydrogenation reactions, as in the case of Cu/Pt(332) for hydrogenation of benzene (C10). On the other hand, such a surface should also help in understanding geometric effects: Since the diameter of a benzene molecule corresponds to approx. 3 Pt atoms, its adsorption on a Pt(331) surface, with its only 2 atoms wide terraces might be largely suppressed after step decoration by Cu or Ag. However, the benzene coverage of ca. 0.2 nmol cm^{-2} as determined by DEMS in pure supporting electrolyte after adsorption at 0.3 V and electrolyte exchange, is similar to that of Pt(332) after step decoration by Cu or Ag, and only reduced by 50% with respect to the undecorated surface. Obviously, binding to only one row of accessible Pt atoms after step decoration is sufficient for strong, irreversible binding (C11).

As an alternative to obtaining a bimetallic surface with alternating atoms of a catalytically active and inactive metal, Pd UPD-deposition on Au (332) is used in this work. Underpotential deposition of Pd on smooth Au(111) surfaces has been described by a number of authors (C12-C15).

Experimental

Disc-shaped gold single crystals (Metal Crystals and Oxides LTD, 10 mm diam.) were prepared by flame annealing. After 2 minutes of annealing, they were transferred to the electrochemical cell and cooled down for 4 minutes over deaerated Millipore water

in a controlled atmosphere of either ultra pure argon (99.999%, Air Products) or in a reductive atmosphere of Ar:H_2 (2:1 vol.). After cooling, the quality of the surface was checked by cyclic voltammetry in 0.1 M H_2SO_4 (Merck supra pur). All measurements were made at room temperature. In some experiments the surface quality was also controlled taking STM images. Examples are shown in Fig. C-1. It is clear from these images that cooling in Ar leads to faceting of stepped surfaces (similar to Pt, see (C16)), whereas after cooling in the hydrogen containing atmosphere the step width is close to the nominal width. If the crystal is cooled in air, faceting is even more pronounced and the terrace width gets larger, an effect that is evident in older STM images (C17).

Millipore water was used to prepare all the solutions. A reversible hydrogen electrode (RHE) in 0.1 M H_2SO_4 served as reference electrode for all the voltammetric experiments, while a Pt wire was used in the STM-cell as quasi reference electrode. The cyclic voltammograms were recorded in a glass cell in the hanging meniscus arrangement. Solutions were deaerated with ultra pure argon.

Two kinds of solutions were employed for the Pd deposition in the UPD-regime, namely one with chloride (0.1 mM $PdCl_2$ + 0.6 mM HCl + 0.1 M H_2SO_4) and one chloride-free (0.1 mM $PdSO_4$ + 0.1 M H_2SO_4). $PdSO_4 \cdot 2H_2O$ and $PdCl_2$ were obtained from Merck. The electrode was immersed at a potential of 1.16 V vs. RHE, where no Pd deposition takes place, and the potential was cycled slowly (v = 1 mV/s) in the cathodic direction until the UPD peak appeared. The charge under the UPD curve was used as a measure of the amount of Pd deposited, taking Q = 440 _C cm^{-2} as the equivalent charge for a full monolayer on the Au(111) surface. The integration was performed with the trapezoidal rule. To attain fractional coverage, the potential was stopped at a given value before the UPD peak was complete, breaking immediately the contact with the electrolyte and rinsing the electrode with water. This method was found to give more reproducible results than the selective dissolution of a previously deposited full Pd monolayer.

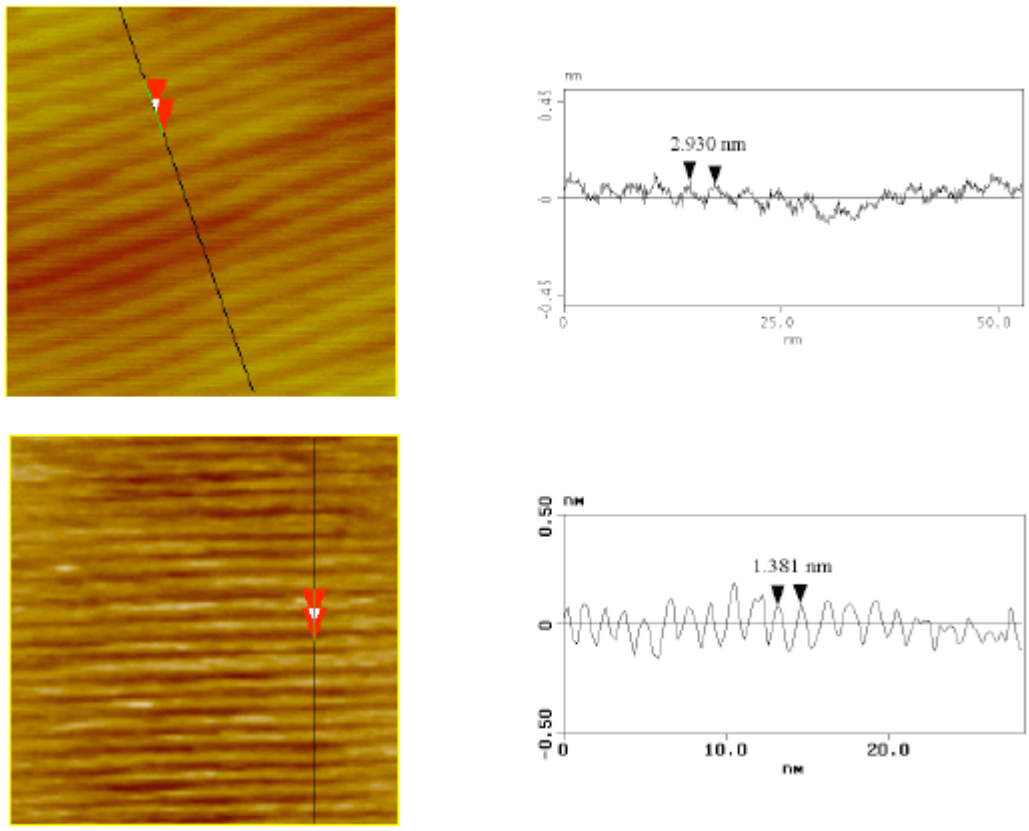

Fig. C-1: STM-images of flame annealed Au(332). *Top:* 53 x 53 nm^2 , after cooling down in Ar. *Bottom:* 28 x 28 nm^2 , after cooling in Ar:H_2 atmosphere.

At the end of any experiment involving Pd deposition, the electrode was cycled in a solution containing 0.1 M H_2SO_4 and 0.6 mM HCl at 50 mV/s between 0 and 1.7 V until a steady response was attained, changing the electrolyte several times if necessary. This procedure proved to be enough to dissolve all the deposited Pd, leaving a clean gold single crystal that can be annealed and used again. Details of differential electrochemical mass spectrometry (DEMS) are described elsewhere (C18).

CO adsorption was performed for 3 min under potential control (0.35 V) using a CO-saturated 0.1 M H_2SO_4 solution. After adsorption, the cell was rinsed with supporting electrolyte at the same adsorption potential. Scan was started cathodically to check the suppression of the H ads/des signals between 0.30 V and 0.10 V. After that, the positive switching potential was extended to 1.30 V.

Results and Discussion

Fig. C-2 summarizes the cyclic voltammetry for Au(332) covered by varying amounts of Pd. The pair of peaks at around 0.3 V corresponds to hydrogen adsorption and to some extent to anion desorption. The anodic peak at 0.9 V is independent of the Pd coverage whereas that above 1.0 V strongly depends on the Pd coverage. We, therefore, conclude that the latter is due to oxygen adsorption on Pd (UPD) terraces (and subsequent Pd dissolution) whereas the former is due to oxygen adsorption at steps. Its independence on the Pd coverage signifies that Pd decorates the steps indeed. If Pd islands on the Au terraces would form, their total edge length certainly would vary with Pd coverage. The Pd/Au(111) surface only shows the second peak. A further hint for step decoration is the height of the peak at 0.3V: at a coverage of 47% its height is only 1/3 of that of full Pd coverage. A plot of the peak current vs. coverage and extrapolation to zero peak height shows that hydrogen adsorption becomes appreciable only above a coverage of around 20%, which just corresponds to a decoration of the step edges with one row of Pd atoms.

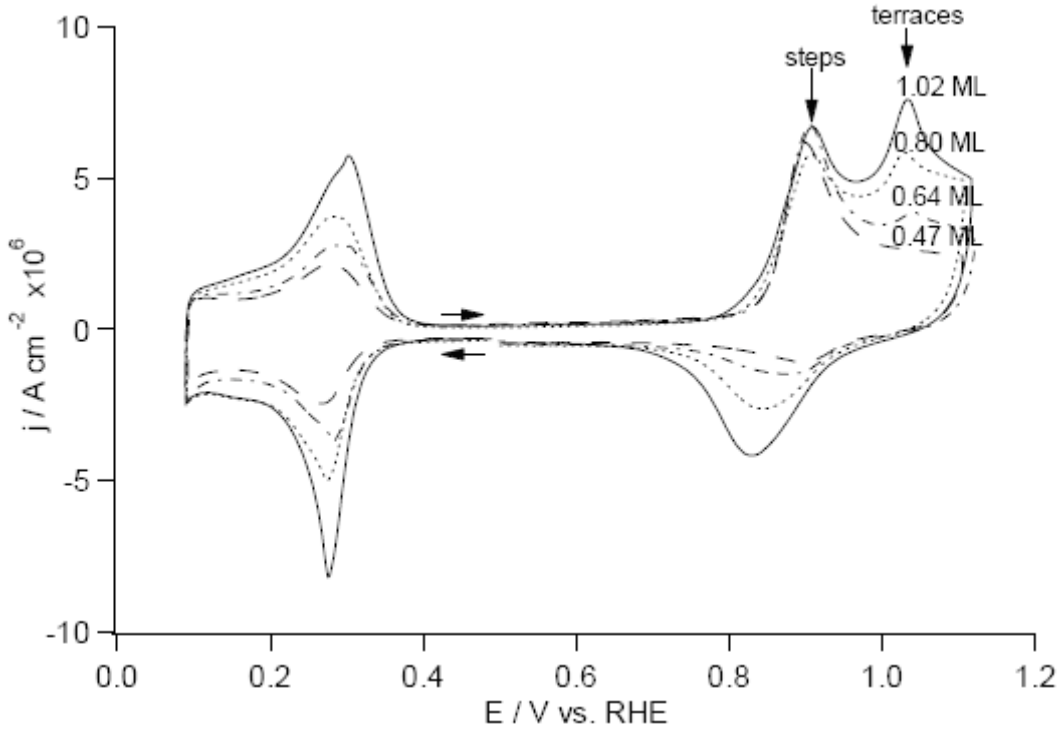

Fig. C-2: First voltammetric cycle for Pd/Au(332) in 0.1 M H_2SO_4 with different Pd coverage. Starting potential 0.5 V, scan rate of 5 mV/s. Pd was deposited from $PdSO_4$ solution.

Hydrogen adsorption on Au electrodes is usually not believed to occur. Recent theoretical calculations have shown that the adsorption energy of hydrogen on Au is much lower that that of Pd (C19). On the other hand, hydrogen evolution observed during formaldehyde oxidation in alkaline solution on Au, Ag and Cu electrodes is known to occur via adsorbed hydrogen (C20). Adsorbed hydrogen on Ag is formed during the injection of hot electrons in MIM structures (C21). Recently, Stimming and co-workers interpreted their results on hydrogen evolution at Pd clusters generated from an STM tip by a spillover of hydrogen atoms onto the Au surface and their subsequent recombination on Au (C22). Therefore, we have also studied the hydrogen evolution at the Pd decorating the steps of Au(332). The results are summarised in Fig. C-3, which gives the current-voltage curves in a hydrogen-saturated sulphuric acid solution at small overpotentials. Whereas at pure Au the exchange current density is negligible, at surfaces covered by submonolayers of Pd it is more than twice that of the exchange current measured at a surface covered by nearly 2 monolayers. Interestingly, the current density hardly depends on the Pd coverage as long as it is below one monolayer. At all surfaces, the scan rate had no influence.

A higher catalytic activity of UPD Pd as compared to that of bulk Pd has already been found by Kibler et al. and has been explained by the shift of the d-band centre. For submonolayers of Pd on Au(111) Stimming and co-workers have found that the exchange current density is not proportional to the coverage of Pd on Au(111); when normalized to the Pd coverage it decreases. This was interpreted by the spillover of hydrogen atoms from Pd to the uncovered Au surface, where formation of H_2 takes place more efficiently. This spillover of hydrogen atoms had already been suggested to explain the large catalytic activity of Pd nanoclusters on Au (C22).

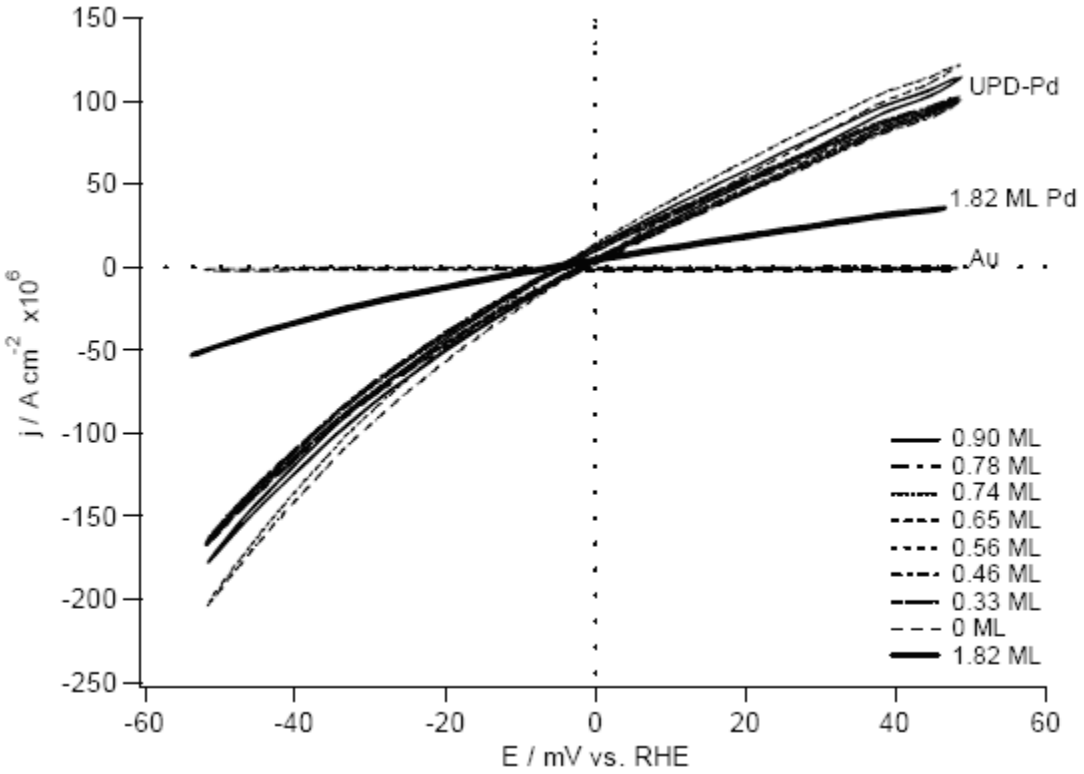

Fig. C-3: H_2-evolution on Pd/Au(332) as a function of Pd-coverage. Current-voltage curves in 0.1 M H_2SO_4 saturated with H_2, 25 mV/s (no effect of scan rate was found).

The independence of the reaction rate on coverage suggests that the rate of hydrogen evolution is proportional to the total step length. Assuming step decoration, this length does not vary with increasing Pd coverage on a stepped Au surface, whereas it does vary with coverage on Au(111) surfaces due to a changing number and size of Pd islands. Note that the step length is identical to the length of the boundary between Pd and Au as long as the coverage is below one monolayer. Therefore, this effect may be due to a particular catalytic activity of Pd steps, or to the importance of the Pd-Au boundary, which, assuming the hydrogen spillover to Au to be true, would limit the overall rate.

The decrease of the catalytic activity after deposition of a second monolayer probably has to be explained by an electronic effect. However, a change of the morphology also has to be considered. In Fig. C-4, the STM images during deposition of a second monolayer are shown. The result is a facetted surface; terraces become broader, but they are not continuous in step direction. This has to be compared to overpotential deposition of Pd on Au(111) which occurs in a layer-by-layer growth mode, however, the thicker the Pd layer, the less continuous the Pd layers are (C12,C13,C15,C23,C24).

Oxidation of adsorbed carbon monoxide also demonstrates step decoration by Pd (Fig C-5). Differential electrochemical mass spectrometry (DEMS) was used here in order to distinguish the oxidation currents from (pseudo-) capacitive currents. On a surface covered by 0.78 monolayer of Pd, a peak at 0.93 V and a shoulder at 1.1 V are visible. When essentially only the steps are decorated by Pd (approx. 0.34 monolayers) only an oxidation peak at 1.1 V is visible, coinciding with the shoulder observed for the higher Pd coverage. This latter peak corresponds, therefore, to CO adsorbed either at Pd step sites or to sites in the direct vicinity of Au (steps of the substrate). Since it is improbable that the neighborhood to Au increases the adsorption strength, we favor the interpretation that the more anodic peak corresponds to CO adsorbed at step sites. Nevertheless, the oxidation may proceed at step sites also from molecules adsorbed at terrace sites, i.e. oxidation may well start at steps. But CO molecules diffuse from terrace sites to the steps and quickly refill those sites.

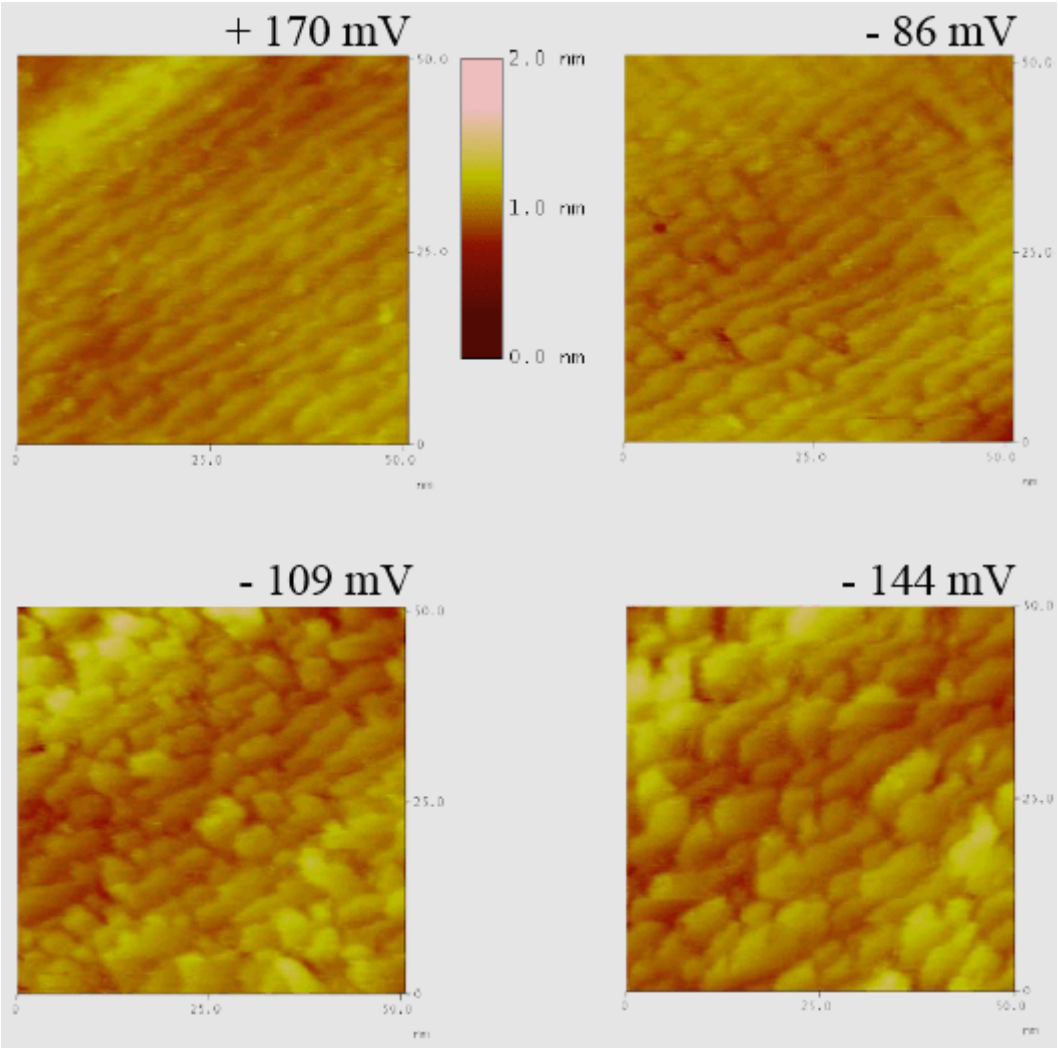

Fig. C-4: Sequence of STM-images for Pd deposition from $PdSO_4$ solution on Au(332). *Top left:* original surface; *Top right:* 1st. Pd layer is complete. *Bottom:* Growth of subsequent layer. All potentials vs. Pt QRE. Area is 50 x 50 nm^2.

Desorption of irreversibly adsorbed benzene on a Pd-modified Au(332) surface is monitored by the DEMS experiment shown in Fig C-6. From a surface fully covered by Pd, part of the adsorbate is desorbed during a potential sweep in the negative direction without hydrogenation. Some residual benzene is displaced by adsorbing oxygen in the subsequent anodic potential sweep. Qualitatively, a similar behavior had been observed for benzene adsorbed on polycrystalline Pd (C25). When only the steps are decorated by Pd, no benzene is desorbed at low potentials, but only in the oxygen adsorption region. Oxidation to CO_2 is negligible in both cases. The obvious interpretation is that benzene adsorbed at step sites is strongly adsorbed and is only displaced by oxygen, whereas benzene at terraces is desorbable at low potentials. Table C-1 summarizes the results including the Au(111) face. Note that from an Au(111) electrode largely covered by Pd, nearly all of the benzene desorbs at low potentials.

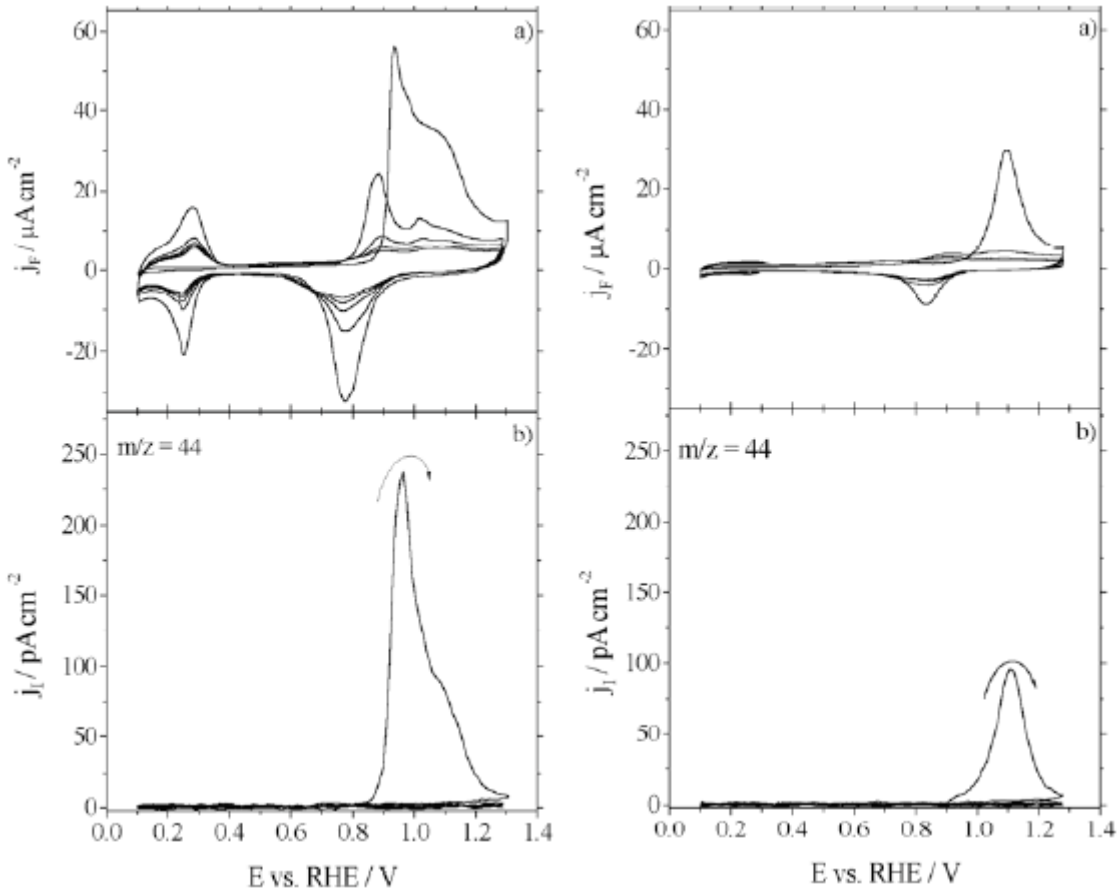

Fig. C-5: CO oxidation on Pd/Au(332) surfaces. *a)* Cyclic voltammogram (CV) after CO adsorption, *b)* mass spectrometric cyclic voltammogram (MSCV) for m/z = 44, corresponding to CO_2. E_{ad}= 0.35 V, v = 10mV/s, 0.10 M H_2SO_4. *Left:* 0.78 ML Pd, *right:* 0.34 ML Pd.

Table C-1: Summary of DEMS results for benzene desorption on Pd/Au(332) and Pd/Au(111).

Surface	$\Gamma_{benzene}$ / nmol cm^{-2}	
	Hydrogen region	**Oxide region**
0.94 ML Pd/Au(332)	113.4	74.1
0.16 ML Pd/Au(332)	15.6	79.5
0.60 ML Pd/Au(111)	161.8	12.7

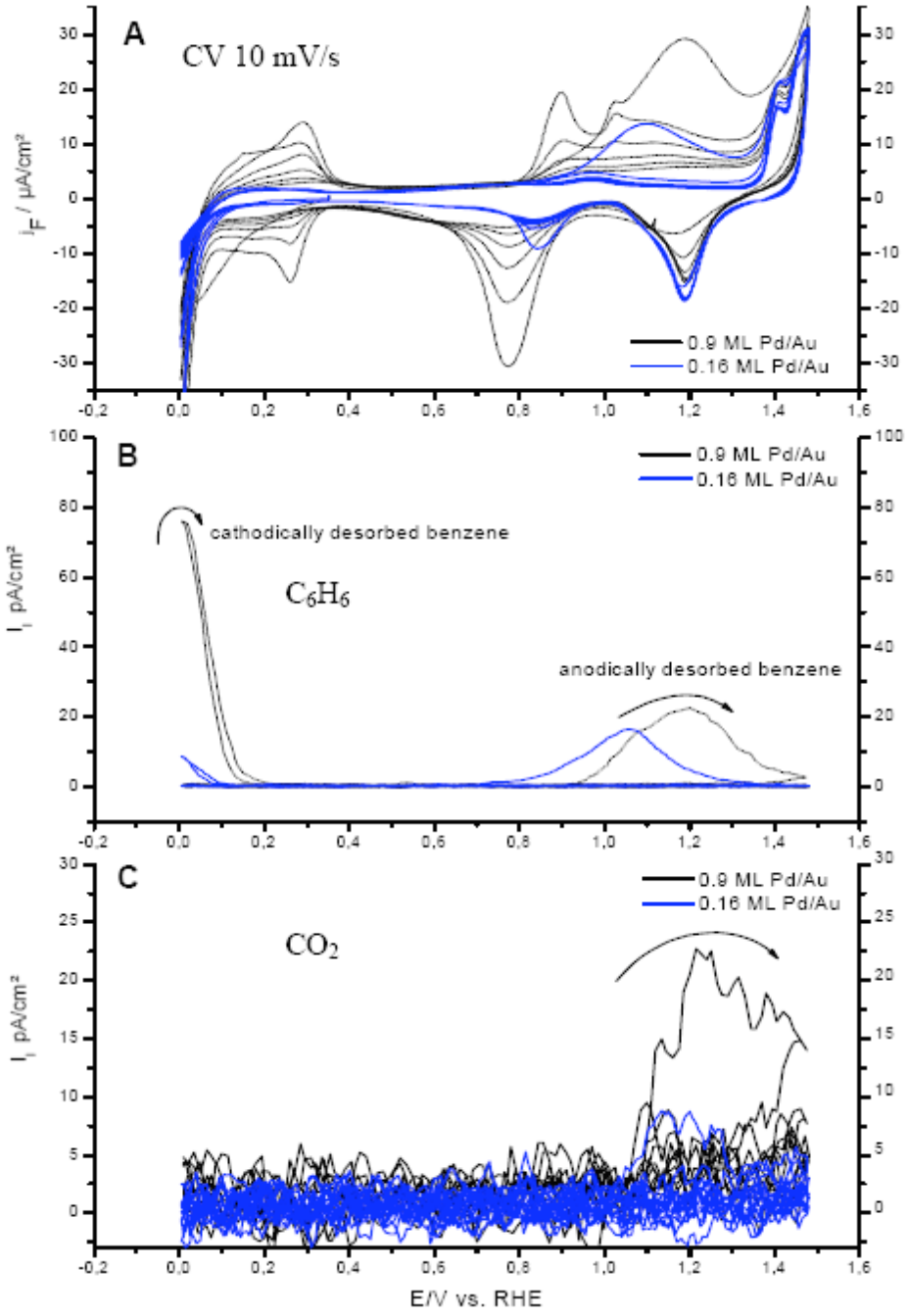

Fig. C-6: Desorption of benzene on Pd/Au(332) surfaces. *a)* Cyclic voltammogram (CV) after benzene adsorption, *b)* mass spectrometric cyclic voltammogram (MSCV) for m/z = 78, benzene and *c)* MSCV for m/z = 44, CO_2. Two different Pd coverages are shown.

Acknowledgments

This project would have not been possible without the support of the Deustche Forschungsgemeinschaft (DFG). Fernando Hernandez and Jean Sanabria-Chinchilla thank the German Academic Exchange Service (DAAD) for their research grants.

References

C1. Hayden, B. E.; Rendall, M. E.; South, O. *J. Am. Chem. Soc.* **2003,** *125*, 7738-7742.

C2. Stamenkovic, V. R.; M., A.; C.A., L.; Gallagher, M. E.; Ross, P. N.; Markovic, N. M. *J. Am. Chem. Soc.* **2003,** *125*, 2736-2745.

C3. Clavilier, J.; Feliu, J. M.; Aldaz, A. *J. Electroanal. Chem.* **1988,** *243*, 419-433.

C4. Massong, H.; Tillmann, S.; Langkau, T.; Abd El Meguid, E. A.; Baltruschat, H. *Electrochim. Acta* **1998,** *44*, 1379-1388.

C5. Berenz, P.; Tillmann, S.; Massong, H.; Baltruschat, H. *Electrochim. Acta* **1998,** *43*, 3035-3043.

C6. Tillmann, S.; Samjeske, G.; Friedrich, A.; Baltruschat, H. *Electrochim. Acta* **2003,** *49*, 73-83.

C7. Massong, H.; Wang, H. S.; Samjeske, G.; Baltruschat, H. *Electrochim. Acta* **2000,** *46*, 701-707.

C8. Samjeske, G.; Xiao, X.-Y.; Baltruschat, H. *Langmuir* **2002,** *18*, 4659-4666.

C9. Samjeské, G.; Wang, H.; Löffler, T.; Baltruschat, H. *Electrochim. Acta* **2002,** *47*, 3681 - 3692.

C10. Löffler, T.; Bussar, R.; Drbalkova, E.; Janderka, P.; Baltruschat, H. *Electrochim. Acta* **2003,** *48*, 3829 - 3839.

C11. Bußar, R. Diploma thesis, University of Bonn, Bonn, 2002.

C12. Naohara, H.; Ye, S.; Uosaki, K. *Colloid Surf. A-Physicochem. Eng. Asp.* **1999,** *154*, 201-208.

C13. Takahasi, M.; Hayashi, Y.; Mizuki, J.; Tamura, K.; Kondo, T.; Naohara, H.; Uosaki, K. *Surface Sci.* **2000**, 213-218.

C14. Baldauf, M.; Kolb, D. M. *Electrochim. Acta* **1993,** *38*, 2145-2153.

C15. Kibler, L. A.; Kleinert, M.; Randler, R.; Kolb, D. M. *Surface Sci.* **1999,** *443*, 19-30.

C16. Herrero, E.; Orts, J. M.; Aldaz, A.; Feliu, J. M. *Surface Sci.* **1999,** *440*, 259-270.

C17. Adzic, R. R.; Hsiao, M. W.; Yeager, E. B. *Surface Science Letters* **1992,** *273*, L425-L429.

C18. Baltruschat, H. In *Interfacial Electrochemistry*; Wieckowski, A., Ed.; Marcel Dekker, Inc.: New York, Basel, 1999, pp 577 - 597.

C19. Roudgar, A.; Groß, A. *J. Electroanal. Chem.* **2003,** *548*, 121-130.

C20. Stadler, R.; Z., J.; Baltruschat, H. *Electrochim. Acta* **2002,** *47*, 4485-4500.

C21. Diesing, D.; Rüße, S.; Otto, A.; Lohrengel, M. M. *Ber. Bunsenges. Chem.* **1995,** *99*, 1402-1405.

C22. Meier, J.; Schiotz, J.; Liu, P.; Norskov, J. K.; Stimming, U. *Chem. Phys. Lett.* **2004,** *390*, 440-444.

C23. Naohara, H.; Ye, S.; Uosaki, K. *J. Phys. Chem. B* **1998,** *102*, 4366-4373.

C24. Quayum, M. E.; Ye, S.; Uosaki, K. *J. Electroanal. Chem.* **2002,** *520*, 126-132.

C25. Schmiemann, U.; Jusys, Z.; Baltruschat, H. *Electrochim. Acta* **1994,** *39*, 561-576.

VITA

JEAN SANABRIA-CHINCHILLA

Department of Chemistry
Texas A&M University
TX 77843-3255

E-mail: jeansanabria@yahoo.com
Phone: 832-798-0302

EDUCATION

Ph.D., Chemistry. Texas A&M University, College Station, TX. 2006

B.S., Chemistry. Universidad de Costa Rica, San José, Costa Rica. 1997

PUBLICATIONS

1. J. Sanabria-Chinchilla, M.P. Soriaga, R. Bussar, H. Baltruschat. "A DEMS Study of the Electrocatalytic Hydrogenation and Oxidation of p-Dihydroxybenzene at Polycrystalline and Monocrystalline Platinum Electrodes." J. Appl. Electrochem. Accepted, 2006.
2. F. Hernandez, J. Sanabria-Chinchilla, M.P. Soriaga, H. Baltruschat, "Step Decoration at Au Single-Crystal Electrodes. Impact on Adsorption and Catalysis." Proc. Electrochem. Soc. 18 (2005) 15-24.
3. X. Chen, J. Sanabria-Chinchilla, M.P. Soriaga, "The Use of Thin-Layer Electroanalysis in the Study of the Chemisorption and Anodic Oxidation of Aromatic Molecules at Smooth Polycrystalline Palladium." Electroanalysis 17 (2005) 2121-2127.
4. Y.-G. Kim, X. Chen, Y.-S. Park, J.H. Baricuatro, J. Sanabria-Chinchilla, M.P. Soriaga, "Surface Organometallic Chemistry of Well-Defined Palladium Electrodes." J. Arg. Chem. Soc. 91 (2003) 1-22.
5. D. Chong, I.P. Georgakaki, R. Mejia-Rodriguez, J. Sanabria-Chinchilla, M.P. Soriaga, M. Y. Darensbourg, "Electrocatalysis of Hydrogen Production by Active Site Analogues of the Iron Hydrogenase Enzyme: Structure/Function Relationships." J. Chem. Soc., Dalton Trans. 21 (2003) 4158-4163.
6. J.B. Abreu, J.M. Sanabria-Chinchilla, M.P. Soriaga, J.F. Garst, J.L. Stickney, "The Interfacial Chemistry of Grignard Reagent Formation: Reactions of Clean Mg(0001) Surfaces", in Thin films: Preparation, Characterization, Applications, M.P. Soriaga, J.L. Stickney, Y.-G. Kim (Eds.), Kluwer Academic/Plenum Publishers, New York, 2002, p.185-196.